Role of the Rab GTPase activating protein TBC1D4 in ischemia/reperfusion-induced myocardial injury

Inaugural-Dissertation

zur Erlangung des Doktorgrades
an der Mathematisch-Naturwissenschaftlichen Fakultät
der Heinrich-Heine-Universität Düsseldorf

vorgelegt von

Christian Binsch
aus Münster (Westf.)

Düsseldorf, Dezember 2020

Aus dem Institut für Klinische Biochemie und Pathobiochemie
des Deutschen Diabetes-Zentrums,
Leibniz-Zentrum für Diabetesforschung
an der Heinrich-Heine-Universität Düsseldorf

Gedruckt mit der Genehmigung der
Mathematisch-Naturwissenschaftlichen Fakultät der
Heinrich-Heine-Universität Düsseldorf

Berichterstatter:

1. Prof. Dr. Hadi Al-Hasani
2. Prof. Dr. Michael Feldbrügge

Tag der mündlichen Prüfung: 04.11.2021

Table of Contents

Summary

Type 2 Diabetes mellitus (T2DM) represents a significant risk factor for the development and the course of cardiac diseases. Patients suffering from T2DM exhibit an increased prevalence for myocardial infarction (MI) and reduced survival rate. In T2DM, the cardiac metabolic flexibility, i.e. the switch between carbohydrates and lipids as energy source, is disturbed. The signaling protein TBC1D4/AS160 is a crucial regulator of glucose and fatty acid utilization for energy production in skeletal muscle and adipose tissue. Moreover, a TBC1D4 p.Arg684Ter loss-of-function variant defines a specific form of T2DM and accounts for more than 10% of T2DM in arctic populations. Therefore, the aim of this study was to elucidate the function of TBC1D4 in cardiac substrate metabolism and adaption under conditions of ischemia/reperfusion (I/R)-induced myocardial injury.

The results of the present study identified TBC1D4 as a crucial mediator of cardiac glucose homeostasis and adequate adaptation towards ischemia/reperfusion injury-induced myocardial damage. *Tbc1d4*-deficient C57BL/6J mice showed no insulin-stimulated increase in glucose uptake in the heart *ex vivo* and *in vivo*, and exhibited a marked decrease of cardiac GLUT4 content while GLUT1 abundance remained unchanged. At the same time, mitochondrial function and number as well as cardiac lipid composition were not altered due to the loss of *Tbc1d4*. Three weeks following cardiac I/R-intervention, deficiency of *Tbc1d4* led to reduced cardiac function along with a markedly increased infarction size. At the molecular level, cardiac transcriptome analysis of *Tbc1d4*-knockout hearts revealed distinct differential gene regulation in pathways regarding the unfolded protein response (UPR) and extracellular matrix (ECM) remodeling processes. Further biochemical analysis identified specific alterations of the cardiac unfolded protein response via the ATF4/eIF2α mediated pathway and decreased expression of cardiac matrix metalloproteinases (MMPs) as well as reduced ratios to their inhibitors (TIMPs). A *Tbc1d4*-associated impairment of ECM remodeling in the heart was further supported by morphometry using transmission electron microscopy (TEM) which demonstrated increased ECM area in hearts of *Tbc1d4*-deficient mice. Collectively, the impaired cardiac recovery after I/R in *Tbc1d4*-deficient mice is linked to i) defects in metabolic flexibility, ii) altered response to ER-stress through the UPR system, and iii) changes in remodeling of the cardiac ECM which may relate to altered synthesis and/or secretion of matrix proteases.

Further studies will focus on the exact molecular pathways of TBC1D4 action on the unfolded protein response and ECM remodeling. The importance of TBC1D4 for glucose homeostasis in humans, as seen in Greenlandic Inuit, renders it as a potential target for therapeutically intervention.

Zusammenfassung

Typ-2 *Diabetes mellitus* (T2DM) ist ein wesentlicher Risikofaktor für Entstehung und Verlauf von Herzerkrankungen. Patienten mit T2DM haben eine erhöhte Prävalenz für Myokardinfarkt (MI) sowie eine verminderte Überlebensrate. Die kardiale metabolische Flexibilität, d.h. der adäquate Wechsel zwischen Kohlenhydraten und Lipiden als Energiequelle, ist in T2DM gestört. Das Signalprotein TBC1D4/AS160 ist ein essentieller Regulator der Energiegewinnung durch Glukose und Fettsäuren in Skelettmuskel und Fettgewebe. Eine p.Arg684Ter Mutation von *TBC1D4* ist für über 10% der T2DM-Fälle in grönländischen Inuit Populationen verantwortlich. Ziel dieser Studie ist die Entschlüsselung der Funktion von TBC1D4 auf den kardialen Substratmetabolismus und die Adaptation an Ischämie/Reperfusion (I/R) - vermittelte Schädigung des Myokards.

Die Ergebnisse der vorliegenden Studie konnten TBC1D4 als essentiellen Mediator des kardialen Glukosestoffwechsels und der adäquaten Adaptation an I/R-vermittelten Myokardschaden identifizieren. T*bc1d4*-defiziente C57BL/6J Mäuse zeigten keine Erhöhung der kardialen Glukoseaufnahme nach Insulinstimulation *ex vivo* und *in vivo*. Zugleich war der kardiale Gehalt des insulin-abhängigen Glukosetransporters GLUT4 vermindert, nicht aber der des Glukosetransporters GLUT1. Die TBC1D4 Defizienz führte weder zu Veränderungen in Bezug auf Funktion und Zahl der Mitochondrien, noch zu Änderungen des kardialen Lipidprofils. Drei Wochen nach I/R-Intervention zeigte sich durch *Tbc1d4* Defizienz eine reduzierte Herzfunktion sowie eine deutlich vergrößerte Infarktfläche. Die Analyse des kardialen Transkriptoms identifizierte differentielle Genregulation durch *knockout* von *Tbc1d4* bezüglich Signalwegen, welche mit der Stressantwort des endoplasmatischen Retikulums (ER) und des strukturellen Umbaus der kardialen extrazellulären Matrix (ECM) assoziiert sind. Weitere Analysen identifizierten spezifisch über den ATF4/eIF2α Signalweg vermittelte Störungen der kardialen ER-Stress Antwort, sowie verminderte Expression kardialer Matrix-Metalloproteasen (MMPs) und eine verminderte Ratio zu ihren Inhibitoren (TIMPs). Eine *Tbc1d4*-assozierte Störung der ECM Modellierung konnte unterstützend durch Morphometrie anhand von Transmissionselektronenmikroskopie eine Erhöhung der ECM Fläche in *Tbc1d4*-defizienten Herzen identifiziert werden. Zusammengefasst ist die gestörte kardiale Genesung nach I/R in *Tbc1d4*-defizienten Mäusen assoziiert mit i) Defekten in der metabolischen Flexibilität, ii) gestörter ER-Stressantwort und iii) veränderter Modellierung der kardialen ECM, welche mit geänderter Synthese und/oder Sekretion von Matrix-Metalloproteasen assoziiert sein könnte.

Weiterführende Untersuchungen sollen ihren Fokus auf die molekulare Funktion von TBC1D4 in der ER-Stressantwort und Umbau der ECM legen. Die Bedeutsamkeit von TBC1D4 in der Humansituation, wie im Fall der grönländischen Inuit, macht TBC1D4 zu einem potentiellen Ziel therapeutischer Interventionen.

1. Introduction

1.1 Cardiovascular diseases and myocardial infarction

Cardiovascular diseases (CVD) represent the major cause for mortality worldwide. According to the World Health Organization (WHO), an estimated 31% of all global deaths in the year 2016 were caused by cardiovascular diseases, representing 17.9 million cases. While the term “CVD” includes peripheral arterial disease, rheumatic heart disease, congenital heart disease, deep vein thrombosis and pulmonary embolisms, around 85% of all CVD related-deaths are due to cerebrovascular disease and coronary heart disease, including myocardial infarction.

Myocardial infarction (MI) describes the situation of myocardial cell death due to prolonged durations of ischemia, resulting from an imbalanced ratio of oxygen supply and demand (Thygesen et al., 2018). Here, the disrupted or decreased blood flow (ischemia) in specific parts of the heart and limits the oxygen supply from the blood stream (hypoxia). This prolonged lack of supply triggers damage to the thereby undersupplied heart muscle (myocardium). In current clinical classification, a distinction between three types of MI has been introduced (Thygesen et al., 2018).

1) Type 1 myocardial infarction is the result of atherothrombotic artery disease (CAD) and often manifested in atherosclerotic plaque disruption. This leads to occlusive or non-occlusive thrombi due to plaque rupture or erosion.

2) Type 2 myocardial infarction describes other pathophysiological mechanisms leading to ischemia-induced myocardial injury than defined in type 1 MI (e.g. atherosclerosis, vasospasm or coronary microvascular dysfunction)

3) Type 3 myocardial infarction describes the situation when the suspicion for myocardial ischemic situation is high but lacking coherent clinical evidence, for instance via specific biomarkers, mostly due to the prior death of the patient.

In most clinical cases, the impaired blood flow is the result of a blockage of coronary arteries evoked by an atherosclerotic plaque, constituting 70% of all fatal cases (Mechanic & Grossman, 2020).

On a structural level, the resulting damage of these ischemic events has been described to be present already as early as 10-15 minutes after the ischemic incident. Among these are decreased cellular glycogen content, relaxation of myofibrils and sarcolemmal disruption visible on the ultrastructural level (Jennings & Ganote, 1974). Moreover, progressive mitochondrial abnormalities can be observed at this time point already (Virmani, Forman, & Kolodgie, 1990). However, also in later stages, acute inflammatory processes can be detected during the first 4 days after MI and potential repair mechanisms, such as neovascularization, wound healing, myofibroblast activation and scar formation in order to ensure structural integrity take place in the following days up to weeks post-MI (Prabhu & Frangogiannis, 2016).

Since the first regulatory processes of adaptation and also structural damages occur already shortly after the MI incident, in the clinical situation the removal of the blockage is vital in order to limit myocardial damage and preserve cardiac function. While this principle of “time is muscle” (Abreu, 2019), meaning the sooner the blockage is released the better the chances are to maintain viable cardiac tissue, is applied, the actual restoration of blood flow to the prior deprived tissue (reperfusion) leads to causation of additional damage to the ischemic tissue due to inflammatory response and oxidative damage. This phenomenon is referred to as “ischemia-reperfusion injury” (Abreu, 2019).

Although this concept has been highly debated in the past, it has been shown that the reperfusion event on the ischemic myocardium can trigger cardiomyocyte death independent of the ischemia-induced damage itself (Braunwald & Kloner, 1985; Hausenloy & Yellon, 2013; Piper, Garcia-Dorado, & Ovize, 1998; Yellon & Hausenloy, 2007). The clinical consequences of this ischemia-reperfusion injury include reversible forms like reperfusion-induced cardiac arrhythmias and myocardial stunning, but also irreversible damage such as microvascular obstruction and lethal myocardial reperfusion injury (Hausenloy & Yellon, 2013; Piper et al., 1998).

However, while some studies see the origin of this paradoxical effect at the level of reactive oxygen species (ROS) production and oxidative stress which promote endothelial dysfunction, DNA damage and local inflammatory responses (Ornellas et al., 2017; Wu et al., 2018), the exact mechanisms regarding the detrimental effects of reperfusion after MI remain to be elucidated.

1.1.1 Cardiovascular disease and the metabolic syndrome

The WHO reports various risk factors for the development of cardiovascular diseases and myocardial infarction. One major cluster of risk factors is found in the metabolic syndrome.

The metabolic syndrome (also referred to as insulin resistance syndrome or syndrome X) describes the principle of the co-occurrence of several risk factors for the development of cardiovascular diseases. In classical definition, these include five different phenotypes including visceral obesity, insulin resistance, hypertension, high levels of triglycerides and low HDL-cholesterol. These conditions have been described to be highly interrelated and may share common underlying mediators, mechanisms and pathways (Mule, Calcaterra,

Nardi, Cerasola, & Cottone, 2014), however the molecular basis of these relations is still subject to debate (Uzunlulu, Telci Caklili, & Oguz, 2016; Zimmet et al., 2019). Interestingly, these risk factors do not only contribute to the development of cardiovascular diseases but are also associated with type 2 diabetes mellitus, which in turn is a risk factor for developing CVDs itself. In fact, cardiovascular diseases and diabetes mellitus represent two closely related diseases in terms of risk factors and development.

1.2 Diabetes mellitus

Diabetes mellitus represents one of the largest scientific and medical challenges of the present times and constitutes a major risk factor for the development of various deuteropathies, including hypertension, atherosclerosis and heart diseases. With a number of 108 million affected people in 1980, the number of adults suffering from diabetes mellitus has ever since increased to 422 million in the year 2014, with prognosis to further rise to over 700 million cases in the year 2025 (Collaboration, 2016). According to the World Health Organization (WHO), an estimated 1.6 million deaths were directly caused by diabetes in 2016 and the International Diabetes Federation (IDF) reports a number of 4.2 million diabetes-related deaths (Federation, 2019)

1.2.1 Types of diabetes mellitus

The classical definition of diabetes mellitus distinguishes two major types of the disease (Leney & Tavare, 2009):

Type 1 diabetes mellitus (T1DM, previously known as “insulin-dependent” or “juvenile/childhood-onset diabetes”) is caused by an autoimmune destruction of insulin-

producing pancreatic β-cells and thereby characterized by an absolute and primary insulin deficiency.

Type 2 diabetes mellitus (T2DM, previously known as “non-insulin dependent” or “adult-onset” diabetes) is defined as a potentially reversible metabolic state that can be caused by various triggers (e.g. obesity and simultaneous lack of physical activity, insulin resistance, etc.), which results in impairments of insulin action and/or insulin secretion and subsequently to hyperglycemia due to impaired insulin-stimulated glucose uptake by peripheral tissues.

Next to impairments in glucose homeostasis, T2DM can also provoke multiple deuteropathies, including cardiovascular diseases (CVD), nephropathies, retinopathies, and neuropathies and also cardiovascular diseases (Colberg et al., 2010). Especially, life style-related inadequate nutrition including high consumption of glucose and fat with concurrent lack of physical activity causes an impaired balance between energy uptake and energy expenditure towards energy consumption and storage. This leads to an excessive accumulation of body fat and subsequently to obesity, a major risk factor for both, T2DM and cardiovascular diseases.

1.2.2 Type 2 diabetes mellitus and myocardial infarction

Type 2 diabetes mellitus, which constitutes up to 90% of all diabetes mellitus cases worldwide, and the closely associated progressive insulin resistance represent major risk factors for the development of various cardiovascular diseases (CVD) (Dinesh Shah et al., 2015; Gast, Tjeerdema, Stijnen, Smit, & Dekkers, 2012). In this course, T2DM patients exhibit not only an increased prevalence for myocardial infarction (MI), but also impaired recovery and reduced survival rates after the infarction even (Einarson, Acs, Ludwig, & Panton, 2018). The incidence of cardiovascular diseases in T2DM patients is estimated

to be two to eight-fold higher compared to healthy individuals (Martin-Timon, Sevillano-Collantes, Segura-Galindo, & Del Canizo-Gomez, 2014). Moreover, about 60% of all deaths among Type 2 Diabetes patients are due to cardiovascular diseases and predominantly myocardial infarction (Kalofoutis et al., 2007). Interestingly, especially under diabetic conditions, myocardial function and structure can be impaired without the presence of additional cardiac risk factors, like hypertension or coronary artery disease. This phenomenon is referred to as the so-called “diabetic cardiomyopathy” (Jia, Hill, & Sowers, 2018).

1.3 Cardiac metabolic flexibility

A key feature of the healthy heart is its high metabolic flexibility, meaning its capacity to ensure optimal energy supply under various metabolic circumstances of energy availability (e.g. resting state, exercise, ischemia, etc.). This flexibility is achieved by the finely regulated utilization of lipids, glucose and other substrates as source of energy. (Doenst, Nguyen, & Abel, 2013; Goodwin & Taegtmeyer, 2000)

Impairments of this flexibility have been shown to contribute not only to increased cardiac injury during I/R but also to the development of heart failure (Q. Chen & Lesnefsky, 2018). For example, the limited utilization of glucose and simultaneously increased oxidation of lipids has been shown to increase cardiac injury (Kolwicz & Tian, 2009). Moreover, age might also be a crucial factor in this case, since reports describe marked impairments in metabolic flexibility of aged hearts following ischemia/reperfusion events when compared to hearts from younger patients (L. Wang et al., 2018).

Under normal, well-perfused conditions, the major part (60-90%) of energy production in form of ATP in the heart is provided by fatty acids via oxidative phosphorylation in the mitochondria, whereas glucose via glycolysis in the citric acid cycle and lactate only constitute a minor proportion of 10-40% of the total substrate use (Stanley, Recchia, & Lopaschuk, 2005). A lesser portion derived from ketone bodies and amino acids can in addition be utilized for energy production by cardiomyocytes (Henning, Wambolt, Schonekess, Lopaschuk, & Allard, 1996; Opie, 1992).

In situations of increased energy demand, the substrate preference of the heart is shifted towards the predominant utilization of glucose (Shao & Tian, 2015) to ensure sufficient energy supply, since in terms of produced ATP per oxygen consumed glucose can be metabolized more efficiently compared to the use of fatty acids. However, metabolic mal-adaptations in this course can potentially lead to a loss or impairments of the cardiac metabolic flexibility (Oakes et al., 2006). In T2DM patients, this flexibility is disturbed due to an imbalance of glucose and lipid utilization, manifesting in a reduced uptake and utilization of glucose along with an increased oxidation of lipids, which leads to impairments in adequate adaptation in situations of higher energy demand and/or oxygen deprivation.

Therefore, especially in T2DM patients, the impaired metabolic flexibility of the heart might play a role in the mal-adaption to acute myocardial infarction and ischemia/reperfusion events, since in this situation a shift to the use of glucose is of the essence. (Karwi, Uddin, Ho, & Lopaschuk, 2018; King & Opie, 1998; Larsen & Aasum, 2008)

A major impairment in the decreased metabolic flexibility of T2DM patients is the insulin-stimulated uptake of glucose from the bloodstream into the cardiomyocytes. The

transport of glucose into cells is a tightly controlled process involving a variety of signaling factors and cascades.

1.4 Post-prandial glucose uptake, insulin signaling and GLUT4 translocation

As a consequence of elevated post-prandial blood glucose levels, the pancreas secretes insulin. At the molecular level, insulin binds to the membrane-bound insulin receptor on cells of insulin-responsive tissues, such as skeletal muscle, liver, adipose tissue and heart, and thereby triggers a cascade of phosphorylation events, which initially includes the phosphorylation of insulin receptor substrate 1 (IRS1), and subsequently via phosphatidylinositol-3-kinase (PI3K) and 3-phosphoinositide-dependent protein kinase 1 (PDK1). This leads to phosphorylation, and thereby activation, of protein kinase B (AKT) and results ultimately in the translocation of glucose transporter type 4 (GLUT4) containing storage vesicles from the cytosol toward the cell membrane for exocytosis. Due to the increased GLUT4 content on the cell membrane, glucose uptake into the cell is facilitated. A crucial regulator of these translocation processes is the Rab-GTPase activating proteins TBC1D4.

The Rab-GTPase activating proteins (RabGAPs) TBC1 domain family member 4 (TBC1D4, alias AS160, AKT substrate of 160 kDa, Figure 1) and its close homologue TBC1 domain family member 1 (TBC1D1) are downstream targets of RAC-alpha serine/threonine-protein kinase (AKT) and 5'-AMP-activated protein kinase (AMPK). TBC1D4 and TBC1D1 have been shown to key factors in the regulation of insulin-stimulated glucose uptake in skeletal muscle and adipose cells by mediating the reversible translocation of GLUT4 from cytosolic storage vesicles towards the plasma membrane (Chadt et al., 2015; Holman & Cushman, 1994; Leto & Saltiel, 2012).

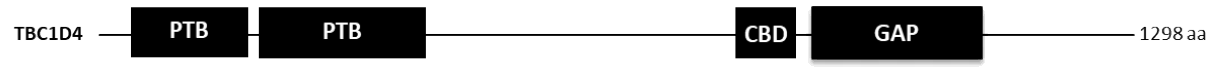

Figure 1: Domain structure of TBC1D4. The protein contains two amino-terminal phosphotyrosine-binding (PTB) domains, a Ca+/calmodulin-binding domain (CBD) and a catalytic Rab-GTPase-activating protein (GAP) domain. Adapted from: (Espelage, Al-Hasani, & Chadt, 2020)

In the GLUT4 translocation cascade, AKT and AMPK phosphorylate TBC1D4 (and also its close homologue TBC1D1) which leads to their inactivation. Since these RabGAPs under active conditions catalyze the hydrolysis of GTP-bound Rab proteins (and thereby inhibiting their function), the inactivation of RabGAPs leads to increased presence of active, GTP-bound Rab proteins which subsequently lead to the translocation of glucose transporter containing vesicles (GSV) form the cytosol towards the plasma membrane and promote exocytosis. Consequently, the increased amount of plasma-membrane located GLUT4 facilitates the glucose uptake form the blood stream into the cell (Figure. 2). In this process approx. 20-50% of cellular GLUT4 is translocated to the plasma membrane, while approx. 50-80% remains in the cytosolic compartment (Stockli, Fazakerley, & James, 2011; Wieringa et al., 2012).

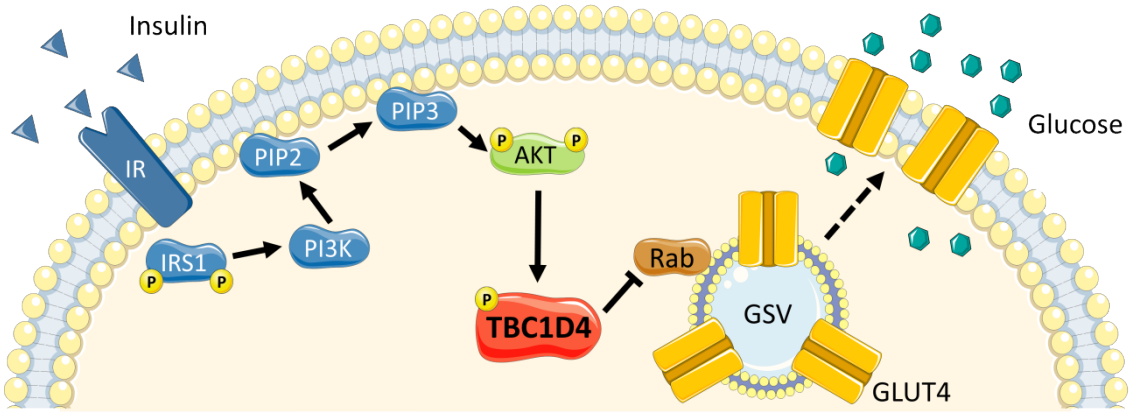

Figure 2: Model of insulin-induced cascade of GLUT4 translocation via TBC1D4. The binding of insulin to the membrane-coupled insulin receptor (IR) induces a cascade of phosphorylation events resulting in phosphorylation of protein kinase B (AKT), which subsequently leads to the phosphorylation of TBC1 domain family member 4 (TBC1D4). In this state the intrinsic GTPase-activating protein (GAP) activity of TBC1D4 is inhibited, leading to an increase in GTP-bound (and thereby activated) Rab GTPases. Consequently, this leads to enhanced translocation of glucose transporter type 4 (GLUT4) containing glucose transporter storage vesicles (GSV) to the plasma membrane and ultimately promotion of cellular glucose uptake.

Genetic ablation of *Tbc1d4* and its close homologue *Tbc1d1* have been described to be responsible for disorders in energy and substrate metabolism (Chadt et al., 2015; Chadt et al., 2008; Dash et al., 2009; Dokas et al., 2013; Stone et al., 2006; Szekeres et al., 2012). In this course it was shown in a mouse model that (whole body) *Tbc1d4*-deficieny in *Tbc1d4* evokes reduced abundance of GLUT4 protein in oxidative soleus skeletal muscle and white adipose tissue, whereas the abundance of GLUT4 protein in glycolytic skeletal muscles, such as the *extensor digitorum longus* (EDL) was not affected due to loss of *Tbc1d4* (Chadt et al., 2015; Hargett, Walker, & Keller, 2016; Lansey, Walker, Hargett, Stevens, & Keller, 2012; Wang et al., 2013; Xie et al., 2016). Additionally, *in vitro* studies revealed that knockdown of either *Tbc1d4* or *Tbc1d1*, as well as overexpression of non-functional mutant constructs of these RabGAPs impaired insulin-stimulated translocation processes of GLUT4 (Brewer, Romenskaia, Kanow, & Mastick, 2011; Eguez et al., 2005; Sun, Bilan, Liu, & Klip, 2010). However, despite of impairments

of insulin-stimulated glucose transport into skeletal muscles and adipocytes in *Tbc1d1*- or *Tbc1d4*-deficient mice, respectively, the impact of either RabGAP-deficiency on whole-body glycaemia was rather small. In vivo models of mice lacking either *Tbc1d1* (Dokas et al., 2013; Szekeres et al., 2012), *Tbc1d4* (Lansey et al., 2012; Wang et al., 2013) or the combination of both orthologues (Chadt et al., 2015) revealed tissue-specific disturbance of insulin-stimulated glucose uptake and rather mild impairments of glycemic control an, but on the other hand showed increased oxidation of lipids in skeletal muscle. Interestingly, the combined knockout of *Tbc1d1* and *Tbc1d4* led to higher intolerance towards glucose and insulin compared to the knockout of *Tbc1d1* or *Tbc1d4* alone. This observation suggests that in case of a single RabGAP-knockout, a compensatory mechanism on the level of the remaining functional RabGAP takes place (Chadt et al., 2015).

In human studies, a muscle-specific loss-of-function mutation of TBC1D4, which is exclusive to its long isoform, has been identified in a Greenlandic Inuit population as a major reason for T2DM prevalence (Moltke et al., 2014). However, up to now cardiovascular data regarding the impact in this population are inconclusive.

TBC1D4 has been shown to be the predominantly expressed RabGAP in oxidative muscle fibers and adipose tissue (Wang et al., 2013). However, its presence and its role on the cardiac metabolism, especially in post-ischemia/reperfusion (I/R) progress, remains to be elucidated. So far, only a few reported studies focused on the presence and action of TBC1D4 in context of the heart One study investigated an AS160-knockout rat model and reported decreased cardiac GLUT4 abundance due to the lack of AS160, but surprisingly increased glucose uptake during hyperinsulinemic-euglycemic clamps (Arias, Zheng, Agrawal, & Cartee, 2019). Others reported a tendency towards increased risk for cardiovascular diseases in carriers of a human TBC1D4 p.Arg684Ter mutation,

however this data is not conclusive at this point (JØRGENSEN et al., 2018). A mouse study using a knock-in mutation of AS160 (Thr649Ala) which inhibits its phosphorylation through Protein Kinase B (AKT), reported no changes in cardiac function or morphology following permanent occlusion of the left anterior descending coronary artery (LAD) (Quan, Xie, Wang, & Chen, 2015).

However, all of these studies laid their focus on the role of TBC1D4 as a mediator of insulin signaling or its role on cardiac function alone. The present study is the first one to investigate the impact of TBC1D4 on cardiac glucose metabolism and I/R-induced myocardial injury and post-infarction healing processes.

1.5 Aim of the study

Previous studies have revealed the vital role of metabolic flexibility of the heart in circumstances of differential energy demand and availability in order to ensure sufficient energy production. Especially under ischemic conditions of myocardial infarction or ischemia/reperfusion-induced injury, the ability to adapt to the hypoxic conditions adequately on a metabolic level might be crucial for the cardiac outcome, prognosis and survival rate after MI. Since in diabetes patients, this flexibility is already disturbed *per se* by impairments of glucose utilization as energy substrate*,* it is a major risk factor for development and also the progression of myocardial infarction. However, key factors and entry points for potential clinical or pharmacological intervention remain to be elucidated.

Since the RabGAP TBC1D4 has not only been shown to be a crucial regulator of metabolic flexibility in skeletal muscle tissue, but also is in terms of RabGAPs is highly present in the myocardium, it represents a potential key regulator “metabolic switch” of substrate flexibility in the heart. Moreover, impairments in TBC1D4 have been associated

with insulin resistance and diabetes, which are important factors for the incidence of CVDs as late-term effects.

Therefore, the aim of this study is to elucidate the role of the RabGAP TBC1D4 in the heart and under conditions of ischemia/reperfusion-induced myocardial injury.

2. Material & Methods

2.1 Material

2.1.1 Experimental animals

All data in the present study have been generated using mice with targeted whole-body deletion of *Tbc1d4* (D4KO) and corresponding wild type littermates. Animals were obtained from Texas A&M Institute for Genomic Medicine (Houston, TX) and backcrossed on a C57BL/6J strain background.

2.1.2 Chemicals

Table 1: Chemicals

Denomination	Supplier
[^{14}C]-palmitic acid	Hartmann Analytic, Brunswick, Germany
[^{3}H]-2-deoxyglucose	Hartmann Analytic, Brunswick, Germany
2-deoxyglucose	Sigma-Aldrich, Steinheim, Germany
3,3′-Diaminobenzidine tablets	Sigma-Aldrich, Steinheim, Germany
Acetic acid 100%	Merck KGaA, Darmstadt, Germany
Acetyl chloride ≥99.5 %	Sigma-Aldrich, Steinheim, Germany
Acetyl chloride ≥99.5 %	Sigma Aldrich, Steinheim, Germany
Acrylamide 30%	BioRad, Munich, Germany
Agarose	Biozym Scientific, Oldendorf, Germany
Albumin from bovine serum	Sigma-Aldrich, Steinheim, Germany
Ammonium persulfate (APS)	MP Biomedicals, Solon, USA
Aniline	Merck KGaA, Darmstadt, Germany
Aprotinin (from bovine lung)	Sigma-Aldrich, Steinheim, Germany
Azocarmine G	Merck KGaA, Darmstadt, Germany
Background reducing antibody diluent	Agilent/Dako, Waldbronn, Germany
Bromophenol blue	Merck, Darmstadt, Germany
BSA Fraction V	Sigma-Aldrich, Steinheim, Germany
Buprenorphine (Temgesic)	RB Pharmaceuticals, Heidelberg, Germany
Calcium chloride ($CaCl_2$)	Merck, Darmstadt, Germany
Chloroform	Applichem, Darmstadt, Germany
Complete proteinase inhibitor	Roche Diagnostics, Mannheim, Germany

Denomination	Supplier
D(+)-Glucose, ≥99.5 %	Sigma Aldrich, Steinheim, Germany
Desoxyribonucleotide triphosphate mix	Roche Diagnostics, Mannheim, Germany
Diprotin A	Bachem, Bubendorf, Switzerland
Dithiothreitol (DTT)	Sigma-Aldrich, Steinheim, Germany
D-mannitol	AppliChem, Darmstadt, Germany
Eosin G	Merck KGaA, Darmstadt, Germany
Ethanol (Abs., 96%, 90%, 70%)	VWR International GmbH, Radnor, USA
Ethanol absolute	Applichem, Darmstadt, Germany
Ethylene diamine tetraacetic acid (EDTA)	Serva, Heidelberg, Germany
Ethylene glycol tetraacetic acid (EGTA)	Serva, Heidelberg, Germany
Glycerol	Aros Organics, NJ, USA
Glycine	Applichem, Darmstadt, Germany
Hematoxylin	British BioCell, South Glamorgan, UK
Heparin	Medical equipment affiliates, North Grand , Tahlequah, OK , USA
Hydrochloric acid (HCl)	Carl Roth, Karlsruhe, Germany
Isopropanol	Applichem, Darmstadt, Germany
Ketamine (Ketaset 100 mg/ml)	Zoetis, Parsippany-Troy Hills Township, NJ, USA
Liquid scintillation universal cocktail	Carl Roth, Karlsruhe, Germany
Methanol	Carl Roth, Karlsruhe, Germany
n-hexane	Applichem, Darmstadt, Germany
n-hexane	AppliChem, Darmstadt, Germany
Orange G	Carl Roth GmbH & Co. KG, Karlsruhe, Germany
Pentadecanoic acid	Sigma-Aldrich, Steinheim, Germany
Pentadecanoic acid	Sigma Aldrich, Steinheim, Germany
Phosphotungstic acid (5%)	Sigma Aldrich, Fluka, St. Louis, USA
PhosSTOP Phosphatase inhibitor cocktail	Roche Diagnostics, Mannheim, Germany
Potassium chloride (KCl)	Merck, Darmstadt, Germany
Potassium hydroxide (KOH)	Merck, Darmstadt, Germany
Shandon™ EZ-Mount™	Thermo Fisher Scientific, Waltham, USA
Skim milk powder	Carl Roth, Karlsruhe, Germany
Sodium chloride (NaCl)	Carl Roth, Karlsruhe, Germany

Denomination	Supplier
Sodium dihydrogen phosphate (NaH_2PO_4)	Merck, Darmstadt, Germany
Sodium dodecyl sulfate (SDS)	Applichem, Darmstadt, Germany
Sodium hydroxide (NaOH) pellets	Applichem, Darmstadt, Germany
Streptavidin/HRP (Conjugate)	Dianova, Hamburg, Germany
Tetramethylethylenediamine (TEMED)	Carl Roth, Karlsruhe, Germany
Tris-HCl	Applichem, Darmstadt, Germany
Triton X-100	Roche Diagnostics, Mannheim, Germany
Tween-20	MP Biomedicals, Solon, USA
Xylazine (Rompun 2%)	Bayer Vital, Leverkusen, Germany
Xylene	VWR International GmbH, Radnor, USA

2.1.3 Antibodies

Table 2: Primary and secondary antibodies

Target protein	Host species, clonality	Supplier	Catalogue number
eIF2α	Rabbit, polyclonal	Cell Signaling, Danvers, MA, USA	#9722
GAPDH	Rabbit, monoclonal	Cell Signaling, Danvers, MA, USA	#2118
GLUT1	Rabbit, polyclonal	Generous gift from Prof. Annette Schürmann, DIfE, Potsdam, Germany	-
GLUT4	Rabbit, polyclonal	Custom-made Hadi Al-Hasani, DDZ, Düsseldorf, Germany	-
HRP-conjugated anti-rabbit IgG	Goat, polyclonal	Jackson ImmunoResearch, West Grove, PA, USA	#107615
PECAM-1/CD31	Rabbit, polyclonal	Abcam, Cambridge, UK	ab28364
Phospho-eIF2α (Ser51)	Rabbit, polyclonal	Cell Signaling, Danvers, MA, USA	#9721
Phospho-SAPK/JNK (Thr183/Tyr185)	Rabbit IgG, monoclonal	Cell Signaling, Danvers, MA, USA	#4668
SAPK/JNK	Rabbit, polyclonal	Cell Signaling, Danvers, MA, USA	#9252

Target protein	Host species, clonality	Supplier	Catalogue number
TBC1D1	Rabbit, polyclonal	Eurogentec, Cologne, Germany	*custom*
TBC1D4/AS160	Rabbit, polyclonal	Merck- Millipore, Darmstadt, Germany	#07-741
VCAM-1	Rabbit, monoclonal	Abcam, Cambridge, UK	ab134047
Biotin-conjugated anti rabbit IgG	Goat, polyclonal	Dianova, Hamburg, Germany	111-065-045

2.1.4 PCR and qRT-PCR primers

Table 3: Primer sequences for genotyping

Target	Sequence (5'→3')
Tbc1d4 forward	5'-AGTAGACTCAGAGTGGTCTTGG-3'
Tbc1d4-wt reverse	5'-GTCTTCCGACTCCAT ATTTGC-3'
Tbc1d4-knockout reverse	5'-GCAGCGCATCGCCTTCTATC-3'

The size of the PCR products revealed the respective alleles for *Tbc1d4*-genotype. The wild type allele (*Tbc1d4*-wt) leads to the generation of a 350 bp product, while the knockout-allele (T*bc1d4*-ko) reveals a 250 bp product. Heterozygous alleles show both products.

Table 4: Primer Sequences for qRT-PCR

Target	Name	Sequence (5'→3')	Product length
Atf4	Activating transcription factor 4	forward: 5'-GAGCTTCCTGAACAGCGAAGTG-3' reverse: 5'-TGGCCACCTCCAGATAGTCATC-3'	113 bp
Atf6	Activating transcription factor 6	forward: 5'-GAACTTCGAGGCTGGGTTCA-3' reverse: 5'-ACTCCCAGAATTCCTACTGATGC-3'	174 bp
Mmp2	Matrix metalloproteinase 2	forward: 5'-ACAAGTGGTCCGCGTAAAGT-3' reverse: 5'-GTAAACAAGGCTTCATGGGGG-3'	189 bp

Target	Name	Sequence (5'→3')	Product length
Mmp8	Matrix metalloproteinase 8	forward: 5'-ACCAGTGCTGGAGATATGACA-3' reverse: 5'-ACTCCTGGGAACATGCTTGG-3'	82 bp
Mmp9	Matrix metalloproteinase 9	forward: 5'-GCCGACTTTTGTGGTCTTCC-3' reverse: 5'-GGTACAAGTATGCCTCTGCCA-3'	80 bp
Mmp13	Matrix metalloproteinase 13	forward: 5'-GCCATTACCAGTCTCCGACG-3' reverse: 5'-GAGCCCAGAATTTTCTCCCTCT-3'	196 bp
Mmp14	Matrix metalloproteinase 14	forward: 5'-TCACTGCCCATGAATGACCC-3' reverse: 5'-CCGGGGCAATAAGTACTACCG-3'	123 bp
Tbc1d1	TBC1 Domain Family Member 1	forward: 5'-ACAGTGTGGGAAAAGATGCT-3' reverse: 5'-AGGTGGAACTGCTCAGCTAG-3'	143 bp
Tbc1d4	TBC1 Domain Family Member 4	forward: 5'-CCAACAGTCTTGCCTCAGAG-3' reverse: 5'-GAATGTGTGAGCCCGTCTTC-3'	146 bp
Tbp	TATA-binding protein	forward: 5'-GCGGCACTGCCCATTTATTT-3' reverse: 5'-GGCGGAATGTATCTGGCACA-3'	236 bp
Timp1	Tissue inhibitors of metalloproteinases 1	forward: 5'-AGCAGATACCATGATGGCCC-3' reverse: 5'-AGCCCTTATGACCAGGTCCG-3'	145 bp
Timp2	Tissue inhibitors of metalloproteinases 2	forward: 5'-GACTTCATTGTGCCCTGGGA-3' reverse: 5'-ATGGGACAGCGAGTGATCTTG-3'	101 bp
Timp3	Tissue inhibitors of metalloproteinases 3	forward: 5'-GAAGAAAAGAGCGGCAGTCC-3' reverse: 5'-CCGGATCACGATGTCGGAGT-3'	173 bp
Timp4	Tissue inhibitors of metalloproteinases 4	forward: 5'-TTCCCTCTGTGGTGTGAAGC-3' reverse: 5'-TGGTACATGGCATTGGCAGC-3'	193 bp
Xbp1 spliced	X-box binding protein 1 (spliced)	forward: 5'-GAGTCCGCAGCAGGTG-3' reverse: 5'-GTGTCAGAGTCCATGGGA-3'	65 bp
Xbp1 *un*spliced	X-box binding protein 1 (unspliced)	forward: 5'-TGAGAACCAGGAGTT AAGAACACGC-3' reverse: 5'-TTCTGGGTAGACCTCTGGGAGTTCC-3'	330 bp

2.1.5 Polymerases, molecular weight size markers and standards

Table 5: Polymerases and PCR standards

Denomination	Supplier
Dream Taq Green DNA	Fermentas GmbH, St. Leon-Rot, Germany
GeneRuler 100 bp DNA Ladder	Fermentas GmbH, St. Leon-Rot, Germany

Table 6: Molecular weight markers

Denomination	Supplier
Dual Color Precision Plus Protein Standard	Bio-Rad, Munich, Germany
Spectra multicolor High Range protein ladder	Thermo Scientific, Brunswick, Germany

2.1.6 Reaction kits

Table 7: Reaction Kits

Denomination	Application	Supplier
BCA Protein Assay Kit	Protein content determination	Pierce, Rockford, IL, USA
GoTaq® qPCR Master Mix	Polymerase-Chain-Reaction (PCR)	Promega, Madison WI, USA
Illumina HiSeq PE Cluster Kit v4 (cBot)	RNA Sequencing	Illumina, San Diego, CA, USA
Illumina HiSeq SBS Kit v4	RNA Sequencing	Illumina, San Diego, CA, USA
InViSorb™ Genomic DNA Kit II	Genomic DNA extraction	InViTek GmbH Berlin, Germany
LabAssay™ Glucose (Mutarose-GOD method)	Glucose measurement in final plasma	Wako, Neuss, Germany
RNeasy Mini Kit	RNA isolation	Qiagen, Hilden, Germany
Western Lightning ECL Pro and Ultra	Detection of chemiluminescent signals in Western blots	Perkin Elmer, Waltham, MA, USA

2.1.7 Buffers and solutions

Table 8: Buffers and solutions

Denomination	Ingredients
10x Dream Taq Green Buffer	Fermentas GmbH (St. Leon-Rot, Germany)
1x TAE-buffer	40 mM Tris-acetate, 1 mM EDTA, pH 8.0
Aniline solution	0.1% Aniline Blue in 90% EtOH)
Aniline-Orange solution	0.1% Aniline Blue, 2% Orange G in *aqua bidest.*, addition 8% glacial acetic acid before boiling and filtration. (Working dilution 1:2)
Anticoagulant for plasma collection	*For 50 ml stock:* 25 ml 0.5M EDTA, 92 mg aprotinin dissolved in 21 ml saline (0.15 M), 4 ml heparin (10,000 U/ml), 21.6 mg diprotin A
Azocarmin solution	0.1% Azocarmine G In 100 ml *aqua bidest*, filtration and addition of 1% glacial acetic acid before staining
Blocking Solution (Immunohistochemistry)	5% normal goat serum, 0.1% Cold Water Fish Skin Gelatin, 5% BSA, in 1x PBS
Blocking Solution (Western Blotting)	5% skim milk/1x TBS-T *or* 5% BSA/1x TBS-T
BSA standard (2 µg/µl)	Thermo Scientific (Perbio Science Germany, Bonn, Germany)
Citrate buffer	1.8 mM citric acid, 8.2 mM sodium citrate in *aqua dest.*, mixed prior to use
Eosin solution	0.1% Eosin G in 70% EtOH, 40 µl glacial acetic acid per 100 ml solution
Hematoxylin solution	British BioCell, South Glamorgan, United Kingdom
HOT medium (*ex vivo* glucose uptake)	19 mM mannitol, 1 mM 2-deoxyglucose, 2.5 µCi/ml [^{3}H]-2-deoxyglucose, 0.7 µCi/ml [^{14}C]-mannitol, with or without 120 nM insulin; solved in KHB
Incubation medium (*ex vivo* glucose uptake)	15 mM mannitol, 5 mM D-glucose, with or without120 nM insulin; solved in KHB
Krebs-Henseleit buffer (KHB)	118.5 mM NaCl, 4.7 mM KCl, 1.2 mM KH2PO4, 25 mM $NaHCO_3$, 4.7 mM KCl, 2.5 mM $CaCl_2 \cdot 2H_2O$, 1.2 mM MgSO4 $\cdot$ $7H_2O$, 5 mM HEPES, 1% BSA
Laemmli sample buffer + DTT	20% (v/v) glycerol, 8% (w/v) SDS, 10 mM EDTA, 250 mM Tris-HCl, 1% (w/v) bromophenol blue + 400 mM DTT

Denomination	Ingredients
Phosphate-buffered saline	137 mmol/L NaCl, 2.7 mmol/L KCl, 10 mmol/L Na_2HPO_4, 1.8 mmol/L KH_2PO_4
Protein lysis buffer	20 mM Tris-HCl, 150 mM NaCl, 1 mM EDTA, 1 mM EGTA, 1% Triton X-100, *Added before use:* Proteinase inhibitors: Complete Proteinase inhibitor cocktail, 40 µl per ml lysis buffer Phosphatase inhibitors: PhosSTOP phosphatase inhibitor, 100 µl per ml lysis buffer
Recovery medium (ex vivo glucose uptake)	15 mM mannitol, 5 mM D-glucose, solved in KHB
Rinse medium (*ex vivo* glucose uptake)	20 mM mannitol, with or without 120 nM insulin; solved in KHB
SDS-PAGE 1x Electrophoresis buffer	25 mM Tris, 192 mM Glycine, 0.1% (w/v) SDS
Separating gel buffer	1.5 M Tris, 0.4% SDS, pH 8.8
Stacking gel	520 µl stacking gel buffer, 260 µl acrylamide (30%), 1.22 ml ddH_2O, 2 mg APS, 2 µl TEMED
Stacking gel buffer	0.5 M Tris, 0.4% SDS, pH 6.8
TBS-T (1x)	10 mM Tris, 0.15 M NaCl, pH 8.0, 0.05% TWEEN-20
Western blot transfer buffer	25 mM Tris, 192 mM Glycine, 20% Methanol

2.1.8 Devices and instruments

Table 9: Devices and instruments

Denomination	Manufacturer
Chemidoc™ XRS+ System	BioRad Laboratories, Munich, Germany
Electrocardiography setup	Hugo Sachs Harvard Apparatus, March, Germany
FS-FFAP-CB-0.25 chromatography column	CS-Chromatographie Service GmbH, Langerwehe, Germany
Gas chromatography system 6890N	Agilent Technologies, Ratingen, Germany
Glucometer and glucose test stripes	Bayer Vital GmbH, Leverkusen, Germany
iMark™ Microplate Reader	BioRad Laboratories, Munich, Germany
Intubation aid and heating system	Uno Roestvasstaal, Zevenaar, Netherlands
Isoflurane anesthesia setup	Hugo Sachs Harvard Apparatus, March, Germany

Denomination	Manufacturer
Light microscope	Leica Microsystems, Wetzlar, Germany
Nanodrop 2000	Thermo Scientific, Peqlab, Wilmington, MA, USA
NMR Whole Body Composition Analyzer	Echo MRI™, Houston, Texas, USA
Olympus DP73 Camera	Olympus Deutschland GmbH, Hamburg, Germany
Perma-hand silk 4/0 suture	Ethicon, Somerville, NJ, USA
Prolene 7/0 suture	Ethicon, Somerville, NJ, USA
Retraction Kit and surgery tools	Fine Science Tools, Heidelberg, Germany
Rotation microtome HM 360	Mikron, Biel, Switzerland
Thermomixer Compact	Eppendorf, Wesseling-Berzorf, Germany
TissueLyser II	Qiagen, Hilden, Germany
Uniprep Gyrator	UniEquip, Munich, Germany
Vevo 3100 ultrasound scanner	VisualSonics, Toronto, Canada

2.1.9 Software

Table 10: Software

Denomination	Manufacturer
ConsensusPath Database	MPI for Molecular Genetics, Berlin, Germany (Kamburov, Wierling, Lehrach, & Herwig, 2009)
ECG analysis software	Hugo Sachs Harvard Apparatus,
Graph Pad Prism 7	GraphPad Software, San Diego, CA, USA
ImageLab 6	BioRad Laboratories, Hercules, CA, USA
Ingenuity pathway analysis (IPA)	Qiagen, Hilden, Germany
Microplate Manager 6	BioRad Laboratories, Hercules, CA, USA
Nanodrop 2000/2000c software	Thermo Scientific, Peqlab, Wilmington, MA, USA
Office 2016	Microsoft, Redmond, WA, USA
Software cellSens Dimension 1.16	Olympus GmbH, Hamburg, Germany
STAR software for RNASeq alignment	Alexander Dobin (Dobin et al., 2013)
StepOne v2.3	Applied Biosystems, Foster City, CA, USA

2.1.10 Mouse diets

Table 11: Mouse diets

Standard diet **(Ssniff, Soest, Germany; *Cat.-no. V1126 M-Z Extrudat)***		**Mass (%)**	**Calories (%)**
Protein		22.1	36
Carbohydrate		53.3	53
Fat		4.5	11
Total calorie content (kcal/g)	3.3		
High-fat diet **(Research Diets, New Brunswick, NJ, USA; *Cat.-No. D12492)***		**Mass (%)**	**Calories (%)**
Protein		26.2	20
Carbohydrate		26.3	20
Fat		34.9	60
Total calorie content (kcal/g)	**5.2**		

2.2 Methods

2.2.1 General Animal Housing and pre-treatment of animals

All experiments were approved by the Ethics Committee of the State Ministry of Agriculture, Nutrition and Forestry (North Rhine-Westphalia, Germany; reference number 84-02.04.2014.A392) and mice were kept in accordance with National Institutes of Health guidelines for the care and use of laboratory animals. Three to six wild type (WT) and *Tbc1d4*-knockout (D4KO) mice were housed per cage per cage (makrolon type-III) with dustless wooden splint as bedding, red-transparent houses and nesting material as enrichment, under constant temperature conditions of 22 °C and humidity, and a 12 h light-dark cycle (lights on at 6 a.m.). Ear notching was used for mouse identification and tail tip biopsies were collected for genotyping. After weaning at 19-21 days of age, mice had *ad libitum* access to tap water and standard chow diet (ssniff, Soest, Germany) or 60% high-fat diet (HFD) (Research Diets, New Brunswick, NJ, USA), respectively.

2.2.2 Genotyping

For determination of the animals' genotype to wild type (WT), *Tbc1d4*-heterozygous (*Tbc1d4*$^{+/-}$) or *Tbc1d4*-knockout (*Tbc1d4*$^{-/-}$), genomic DNA was isolated from tail tip biopsies and subsequently analyzed via polymerase chain reaction (PCR) and agarose gel electrophoresis.

2.2.2.1 Genomic DNA extraction and determination of DNA concentration

A small tail biopsy was collected from mice and gDNA was extracted using InViSorb Genomic DNA Kit II (InViTek GmbH Berlin, Germany) according to the manufacturer's instructions. Briefly, the tail biopsies were lysed in 200 µl lysis buffer containing 10 µl of Proteinase K o/n at 60 °C and shaking at 1200 rpm. After centrifugation for 1 min at 15,800 x g, supernatant was collected and added to 450 µl mixed "Binding buffer", in order to bind extracted DNA to specific beads. Samples were incubated for 5 min at RT, centrifuged for 1 sec at 15.800 x *g* and supernatant was discarded. Subsequently, the pellet was washed using 650 µl washing buffer, before resuspending in the Uniprep Gyrator (UniEquip, Munich, Germany). The samples were briefly centrifuged at 15,800 x *g* and supernatant was again discarded. The washing step was repeated two more times before the pellet was dried for approx. 10 min at 60 °C in order to evaporate the remaining EtOH of the "Washing buffer" and subsequently for 3 min at RT. This step was followed by the addition of 200 µl pre-warmed (60 °C) "Elution buffer" and incubation for 3 min at 60 °C in order to release the bound DNA from the beads. In the last step, after centrifugation for 2 min at 18,000 x *g*, supernatant was collected.

In the following step, DNA concentration was determined photometrically with the NanoDrop 2000 (Thermo Scientific, Peqlab Wilmington, MA, USA) at a wavelength of 260 nm.

2.2.2.2 Polymerase chain reaction (PCR)

For genotyping purposes, genomic DNA from mouse-tail biopsies served as template for the PCR according to the following program (Table 12).

Table 12: Reaction mix setup and program of *Tbc1d4* genotyping PCR

PCR	**Volume (concentration)**	**PCR program**		
5x GreenGoTaq-Buffer	4 µl	**Initialization**	95 °C 2 min	
dNTPs	2 µl (8 mM)	**Denaturation**	95 °C 30 sec	Repeat (30x)
Tbc1d4 forward	2 µl (10 nM)	**Annealing**	60 °C 30 sec	
Tbc1d4-wt reverse	1 µl (10 nM)	**Elongation**	72 °C 1 min	
Tbc1d4-knockout reverse	1 µl (10 nM)			
Aqua bidest.	5.8 µl			
GoTaqPolymerase	0.2 µl (2 U/µl)			
Template DNA (genomic DNA, 10ng/µl)	4 µl			
Total	**20 µl**			

2.2.2.3 Agarose gel electrophoresis

For separation of PCR products, 1% agarose (Biozym Scientific GmbH, Oldendorf, Germany) was added to 1 x TAE buffer and boiled until the agarose was completely solubilized. After cooling down to ~60 °C, 0.1 µg/ml ethidium bromide (MP Biomedicals, Heidelberg, Germany) was added to the solution. Subsequently, 20 µl of PCR product was loaded into each pocket and electrophoresis was performed at constant 90 V in an electrophoretic chamber with 1xTAE buffer. In order to determine the correct size of the

visual band of amplified PCR product, a 100 bp ladder was used as standard and verification of size. Visualization occurred with UV light (254 nm) with the ChemiDoc XRS+ system and subsequent documentation of the image using Image Lab software.

2.2.3 Ischemia/Reperfusion surgery procedure and electrocardiographic monitoring

Mice were subjected to cardiac ischemia/reperfusion surgery (Figure 3) in a closed chest and open chest model, respectively, as described below:

Open chest model: Mice were anesthetized via an intraperitoneal injection with Ketamine (100 mg/kg body weight) and Xylazine (10 mg/kg body weight), intubated and fixated on a pre-heated (37.5 °C) surface. Constant respiration was applied with O_2-enriched (40% O_2) air and 2% Isoflurane. Mice were constantly monitored via electrocardiography during the operation and maintained body temperature during the whole procedure at 37-38 °C. Subsequently, the thorax was opened via lateral thoracotomy and cardiac ischemia was triggered by ligation of the left anterior descending (LAD) coronary artery. A ligature was placed around the LAD with a suture and reversibly occluded using a piece of polyethylene tubing. Occlusion was ensured via visible paling of the proximal cardiac tissue and elevation of ST segment of ECG (Figure 4). Ischemia was maintained for 45 minutes. After this time, the ligation was removed and the thorax was closed with sutures. Isoflurane application was terminated and mice were respired for some more minutes and subsequently extubated. During the following 5 days mice were treated with Buprenorphine (0.05 mg/kg body weight) every 6 hours.

Closed chest model: The LAD was surrounded with a suture and a piece of polyethylene tube, but not occluded. The ends of the suture were removed from the thorax and placed under the skin with a knot. Thorax and skin were closed. Isoflurane application

was terminated and mouse rested for 3 days with close observation. For post-operative treatment, mice were subcutaneously injected with Buprenorphine (0.05 mg/kg body weight) every 6 hours. Three days after the ligature, mice were anesthetized with oxygen enriched air (40% O_2) and 2% Isoflurane. Under constant ECG and temperature monitoring, skin was incised and ischemia was induced by closing of the ligature by pulling at the end of the sutures. After 60 minutes of ischemia, sutures were cut and skin closed. Isoflurane was removed and mice were respired for some more minutes and subsequently extubated. During the following 5 days mice were treated with Buprenorphine (0.05 mg/kg body weight) every 6 hours.

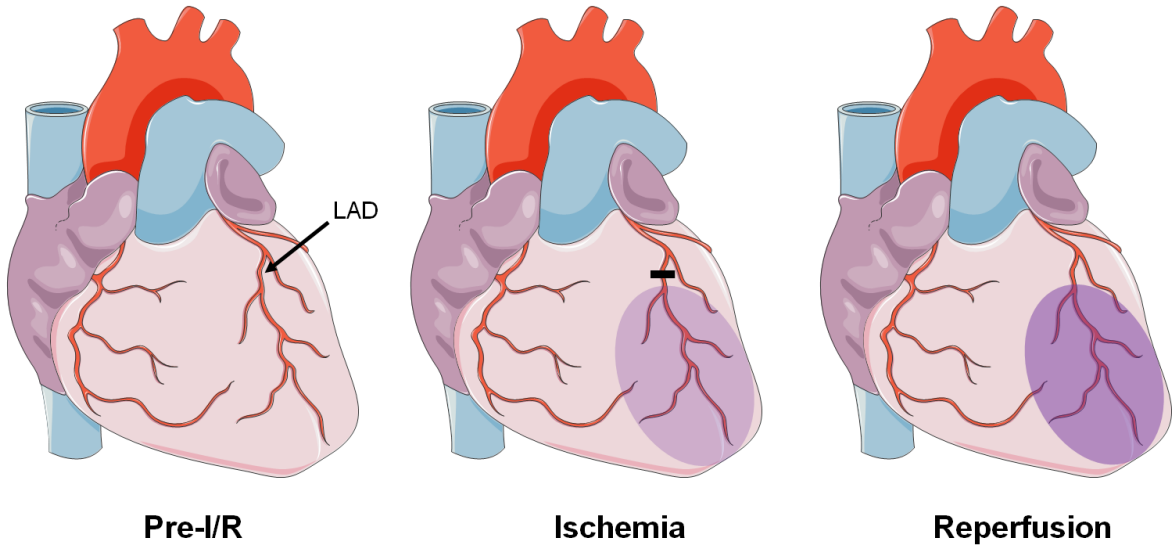

Figure 3: Schematic overview of ischemia/reperfusion surgery procedure. After identification and location of the left anterior descending coronary artery (LAD) in the pre-I/R state, a ligature is placed around the LAD (black bar) in order to trigger ischemia to the following tissue. Subsequently, the ligature is removed and reperfusion is restored.

During the complete surgical interventions, the mice were constantly monitored via electrocardiogram (ECG) in order to monitor electric activity in the heart. Moreover, ECG was used to verify the correct placement of the ligature and occlusion of the LAD by visible

elevation of the ST-Segment during ischemia and subsequent normalization during reperfusion. For this, ECG was recorded via a suitable setup (Hugo Sachs Harvard Apparatus, March, Germany) before and during ischemia, as well as in the acute reperfusion phase.

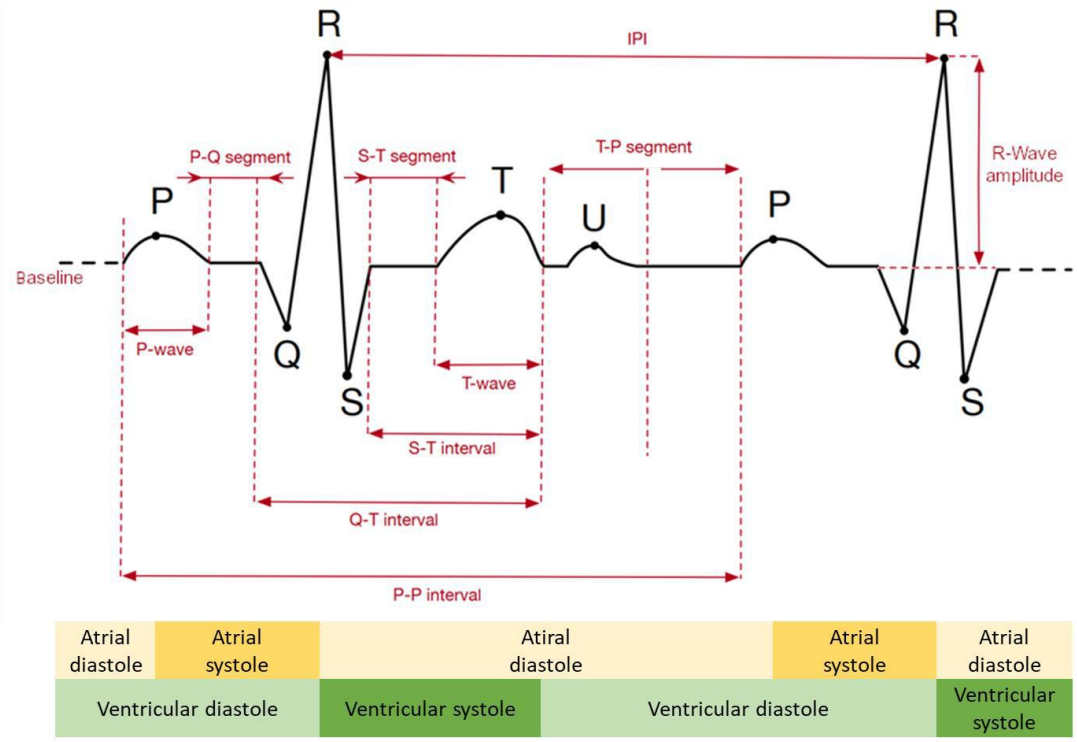

Figure 4: Typical pattern of an electrocardiogram (ECG). The main wave peaks (P, Q, R, S, T, and U) are displayed, as well as corresponding segments and intervals. R-wave amplitude is indicated as the distance between R-wave peak and the baseline. At the bottom, the corresponding course of systole and diastole for atria and ventricles is shown. IPI = Inter-Pulse-Interval. Adapted from: (Ortiz-Martin, Picazo-Sanchez, Peris-Lopez, & Tapiador, 2018)

2.2.3.1 Cardiac ultrasound imaging and echocardiography

Echocardiography was performed using a Vevo 3100 high-resolution ultrasound scanner with 18 to 38 MHz linear transducer (VisualSonics Inc., Toronto, Canada). and performed as previously described (Gorressen et al., 2015), before MI and at time points of 24h, 1 week and 3 weeks after reperfusion, respectively. Parameters of LV end-systolic and end-diastolic volumes were measured.

1.2.4 *Ex vivo* [^{3}H]-deoxyglucose uptake assay of left ventricular papillary muscle

This work was performed in collaboration with David Barbosa. [^{3}H]-2-deoxyglucose uptake in intact isolated left ventricular papillary muscle was essentially performed as previously described for skeletal muscle incubations (Chadt et al., 2008) with some modifications. Briefly, mice were injected with 100 U heparin, subsequently euthanized via cervical dislocation and cardiac left ventricular papillary muscles were dissected in pre-oxygenated (95% O_2 / 5% CO_2) Krebs-Henseleit buffer (KHB) supplemented with 5 mmol/L glucose and 15 mmol/L mannitol. For recovery samples were incubated for 30 min at 30 °C in KHB buffer supplemented with 5 mmol/L glucose and 15 mmol/L mannitol (recovery medium, see section 2.1.7) under constant gas supply (95% O_2 / 5% CO_2) under gentle agitation in a water bath. After recovery, muscles were transferred to new vials for pre-incubation. For this, samples were placed for 10 min in KHB supplemented with 15 mmol/L mannitol and 5 mmol/L glucose under basal conditions or with 120 nmol/L insulin respectively under constant gas supply (incubation medium, see section 2.1.7). In order to remove glucose, muscles were rinsed for 10 min in rinse buffer (see table 8) for 10 min. Afterwards, muscles were transferred into the “hot” incubation medium, containing the same ingredients as before with the presence of 1 mmol/L [^{3}H]-2-deoxyglucose and 19 mol/L [^{14}C]mannitol for 20 min (HOT medium, see section 2.1.7). After incubation, muscles were immediately frozen in liquid nitrogen and stored at -80 °C. Incorporated radioactivity was assessed in cleared protein lysates of LV papillary muscles by scintillation counting of [^{3}H]. [^{14}C] counts from mannitol were determined for extracellular space correction.

1.2.5 *In vivo* [^{18}F]-fluorodeoxy-D-glucose uptake assay via positron emission tomography (PET) scan

This work was performed in collaboration with Dr. Heiko Backes, Anna Lena Cremer and Prof. Jens C. Brüning, Max Planck Institute for Metabolism Research, Cologne. Mice anesthetized with ~2% isoflurane in a 70% N_2O / 30% O_2 gas mixture and the radiotracer was injected via a catheter in the tail vein. At the start of the 45 minutes PET data acquisition the animals received an injection of 10 µCi/g(BW) [^{18}F]-fluorodeoxy-D-glucose (FDG) mixed with 1 mg/g[BW] glucose via the tail vein and glucose uptake over time into different tissues/organs was monitored via a preclinical PET/CT scanner (Inveon, Siemens) followed by a CT scan (180 projections/360°, 200 ms, 80 kV, 500 µA) for attenuation correction. PET data were subsequently histogrammed, corrected for attenuation and decay and reconstructed. Image analysis was performed using VINCI software (VINCI 4.90, MPI for Metabolism Research). Total activity in the heart was normalized to whole body activity.

2.2.6 General tissue collection

Animals were euthanized via cervical dislocation. For biochemical analyses, tissues were dissected, immediately frozen in liquid nitrogen and subsequently stored at -80 °C until further processing. For histological analyses, tissues were dissected, transferred to 4% Paraformaldehyde/1xPBS for 24h and subsequently embedded in paraffin via incubation in Ethanol solutions of increasing concentration (50%, 70%, 96%, EtOH abs.) for denaturation, followed by incubation in xylene and paraffin.

2.2.7 Histological processing and chemical tissue staining

Paraffin-embedded tissues were cut to sections of 5 µm using a rotation microtome HM 360 (Mikron, Biel, Switzerland), stretched in a water bath at 45 °C and subsequently transferred to glass slides. Twenty sections per level were collected and subsequently, 250 µm of tissue were discarded to reach the next level until the end of the prepared block was reached. Before staining, sections were dried o/n at RT. Samples were subsequently stained using Hematoxylin-Eosin (HE)-staining, Azan staining or immunohistochemical staining.

2.2.7.1 Hematoxylin-Eosin (HE)-staining

For HE-staining, sliced samples were rehydrated and de-paraffinized in Xylene and decreasing EtOH solutions (2x xylene, 2x EtOH abs., 2x 96% EtOH, 2x 70% EtOH, 5 min each). Subsequently, the samples were placed for 2 min in Hematoxylin solution, rinsed with *aqua bidest*. and incubated for 10 min under running tap water. Subsequently, sections were incubated for 2 min in 70% EtOH and transferred into the Eosin solution for 30 sec before a brief rinsing in 96% EtOH and subsequent dehydration (96% EtOH, 2x 100% EtOH abs.2x Xylene for 5 min each) and mounting of the slides. Afterwards, slides were imaged via light microscopy and analyzed.

2.2.7.2 Azan staining

For Azan staining, samples were de-paraffinized and re-hydrated (2x xylene, 2x EtOH abs., 2x 96% EtOH, 2x 70% EtOH, 5 min each). Subsequently, samples were rinsed briefly with *aqua bidest.* (5 min) and incubated for 10 minutes in 56-60 °C warm Azocarmine-solution (see section 2.1.7). After rinsing with *aqua bidest. for* 5 min, samples were differentiated in pre-warmed (56 °C) Aniline solution (see section 2.1.7) for another

10 minutes. This was followed by incubation of samples in 1% acetic acid/96% EtOH solution for 1 min and 5% phosphotungstic acid for 1h at RT. After brief rinsing in *aqua bidest*., samples were incubated for 1h in Aniline-Orange-solution (see section 2.1.7) for 1h at RT. Subsequently, samples were briefly rinsed in *aqua bidest*., differentiated in 96% EtOH. Afterwards, samples were dehydrated (2x EtOH abs., 2x Xylene, 5 min each) and mounted for microscopy. Slides were imaged via light microscopy and heart structure was analyzed was analyzed via morphometry. Infarction size of hearts was determined via threshold analysis software of blue stained fibrotic tissue.

2.2.7.3 Immunohistochemical staining

For immunohistochemical staining, samples were de-paraffinized and re-hydrated (2x xylene, 2x EtOH abs., 2x 96% EtOH, 2x 70% EtOH, 5 min each). After brief rinsing in PBS, samples were incubated for 3 min in 3% H_2O_2 / PBS for 3 min, followed by 5 min incubation in PBS at RT. For retrieval of antigens, samples were boiled for 20 min in citrate buffer (see section 2.1.7) via a pressure cooker. As soon as the samples cooled down to RT, they were incubated in 0.05 M glycine / PBS solution for 15 min at RT in order to block aldehydes, followed by 5 min washing in PBS. In order to block unspecific binding sides, samples were incubated with blocking solution (see section 2.1.7) for 30 min at RT and subsequently washed for 5 min in PBS.

Subsequently, sections were incubated with primary antibodies against PECAM-1 (dilution: 1:50) and VCAM-1 (dilution: 1:500) over night at 4 °C. Antibodies were diluted in background reducing diluent (see section 2.1.2). On the next day, samples were washed in PBS for 5 min at RT and subsequently incubated with biotin-conjugated secondary antibody against the respective primary antibody. For this, the secondary antibody was diluted in background reducing diluent (1:200) and added to the sections

for 30 min at RT. After a brief washing step for 5 min in PBS, streptavidin with conjugated horseradish peroxidase (HRP) was added to the sections (dilution 1:200 in background reducing diluent) for 30 min at RT. The streptavidin binds to the biotin-tag on the secondary antibodies in order to introduce the HRP to the sites of antibody binding. Samples were washed for 5 min in PBS and subsequently stained using 3,3'-diaminobenzidine (DAB) and accompanied urea hydrogen peroxide for approx. 10 min at RT until proper staining intensity was reached. The HRP catalyzed for a chemical reaction of DAB with hydrogen peroxide that results in the formation of a brown precipitate at the respective site. Samples were washed for 5 min in PBS and 2x 5 min in *aqua bidest*. Subsequently, samples were counter-stained in hematoxylin solution for 2 min at RT and differentiated for 10 min in tap water. Afterwards, slides were mounted, imaged via light microscopy and analyzed.

2.2.8 Transmission electron microscopy (TEM)

Heart muscle tissues were fixed for 2h at room temperature by immersion in 2.5% glutaraldehyde in 0.19 M sodium cacodylate buffer at pH 7.4, postfixed in 1% reduced osmium tetroxide in *aqua bidest.* for 60 min, and subsequently stained with 2% uranyl acetate in maleate buffer, pH 4.7. The specimens were dehydrated in graded ethanol-series and embedded in epoxy resin (Spurr, 1969). Ultrathin sections were picked up onto Formvarcarbon-coated grids, stained with lead citrate, and viewed in a transmission electron microscope (TEM 910; Zeiss Elektronenmikroskopie, Oberkochen, Germany).

Morphometric evaluation of extracellular matrix area (ECM) was done using comparable ROI (regions of interest) of heart muscle sections excluding cellular components inside the ECM area. For evaluation, threshold analysis was used. Mitochondrial density was quantified manually using CellSense software.

2.2.9 Biochemical methodology – Gene expression analysis

2.2.9.1 RNA extraction from heart tissue using the trizol/chloroform method

Frozen heart tissue was homogenized in liquid nitrogen. Subsequently, 30 mg of the homogenate was added to 500 µl Trizol reagent in a reaction tube. After addition of a steel bead, the tissue was lysed in a TissueLyser (QIAGEN Hilden, Germany) for 5 min at 25 Hz. After lysis, the samples were incubated at RT for 5 min and subsequently centrifuged at 12,000 x *g* and 4 °C for 10 min. After this step, the processing of the samples was depending on the experimental setup applied.

For qPCR experiments, RNA extraction occurred as follows: The supernatant was recovered into a fresh vial and 100 µl Chloroform were added with subsequent inverting for 15 sec, incubation for 3 min and centrifugation at 12,000 x *g* and 4 °C for 15 min. The upper aqueous phase was transferred into a new vial and 250 µl Isopropanol was added. After brief inverting, samples were incubated for 10 min at RT and centrifuged at 12,000 x *g* and 4 °C for 10 min. The supernatant was discarded and the remaining pellet was washed using 500 µl of 75 % Ethanol and subsequently vortexed, followed by another centrifugation step at 7,500 x *g* and 4 °C for 5 min. The supernatant was discarded and washing steps were repeated two additional times. Afterwards, the pellet was dried for 30 min at RT and subsequently re-suspended in 30 µl RNAse-free water followed by incubation for 10 min at 300 rpm and 60 °C in a thermomixer compact (Eppendorf, Wesseling-Berzorf, Germany). After incubation for further 2 min at RT, brief vortexing and centrifugation at 10,000 x *g* for 10 sec, RNA concentration was determined via NanoDrop 2000 device (Thermo Scientific, Peqlab Wilmington, MA, USA) at a wavelength of 260 nm and subsequently introduced to cDNA synthesis.

For RNA-Sequencing analysis, RNA extraction was conducted using the RNeasy Mini Kit (Qiagen, Hilden, Germany) as follows: The supernatant was recovered and

transferred to QiaShredder-columns and centrifuged for 2 min at 14,000 x *g*. The passage was transferred to MaXtract tubes and added to 140 µl of Chloroform before inverting and incubation for 3 min at RT. Samples were subsequently centrifuged at 12,000 x g and 4 °C for 15 min. The upper aqueous phase was recovered into a new vial and Ethanol absolute (1.5 times of its volume) was added. Samples were transferred to miRNeasy-colums, washed 3 times with Ethanol absolute and subsequently eluted in RNAse-free water. Samples were stored at -80 °C until further processing.

2.2.9.2 Complementary DNA (cDNA) synthesis

For cDNA synthesis, 2 µg of isolated RNA (solved in 10 µl of H_2O) were used for a reverse transcriptase PCR (RT-PCR). For this, isolated RNA was added to 2 µl hexanucleotide primers (0.1 µg/µl) and 1 µl dNTPs (0.25 mM), and pre-incubated for 5 min at 65 °C in a thermocycler to remove possible RNA secondary structures (Table 13). After 1 min incubation on ice and brief centrifugation at 10,000 x *g*, 4 µl GoScript 5x reaction buffer, 1 µl GoScript Reverse Transcriptase (Promega, Fitchburg, WI, USA) as well as 2 µl of $MgCl_2$ were added to the sample introduced to cDNA synthesis (Table 13). The RT-PCR was performed under the conditions described in Table 14. Produced cDNA samples were stored at -20 °C until further processing.

Table 13: Reaction mix setup for RT-PCR

Step 1 – Pre-incubation **Ingredient**		 **Volume**
RNA (2 µg)		10 µl
dNTPs (0.25 mM)		1 µl
Hexanucleotidprimer (0.1 µg/µl)		2 µl
Total Volume		**13 µl**
Step 2 - cDNA synthesis **Ingredient**		 Volume
Product of pre-incubation step		13 µl
GoScript 5x reaction buffer		4 µl
Accompanied $MgCl_2$		2 µl
GoScript Reverse Transcriptase		1 µl
Total volume		**20 µl**

Table 14: Program setup for RT-PCR

Step 1 – Pre-incubation **Step**		 **Temperature**	 **Time**
Pre-incubation		65 °C	5 min
Storage		4 °C	∞
Step 2 – cDNA synthesis **Step**		 Temperature	 Time
Annealing		25 °C	5 min
Synthesis		42 °C	60 min
Reverse transcriptase inactivation		70 °C	15 min
Storage		4 °C	∞

The cDNA was diluted 1:40 in nuclease-free water and transferred to qRT-PCR analysis.

2.2.9.3 Quantitative Real-time PCR (qRT-PCR)

For qRT-PCR, 4 µl of diluted cDNA was mixed with 5 µl 2x GoTaq qPCR Master Mix (Thermo Fisher Scientific, Waltham, MA, USA) containing CXR Reference Dye (20 µl CXR per 1 mL 2x GoTaq qPCR Master Mix) for internal control and 0.5 µl of each respective forward and reverse primer (see table 15). General qRT-PCR program is shown in Table 16. Samples were analyzed using the $\Delta\Delta C_t$ method (Livak & Schmittgen, 2001). For normalization, respective gene expression values of *TATA-Box Binding Protein* (*Tbp*) were used.

Table 15: Reaction mix for qRT-PCR

Ingredient	Volume
2x GoTaq qPCR Master Mix	5 µl
forward primer	0.5 µl
reverse primer	0.5 µl
cDNA (1:40 dilution)	4 µl
Total	**10 µl**

Table 16: Program setup for qRT-PCR

Step	Temperature	Time	Cycles
Hot Start	95 °C	2 min	1x
Denaturation	95 °C	15 sec	40x
Primer annealing and extension	60 °C	1 min	
Dissociation (Melting)	60-95 °C	-	1x

2.2.10 Biochemical methodology – Western Blot analysis

2.2.10.1 Protein isolation from frozen tissue samples

15 mg frozen heart tissue was added to 400 µl of ice-cold lysis buffer (Table 8). The samples were homogenized (TissueLyser II, Qiagen, Hilden, Germany) at 17,000 x *g* for 5 min, incubated on ice for 1 min and centrifuged at 17,000 x *g* and 4 °C. The

supernatant was recovered and protein content was determined via BCA Protein Assay Kit (Pierce, Rockford, IL, USA).

2.2.10.2 Protein content determination

Protein concentrations of tissue lysates were measured via BCA Protein Assay Kit (Pierce, Rockford, IL, USA) according the manufacturer`s prescription. Prior to the measurement, samples were diluted 1:20 with ddH_2O and a calibration curve was set up using BSA standard concentrations in a range of 0.02-2.00 µg/µl. The measurement was carried out photometrically with an iMark plate reader (BioRad, Munich, Germany) at a wavelength of 560 nm. Based on these results, suitable dilutions of the samples were prepared for Western blot analysis.

2.2.10.3 Sodium dodecyl sulfate polyacrylamide gel electrophoresis (SDS-PAGE)

After protein content determination, protein lysates of murine hearts were mixed with 4x Laemmli sample buffer, containing SDS and dithiothreitol (DTT) and subsequently boiled for 5 min at 95 °C in order to denature the proteins. Samples were chilled on ice for 1 min and briefly centrifuged before loading on the SDS polyacrylamide gel. Respective gel compositions are shown in table 17. The gel was allowed to run at a constant voltage of 70 V until the samples reached the border of the separating gel. From this point, a voltage of 150 V was applied until the desired resolution was reached. For control of the running conditions and later identification of protein band sizes, a pre-stained marker was loaded along with the samples into an individual well. The choice of the marker was depending on the expected size of the protein of interest.

Table 17: Compositions of separating gel for SDS-PAGE

Acrylamide concentration	Ingredients
10%	1.56 ml separating gel buffer, 2 ml acrylamide (30%), 2.44 ml ddH_2O, 6 mg APS, 6 µl TEMED
12%	1.56 ml separating gel buffer, 2.4 ml acrylamide (30%), 2.04 ddH_2O, 6 mg APS, 6 µl TEMED
14%	1.56 ml separating gel buffer, 2.8 ml acrylamide (30%), 1.64 ml ddH_2O, 6 mg APS, 6 µl TEMED

2.2.10.4 Tank Western Blot technique

Proteins were blotted from the SDS polyacrylamide gels onto nitrocellulose membranes (Oehmen, Essen, Germany) polyvinylidenfluorid (PVDF) membranes via tank blot technology using horizontal electrophoresis. In detail, the gel and membrane, surrounded by Whatman paper and sponges, were placed in a tank filled with cold transfer buffer (Table 8) and kept refrigerated with a water-cooling system. The time of blotting was chosen according to the molecular weight of the protein of interest (2 h up to o/n blotting) at a constant current of 200 mA. After blotting, membranes were removed from the cassettes, briefly washed in TBS-T and subsequently incubated in 5% skim milk/TBS-T in order to block unspecific antibody binding sites.

2.2.10.5 Antibody staining and signal detection

Normalization occurred by using glyceraldehyde 3-phosphate dehydrogenase (GAPDH) as housekeeping protein.

Respective proteins on the membranes were stained with epitope-specific primary antibodies and species-specific IgG horseradish peroxidase (HRP)-linked secondary antibodies. The antibodies were diluted in 5% skim milk/TBS-T or 5% BSA/TBS-T,

respectively (Table 18); Diluent, antibody concentration and incubation parameters of time and temperature were selected depending on the targeted protein, based on prior investigations in the lab (Table 18).

Table 18: Antibody dilutions and incubation parameters

Target protein	Dilution	Diluent	Incubation time/ temperature
eIF2α	1 : 2,500	5% BSA/1x TBS-T	o/n, 4 °C
GAPDH	1 : 5,000	5% skim milk/1x TBS-T	1.5 h, RT *or* o/n, 4 °C
GLUT1	1 : 1,000	5% skim milk/1x TBS-T	1.5 h, RT
GLUT4	1 : 1,000	5% skim milk/1x TBS-T	1.5 h, RT
HRP-conjugated anti-rabbit IgG	1 : 20,000	Same diluent as 1st AB	1 h, RT
Phospho-eIF2α (Ser51)	1 : 1,000	5% skim milk/1x TBS-T	o/n, 4 °C
Phospho-SAPK/JNK (Thr183/Tyr185)	1 : 1,000	5% skim milk/1x TBS-T	o/n, 4 °C
SAPK/JNK	1 : 1,000	5% skim milk/1x TBS-T	o/n, 4 °C
TBC1D1	1 : 1,000	5% BSA/1x TBS-T	o/n, 4 °C
TBC1D4/ AS160	1 : 1,000	5% skim milk/1x TBS-T	o/n, 4 °C

Detection was performed with enhanced chemiluminescence (ECL) via ECL Pro or Ultra (PerkinElmer, Waltham, MA, USA) respectively, according to the manufacturer's instructions. The HRP-catalyzed reaction of the reagents leads to the emission of chemiluminescent light, which was detected by a light-sensitive camera in the ChemiDoc System (BioRad, Munich, Germany). Subsequent quantification of band intensity was done with Image Lab Software (BioRad, Munich, Germany).

2.2.11 Gas chromatography (GC) analysis of cardiac fatty acid composition

Determination of cardiac fatty acid composition was assessed using gas chromatography. For saponification of fatty acids, 40 mg of frozen heart tissue were incubated with 200 µl pentadecanoic acid (1 µg/µl in n-hexane) and 1 ml 1 M methanolic NaOH (4 g NaOH pellets dissolved in 100 ml MeOH) in a water bath for 60 min at 90 °C. As soon as samples cooled down to RT, they were transferred to glass vials containing 1 ml n-hexane. Subsequently, samples were vortexed for 30 sec and centrifuged for 5 min at 1,400 x *g*. After removal of the upper hexane phase, the lower phase was neutralized by addition of 1 M HCl. Consequently, 4 ml n-hexane were added to the samples before mixing and centrifugation for 5 min at 1,400 x *g*. After that, 3 ml of the upper organic phase were transferred to a new vial and the volume was evaporated with N_2 at 40 °C. In the next step, 110 µl derivatization solution (100 % MeOH with 0.9 M acetyl chloride) were supplemented to the samples and the suspension was incubated for 30 min at 90 °C. After cooling down to 50-60 °C, the volume of the samples was completely evaporated using N_2. Subsequently, samples were resolved in 500 µl n-hexane before transferring them into a chromatography column and introducing for gas chromatography. For identification of retention times to the respective fatty acids, a custom-made standard containing 200 µg/µl of defined fatty acids was introduced to the GC analysis (Table 19). The results are shown as peak amplitude [pA] plotted over the retention time [min].

Table 19: Composition of fatty acid reference standard

Trivial name	Carboxyl-reference	ω-reference
Myristic acid	C14:0	C14:0
Pentadecanoic acid	C15:0	C15:0
Palmitic acid	C16:0	C16:0
Palmitoleic acid	C16:1 Δ9	C16:1 (ω-7)
Margaric acid	C17:0	C17:0
Stearic acid	C18:0	C18:0
Oleic acid	C18:1 Δ9	C18:1 (ω-9)
Linoleic acid	C18:2 Δ9, 12	C18:2 (ω-6)
α-Linoleic acid	C18:3 Δ9, 12, 15	C18:3 (ω-3)
Arachidonic acid	C20:4 Δ5, 8, 11, 14	C20:4 (ω-6)

For calculations of the respective fatty acid content, the GC-derived values of C15:0 pentadecanoic acid and its amount (200 µg) in the reference standard can be used as an internal correction factor as follows:

$$Internal\ correction\ factor\ [\mu g] = \frac{Amount\ of\ C15{:}0\ standard\ [\mu g]}{pA(C15{:}0)}$$

Using the internal correction factor, the final fatty acid concentration can be calculated as follows:

$$FA\ concentration\ \left[\frac{\mu g}{mg}\right] = \frac{pA\ (respective\ fatty\ acid) x\ C15{:}0\ correction\ factor[\mu g]}{wet\ cardiac\ tissue\ [mg]}$$

Amounts of total saturated fatty acids (SFA) were calculated as the sum of C14:0, C16:0 and C18:0. Total monounsaturated fatty acids (MUFA) were calculated as sum of C16:1 and 18:1. Total polyunsaturated fatty acid (PUFA) contents were calculated as sum of C18:2, 18:3 and 20:4.

Based on the gas chromatographic results several indices of fatty acid handling and processing were calculated.

Desaturase activities:

Desaturation processes in form of the enzyme activity of stearoyl-CoA desaturase-1 (SCD1) which catalyzes the conversion of the saturated fatty acids C16:0 and C18:0 into the monounsaturated fatty acids palmitoleic acid (C16:1 Δ^9) and oleic acid (C18:1 Δ^9), respectively (Flowers, 2009).

Hence, the Δ9-desaturase index for C16 is defined as ratio of C16:1 to C16:0 fatty acids (Tian & Abel, 2001) and analogously the Δ9-desaturase index for C18 is defined as ratio of C18:1 to C18:0 (Katz, Stenbit, Hatton, DePinho, & Charron, 1995; Tian & Abel, 2001):

$$(C16)\ \Delta 9 - desaturase\ index = \frac{C16{:}\,1\ \left[\frac{\mu g}{g}\right]}{C16{:}\,0\ \left[\frac{\mu g}{g}\right]}$$

$$(C18)\ \Delta 9 - desaturase\ index = \frac{C18{:}\,1\ \left[\frac{\mu g}{g}\right]}{C18{:}\,0\ \left[\frac{\mu g}{g}\right]}$$

Activity of Δ5-desaturase which catalyzes the introduction of a double bond at the fatty acid chains fifth carbon atom (C-terminal) was calculated via the ratio of arachidonic acid (C20:4) and α-Linoleic acid (C18:3) (Tian & Abel, 2001):

$$\Delta 5 - desaturase\ index = \frac{C20{:}\,4\ \left[\frac{\mu g}{g}\right]}{C18{:}\,3\ \left[\frac{\mu g}{g}\right]}$$

In a similar manner, activity of Δ6-desaturase which catalyzes the introduction of a double bond at the fatty acid chains sixth carbon atom (C-terminal) was assessed via calculation of a α-Linoleic acid (C18:3) and linoleic acid (C18:2) ratio (Zisman et al., 2000):

$$\Delta 6 - desaturase\ index = \frac{C18{:}3\ \left[\frac{\mu g}{g}\right]}{C18{:}2\ \left[\frac{\mu g}{g}\right]}$$

Elongase activity:

Next to desaturation, elongase activity, which leads to the elongation of fatty acids chains by addition of two carbon atoms, can be calculated for the respective samples. Hence, C16:0 specific elongation index was calculated as the sum of C18:0 and C18:1 content divided the amount of C16:0 (Wende et al., 2017).

$$C16{:}0\ elongation\ index = \frac{(C18{:}0\ \left[\frac{\mu g}{g}\right] + C18{:}1\ \left[\frac{\mu g}{g}\right])}{C16{:}0\ \left[\frac{\mu g}{g}\right]}$$

Elongation index specific for the saturation of fatty acids (SFA) was calculated as the ratio of stearic acid (C18:0) to palmitic acid (C16:0) for saturated fatty acids (SFA) (Quan et al., 2015) and the ratio of oleic acid (C18:1) to palmitoleic acid (C16:1) for monounsaturated fatty acids (MUFA) (Bjerregaard, Young, & Hegele, 2003):

$$SFA\ elongation\ index = \frac{C18{:}0\ \left[\frac{\mu g}{g}\right]}{C16{:}0\ \left[\frac{\mu g}{g}\right]}$$

$$MUFA\ elongation\ index = \frac{C18{:}1\ \left[\frac{\mu g}{g}\right]}{C16{:}1\ \left[\frac{\mu g}{g}\right]}$$

De novo lipogenesis (DNL) index:

In order to assess the index for cardiac *de novo* lipogenesis, the ration of palmitic acid (C16:0) and linoleic acid (C18:2) was calculated (Ronn et al., 2017):

$$De\ novo\ lipogenesis\ index = \frac{C16{:}0\ \left[\frac{\mu g}{g}\right]}{C18{:}2\ \left[\frac{\mu g}{g}\right]}$$

Thioesterase activity index

Activity of thioesterases as part of the fatty acid synthase, was calculated as e ratio of palmitic acid (C16:0) and myristic acid (C14:0) (Weimershaus et al., 2018)

:

$$Thioesterase\ activity\ index = \frac{C16{:}0\ \left[\frac{\mu g}{g}\right]}{C14{:}0\ \left[\frac{\mu g}{g}\right]}$$

2.2.12 RNA-Sequencing and bioinformatical transcriptome analyses

After total RNA isolation, sequencing was performed at the Max-Planck-Institute for Molecular Genetics (Berlin, Germany) using Illumina HiSeq PE Cluster Kit v4 (cBot) and Illumina HiSeq SBS Kit v4 at 100 million reads per sample an paired-end (2x75) sequencing. Subsequent alignment to the mouse GRCm38/mm10 genome was achieved using STAR software and resulting gene expression data was compared among the experimental groups regarding genotype and I/R intervention. For levels of significance,

resulting p-values were corrected for multiple testing following the Benjamini-Hochberg procedure (Benjamini & Hochberg, 1995). Enrichment and canonical pathway analyses as well as potential upstream target analyses were performed using Ingenuity Pathway Analysis (IPA) software (Qiagen, Hilden, Germany) and ConsensusPathDB (Herwig, Hardt, Lienhard, & Kamburov, 2016) based on fold-changes and level of significance (p-value <0.01) for all analyses.

2.2.13 Mitochondrial high-resolution respirometry

Ex vivo mitochondrial respiration was determined with the kind help of Dr. Tomas Jelenik. In this course, freshly isolated mitochondria from mouse hearts were isolated and me respiration was determined using the Oxygraph-2k (Oroboros Instruments, Innsbruck, Austria) as described. (Jelenik et al., 2014). Defined respiratory states were obtained by the following protocols: (i) tricarboxylic acid cycle (TCA)-linked respiration using 2 mM malate, 10 mM pyruvate (state 2, complex I), 2.5 mM ADP, 10 mM glutamate and (state 3, complex I), 10 mM succinate (state 3, complex I þ II), 10 mM cytochrome c (mitochondrial membrane integrity check), and carbonyl cyanide-p-trifluoromethoxyphenylhydrazone (FCCP) (stepwise increments of 0.25 mM up to the final concentration of max. 1.25 mM, uncoupled state) and (ii) b-oxidation-linked respiration using 2 mM malate, 1 mM octanoyl-carnitine (state 2, complex I þ II), 2.5 mM ADP (state 3, complex I þ II), 10 mM cytochrome c (mitochondrial membrane integrity check), and FCCP (stepwise increments of 0.25 mM up to the final concentration of max. 1.25 mM, uncoupled state). No increase in oxygen consumption upon addition of cytochrome c indicated integrity of the outer mitochondrial membrane after saponin permeabilization. Furthermore, ROS production was assessed simultaneously with respiration by measuring the H_2O_2 levels fluorometrically (O2k-Fluorescence Module, Oroboros

Instruments) using Amplex Red (Amplex Red, Invitrogen, Karlsruhe, Germany) (Jelenik et al., 2017). The same protocols as for respiration were used except from addition of 5 nM oligomycin instead of cytochrome C and FCCP, to induce state 4. Citrate synthase activity was measured spectrophotometrically using a commercial kit (Citrate Synthase Assay Kit, Sigma Aldrich, MO, USA) (Jelenik et al., 2017).

2.2.14 Statistical analysis of data

All data was subjected to statistical testing using GraphPad Prism 7/8 software. All data are reported as mean ± SEM and respective biological replicates are presented in the respective figure legends. Significant differences were determined by one-way or two-way ANOVA (post-hoc-test, Bonferroni multiple comparison test) *or* paired two-tailed Student's t-test, as indicated in the respective figure legends. P-values<0.05 were considered statistically significant.

3. Results

3.1 Impact of *Tbc1d4*-deficiency on cardiac glucose uptake

The RabGAP proteins TBC1D4 and its close orthologue TBC1D1 have been shown to be key regulators of carbohydrate and fatty acid metabolism via mediation of insulin-stimulated glucose uptake via GLUT4 and entry of fatty acids via FATP4 into the cell (Chadt et al., 2015; Chadt et al., 2008; Claycomb et al., 1998; Dokas et al., 2013; Espelage et al., 2020; Szekeres et al., 2012). Since both RabGAPs are highly present in various types of skeletal (Chadt et al., 2008; Szekeres et al., 2012), the question of their abundance in the heart and cardiac muscle arose.

3.1.1 RabGAP abundance in murine heart tissue

In order to assess the level of *Tbc1d4* and *Tbc1d1* expression in cardiac tissue, the mRNA copy number was determined in Chow-fed male wild type mice at 36 weeks of age for whole heart tissue and the cardiac left ventricle as main site of affection by injury inflicted due to myocardial infarction. For this experiment, respective target tissues were homogenized in liquid nitrogen prior to the measurement. The results in Figure 5 show that both RabGAPs are expressed in heart tissue, while *Tbc1d4* represents the more abundant form compared to its paralogue *Tbc1d1*, especially in the cardiac left ventricle (Figure 5A). Additionally, PCR analysis revealed that the expressed isoform of *Tbc1d4* was the so-called “long” isoform, similar to the situation in skeletal muscle (Figure 5B, C)

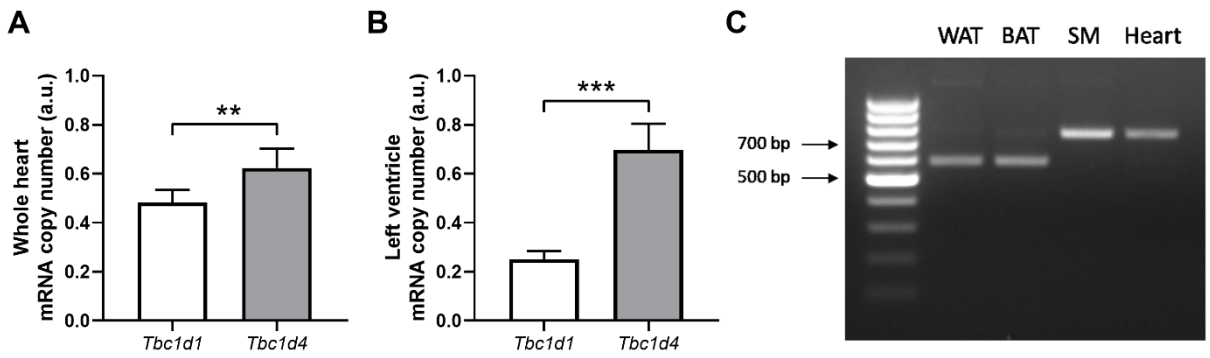

Figure 5: Abundance of *Tbc1d1* and *Tbc1d4* mRNA in whole heart and left ventricle of wild type mice. (A) Cardiac tissue samples of male wild type mice at 36 weeks of age on a Chow diet were introduced into qRT-PCR analysis for *Tbc1d1* (white bars) and *Tbc1d4* (grey bars), respectively. Prior to the measurement, respective tissue samples were homogenized in liquid nitrogen. (B) PCR analysis of *Tbc1d4* isoform expression in heart tissue compared to white adipose tissue (WAT), brown adipose tissue (BAT) and skeletal muscle (SM). The "short" isoform of *Tbc1d4* is detected as PCR product of 555bp, while the "long" isoform is revealed at 782 bp. Data are presented as mean values ± SEM (n = 4). Two-tailed unpaired Student´s t-test with Welch´s correction. **p < 0.01; ***p < 0.001

3.1.2 Impact of *Tbc1d4*-deficiency on cardiac glucose uptake

Since TBC1D4 is a known regulator of glucose uptake into cells of various tissues via the translocation of GLUT4 form intracellular storage vesicles towards the cell membrane and thereby facilitating glucose uptake (Chadt et al., 2015; Espelage et al., 2020), one aim was to assess the cardiac glucose uptake under conditions of *Tbc1d4*-deficiency.

3.1.2.1 *Ex vivo* assay of glucose uptake into left ventricular papillary muscles via [^{3}H]-deoxyglucose uptake assay

In order to assess cardiac glucose uptake, intact papillary muscle was dissected from male *Tbc1d4*-deficient mouse hearts and corresponding wild type mice as controls. This work was performed in collaboration with David Barbosa from the German Diabetes

Center. Dissected muscles were incubated for 20 min with [^{3}H]-deoxyglucose in the absence or presence of 100 nM insulin. Consequently, the muscles were washed, lysed and the amount of incorporated labelled glucose was determined via scintillation counting. While basal glucose uptake is unaltered due to the loss of *Tbc1d4*, insulin response was markedly reduced, leading to no increase in insulin-stimulated glucose uptake (Figure 6).

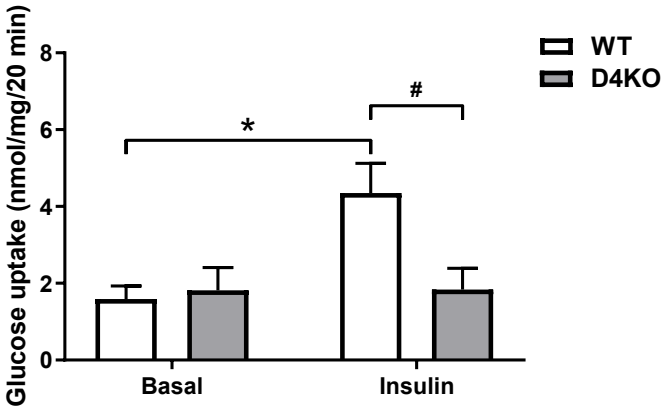

Figure 6: *Ex vivo* insulin-stimulated glucose uptake in papillary muscle of wild type and *Tbc1d4*-deficient mice. The left ventricular papillary muscles of wild type (WT, white bars) and *Tbc1d4*-deficient (D4KO, grey bars) male mice at 16 weeks of age on a Chow-diet were dissected and introduced intact into an insulin-stimulated [^{3}H]-deoxyglucose uptake assay. Data are presented as mean values ± SEM (n=5-6). Two-way ANOVA with Tukey multiple comparisons test. Basal vs. Insulin: *$p < 0.05$; WT vs. D4KO: $^{\#}p < 0.05$

3.1.2.2 *In vivo* assay of cardiac glucose uptake via [^{18}F]-fluorodeoxy-D-glucose positron emission tomography (PET) scan

In vivo cardiac glucose uptake was assessed using [^{18}F]-fluorodeoxy-D-glucose PET/CT) in male, Chow-fed *Tbc1d4*-deficient and wild type mice. This work was performed in collaboration with Dr. Heiko Backes, Anna Lena Cremer, and Prof. Jens C. Brüning, Max Planck Institute for Metabolism Research, Cologne. Briefly, an *i.v.* glucose tolerance test (1 g/kg) was conducted where the distribution of tracer [18F]-fluorodeoxy-D-glucose (FDG) was monitored over time by PET imaging. This technique revealed a

substantial influx of FDG over time into the hearts of WT animals; while in contrast, hearts of D4KO littermates did not show any significant uptake of FDG after glucose injection (Figure 7).

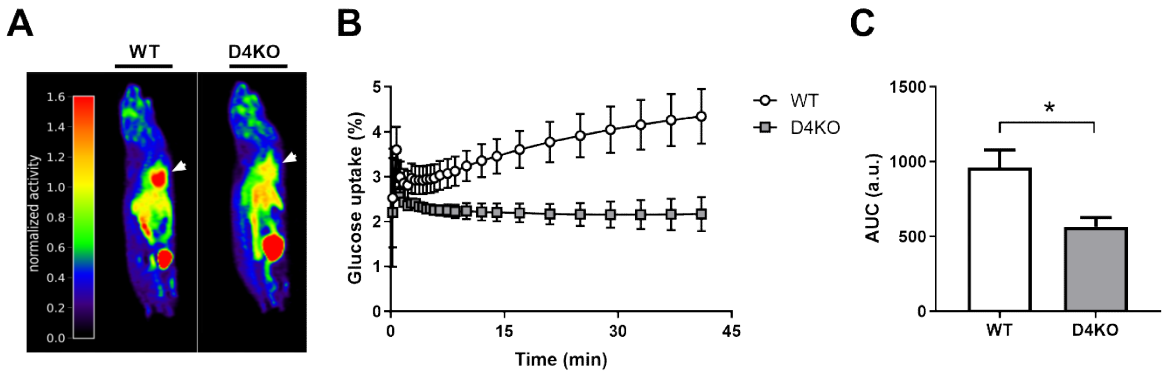

Figure 7: *In vivo* analysis of cardiac glucose uptake over time in wild type and *Tbc1d4*-deficient mice. (A) [18F]-fluorodeoxy-D-glucose positron emission tomography (PET) scan technique was applied in order to visualize glucose uptake into the heart (white arrow) for male *Tbc1d4*-deficient and wild type mice on a Chow-diet. (B) Quantification of cardiac glucose uptake over time with corresponding (C) area under the curve calculation. Data are presented as mean values ± SEM (n = 4). Two-way ANOVA with Tukey multiple comparisons test. Basal vs. Insulin: *p < 0.05; WT vs. D4KO: #p < 0.05. Two-tailed unpaired Student´s t-test with Welch´s correction. *p < 0.05.

3.1.3 Abundance of glucose transporter proteins in *Tbc1d4*-deficient and wild type hearts

The uptake of glucose into the heart is mainly regulated via glucose transporter types 1 and 4 (GLUT1, GLUT4). Interestingly, Western Blot analysis of GLUT1 and GLUT4 protein content in whole heart lysates (Figure 8A) revealed a markedly reduction of GLUT4 content in *Tbc1d4*-deficient hearts compared to wild type controls (Figure 8C), while levels of GLUT1 content remained at comparable levels (Figure 8B).

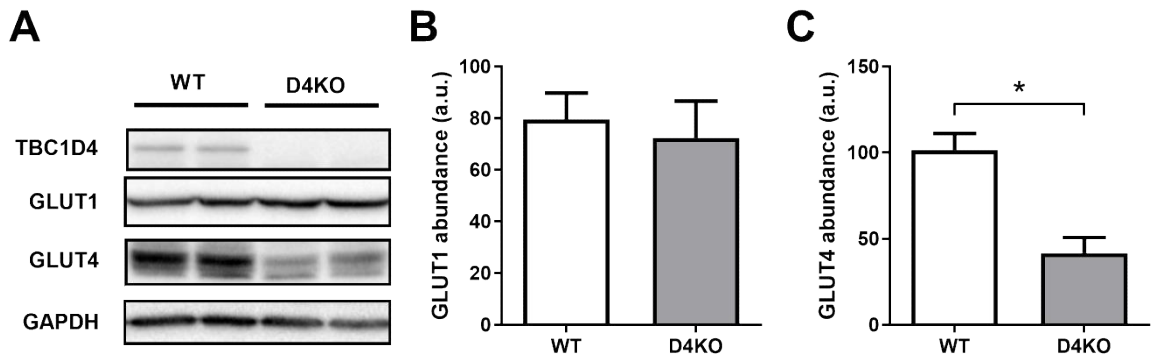

Figure 8: Glucose transporter protein abundance in heart tissue of wild type and *Tbc1d4*-deficient mice. (A) Western Blot analysis of the glucose transporters type 1 (GLUT1) and 4 (GLUT4) in heart tissue in male *Tbc1d4*-deficient and wild type mice on a Chow diet at 36 weeks of age. As loading control, the protein content of GAPDH was assessed. Based on these results, relative abundance of (B) GLUT1 and (C) GLUT4 were calculated. Data are presented as mean values ± SEM (n = 4). Two-tailed unpaired Student´s t-test with Welch´s correction. *p < 0.05

3.2 Effects of *Tbc1d4*-deficiency on cardiac morphology and function following ischemia/reperfusion-induced injury

As a consequence of myocardial infarction, the cardiac muscle tissue undergoes several morphological and structural remodeling processes. Since *Tbc1d4* is a crucial regulator of metabolic flexibility in various tissues, and especially under ischemic conditions during myocardial infarction when an adequate switch from predominantly used lipids towards carbohydrates is needed, it was investigated how its deficiency affected myocardial remodeling following ischemia/reperfusion injury.

3.2.1 Impact of *Tbc1d4*-deficiency and diet on body/heart weight

In order to investigate whether the *knockout* of *Tbc1d4* impacts the heart morphology in terms of size already in pre-infarction state, heart weight of male *Tbc1d4*-deficient mice and wild type controls were analyzed and related to corresponding body weight values under dietary conditions of Chow diet and 60 kcal% HFD. Although no differences in total body weight between WT and D4KO mice were present (Figure 9A, D), mice with *Tbc1d4*-deficiency on a Chow diet showed reduced heart weight compared to WT littermates (Figure 9B), but not on HFD (Figure 9E). However, calculation of the body weight to heart weight ratio revealed no differences between D4KO and wild type mice, independent of the diet (Figure 9C, F).

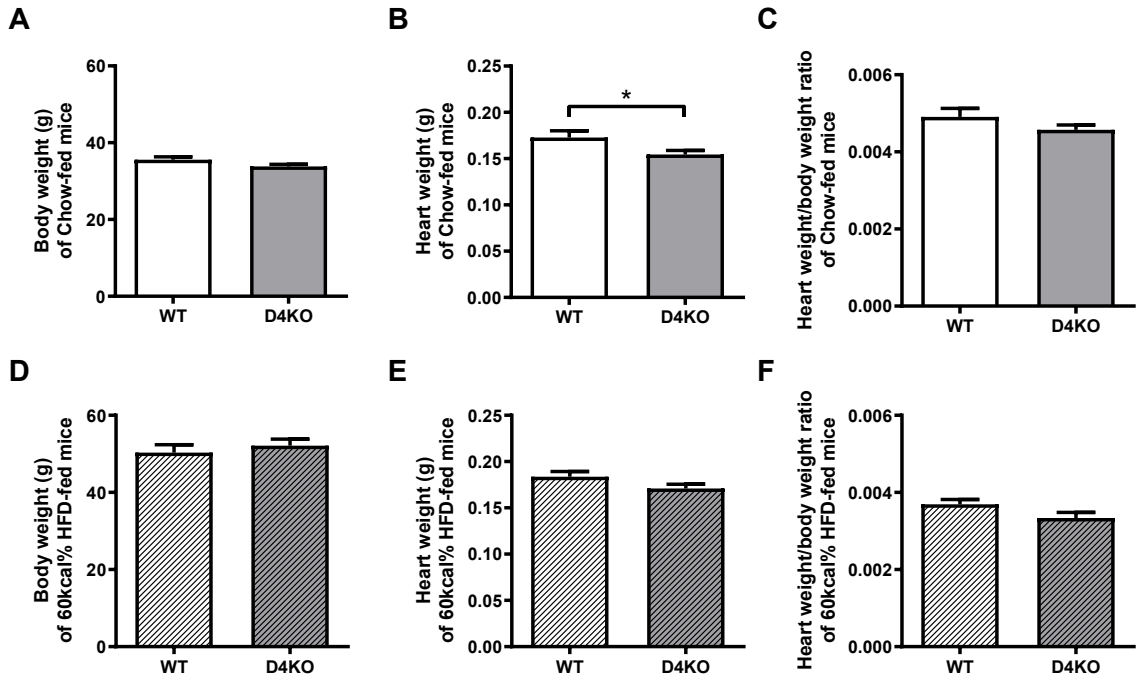

Figure 9: Parameters of body weight and heart weight ratio of wild type and *Tbc1d4*-deficient mice under different dietary conditions. (A, D) Body weight, (B, E) heart weight and (C, F) body weight/heart weight ratio were assessed for wild type (WT; white bars) and *Tbc1d4*-deficient (D4KO; grey bars) male mice at 36 weeks of age on a Chow or 60kcal% high-fat diet (HFD; hatched bars). Data are presented as mean values ± SEM (n = 12-32). Two-tailed unpaired Student´s t-test with Welch´s correction. *p < 0.05

3.2.2 Impact of *Tbc1d4*-deficiency on cardiac morphology following I/R intervention

In order to investigate the effect of *Tbc1d4*-deficiency on ischemia/reperfusion (I/R) induced injury in the heart, male *Tbc1d4*-knockout and wild type mice at an age of 36 weeks and on a 60kcal% HFD were introduced to surgical I/R intervention. Via a close chest model, ischemia was induced by occlusion of the left anterior descending (LAD) artery for 60 min, following reperfusion as described in the method section (see 2.2.3). After 3 weeks of reperfusion, the hearts were dissected and histologically and morphometrically analyzed using Azan staining. The histological staining of WT and D4KO hearts (Figure 10A) revealed a markedly increase in the I/R- induced infarction size due to the knockout of *Tbc1d4* compared to the WT situation (Figure 10B). Consequently the left ventricular wall thickness was reduced (Figure 10C) while at the same time the lumen of the left ventricle was increased (Figure 10D).

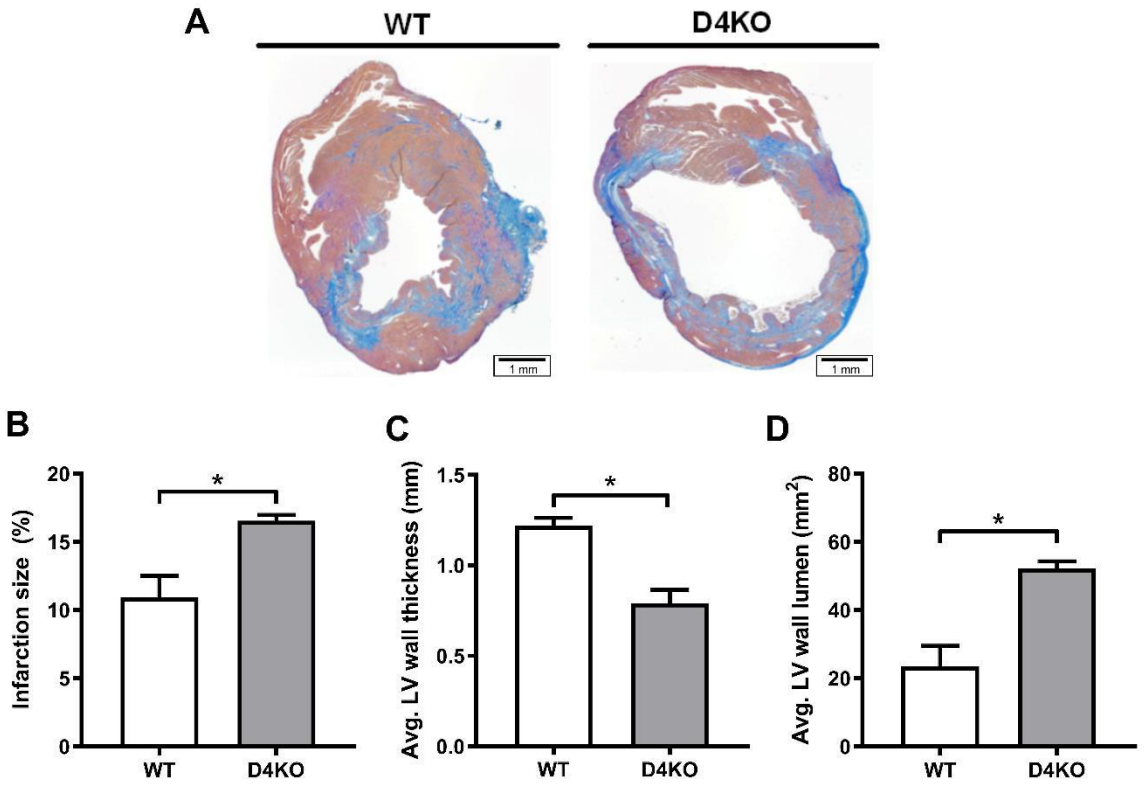

Figure 10: Analysis of cardiac morphology of wild type and *Tbc1d4*-deficient mice 3 weeks after ischemia/reperfusion intervention. Wild type (WT; white bars) and *Tbc1d4*-deficient (D4KO; grey bars) male mice at 36 weeks of age on a 60kcal% high-fat diet underwent surgical occlusion of the left anterior descending coronary artery (LAD) for 60 minutes and subsequent reperfusion for 3 weeks. For each parameter, ten transversal slices, each distanced 250µm from the prior, were integrated. (A) Histological Azan stainings were analyzed and (B) infarction size was calculated vie threshold level analysis. Parameters of (C) left ventricular wall thickness and (D) left ventricular lumen were morphometrically measured. Data are presented as mean values ± SEM (n=3). LV = left ventricle. Two-tailed unpaired Student´s t-test with Welch´s correction. *p < 0.05

Next to cardiac morphometry following I/R-intervention, the abundance and localization of adhesion molecules were assessed using immunohistochemical staining of wild type and *Tbc1d4*-deficient cardiac sections 3 weeks following I/R in the infarction zone. For this, platelet endothelial cell adhesion molecule 1 (PECAM-1) and vascular cell adhesion molecule 1 (VCAM-1) as markers for angiogenesis and inflammatory processes, were assessed via immunohistochemistry of heart sections. The results

revealed that the lack of *Tbc1d4* did not lead to gross alterations in PECAM-1 or VCAM-1 abundance or localization (Figure 11).

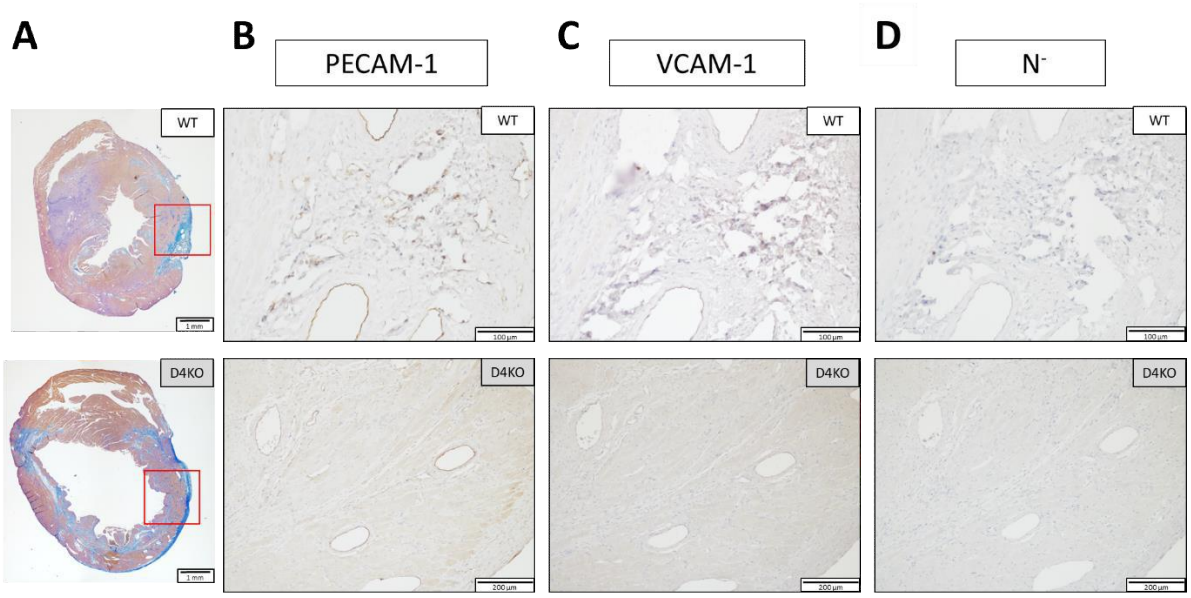

Figure 11: Immunohistochemical stainings for cardiac adhesion molecule abundance in infarcted area of wild type and *Tbc1d4*-deficeint hearts 3 weeks post-I/R. Wild type (WT) and *Tbc1d4*-deficient (D4KO) male mice at 36 weeks of age on a 60kcal% high-fat diet underwent surgical ischemia und subsequent reperfusion for 3 weeks. (A) Azan stainings of heart sections with indication of analyzed area (red rectangle). Immunohistochemical staining for adhesion molecule markers (B) platelet endothelial cell adhesion molecule 1 (PECAM-1) and (C) vascular cell adhesion molecule 1 (VCAM-1) as markers for angiogenesis and inflammatory processes with (D) corresponding negative control of staining. (n=1)

3.2.3 Effect of *Tbc1d4*-deficiency on cardiac function

Before and during the 3 week reperfusion phase, mice were monitored and parameters of cardiac function were assessed regularly using echocardiographic measurements. The measurements were conducted in collaboration with Prof. J. Fischer, Institute for Pharmacology, HHU. The endsystolic volume, which describes the amount of blood remaining in the left ventricle after end of the systole, is unaltered at baseline due to the loss of *Tbc1d4*. However after 1 week and up to the time-point of 3 weeks, the endsystolic volume increased progressively in D4KO hearts compared to WT animals

(Figure 12A), speaking for a decreased pumping function of the heart. For the enddiastolic volume (i.e. amount of blood remaining in the left ventricle after end of the diastole) no differences between D4KO and WT hearts can be observed at these time points (Figure 12B). For further ECG parameters, see supplementary figure 1.

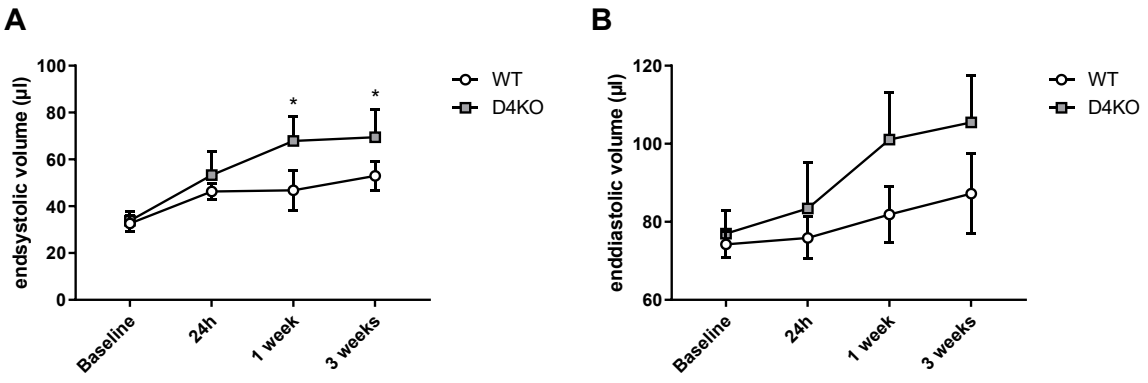

Figure 12: Echocardiographic assessment of heart function parameters of wild type and *Tbc1d4*-deficient mice during 3 weeks following I/R intervention. Following the I/R-intervention phase in male mice at 36 weeks of age on a 60kcal% high-fat diet, animals were monitored for the 3 week reperfusion phase. During this, parameters of cardiac function in terms of (A) endsystolic volume and (B) enddiastolic volume were measured before the intervention (baseline) and at time points of 24 hours, 1 week and 3 weeks after the intervention for type (WT; white) and *Tbc1d4*-deficient (D4KO; grey). Recordings were conducted at ZETT (HHU in collaboration with Prof. J. Fischer, Heinrich-Heine University, Düsseldorf, Germany). Data are presented as mean values ± SEM (n = 6). Two-tailed unpaired Student´s t-test with Welch´s correction. *p < 0.05

3.2.4 Impact of *Tbc1d4*-deficiency on electrocardiographic parameters

Next to the heart histological and echocardiographic approaches in order to determine I/R-induced cardiac impairments, also electrocardiography (ECG) can be introduced to investigate especially the I/R-induced events during the surgical process. The electrical activity during the heart pump cycle can be monitored by ECG, which detects three characteristic waves, “Q”, “R”, and “S”, altogether denominated as the

“QRS” complex. The R-wave is the largest wave in the complex and represents the electrical stimulus as it passes through the thick ventricular walls of the heart. Its amplitude is related to the thickness of the walls.

Under standard conditions, upon placement of the ligature to the LAD and the following 60 minutes of ischemia, the elevation of the R-wave amplitude in the ECG was assessed as a marker in order to verify the ischemia. After release of the blockage in the acute reperfusion phase, the R-wave decreases again. Interestingly, while in both WT and D4KO animals the occlusion induced R-wave amplitude increase in present, the expected decrease after removing of the ligature is missing in D4KO animals (Figure 13)

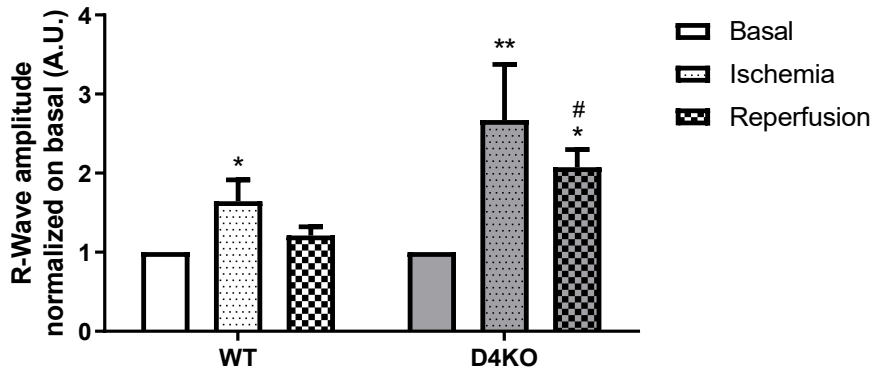

Figure 13: Profile of electrocardiographic R-wave amplitude development at different stages of I/R intervention surgery for wild type and *Tbc1d4*-deficient mice. R-wave amplitude was measured before start of the surgical intervention (basal) after induction of ischemia and acute reperfusion phase for male wild type (WT; white bars) and *Tbc1d4*-deficient (D4KO; grey bars) mice at 36 weeks of age. All values are normalized to the individual basal state. Data are presented as mean values ± SEM (n = 5-7). Two-way ANOVA with Tukey multiple comparisons test. Condition vs. Basal: *p < 0.05, **p < 0.01; WT vs. D4KO: $^{\#}$p < 0.05

3.3 Impact of *Tbc1d4*-deficiency on cardiac fatty acid profile

The main substrates for cardiac energy production are fatty acids. However, under given environmental circumstances, the heart switches between different substrates in order to ensure optimal energy production. Therefore, the cardiac fatty acid profile was investigated via gas chromatography in order to identify the effect of *Tbc1d4*-deficiency and diet intervention on cardiac lipid content and variety. For this, cardiac whole heart samples of wild type and *Tbc1d4*-deficient mice on either a Chow diet or 60 kcal% high-fat diet were analyzed as described in methods section (see 2.2.12).

The results in Table 20 and show that neither genotype nor diet affect cardiac lipid species abundance in most cases. However, the loss of *Tbc1d4* under Chow diet conditions led to a decrease of oleic acid (C18:1) compared to corresponding WT controls. Similarly, levels of the lesser abundant myristic acid (C14:0) are decreased in D4KO hearts on a chow diet compared to WT controls and additionally the high fat diet intervention led to a decrease in the C14:0 wild type situation (see supplemental figure 2).

Based on the results of the lipid profiling, various clusters of lipids were combined in order to investigate the effects of *Tbc1d4*-deficiency on specific lipid classes. In this course, the total amount fatty acids as well as saturated fatty acids (SFA), monounsaturated fatty acids (MUFA) and polyunsaturated fatty acids were calculated. Based on these results, the ratio of MUFA/SFA and PUFA/SFA was also assessed as indicator of total desaturation activity. The results revealed that neither SFA, nor MUFA or PUFA content was altered by either genotype or diet intervention. The same observation was made for total distribution of these lipid clusters as well as for MUFA/SFA and PUFA/SFA ratios (Table 20 and supplemental figure 3).

	WT Chow	D4KO Chow	WT HFD	D4KO HFD
Total	18.03 ± 1.51	15.37 ± 1.12	17.5 ± 1.67	14.98 ± 1.12
SFA				
C14:0	0.16 ± 0.04	0.05 ± 0.01**	0.06 ± 0.01#	0.05 ± 0.01
C16:0	3.40 ± 0.36	2.80 ± 0.15	3.07 ± 0.31	2.59 ± 0.19
C18:0	3.91 ± 0.33	3.60 ± 0.24	4.38 ± 0.31	3.59 ± 0.27
Total SFA	7.39 ± 0.63	6.33 ± 0.42	7.48 ± 0.61	6.20 ± 0.47
MUFA				
C16:1	0.58 ± 0.16	0.27 ± 0.02	0.24 ± 0.07	0.19 ± 0.04
C18:1	3.89 ± 0.36	2.49 ± 0.26*	3.2 ± 0.42	2.49 ± 0.32
Total MUFA	3.52 ± 0.62	2.68 ± 0.31	3.32 ± 0.47	2.59 ± 0.36
PUFA				
C18:2	4.67 ± 0.5	4.28 ± 0.39	4.26 ± 0.43	4.03 ± 0.17
C18:3	0.06 ± 0.01	0.03 ± 0	0.03 ± 0	0.03 ± 0
C20:4	1.97 ± 0.09	2.06 ± 0.14	2.41 ± 0.18	2.13 ± 0.18
Total PUFA	7.11 ± 0.47	6.36 ± 0.5	6.7 ± 0.62	6.18 ± 0.31
Ratios				
MUFA/SFA	0.45 ± 0.05	0.41 ± 0.03	0.43 ± 0.03	0.4 ± 0.02
PUFA/SFA	0.99 ± 0.05	1.01 ± 0.04	0.89 ± 0.02	1.01 ± 0.03

Table 20: Fatty acid profile of cardiac tissue of wild type and *Tbc1d4*-deficient mice. Abundance of individual lipid species and lipid clusters were assessed via gas chromatography analysis for 36 weeks old, male wild type (WT) and *Tbc1d4*-deficient (D4KO) mice on a Chow or 60kcal% high-fat diet (HFD), respectively. In this course, cardiac abundance of saturated fatty acids (SFA), mono-unsaturated fatty acids, and poly-unsaturated fatty acids (PUFA) were assessed. Based on these results, the ratio of MUFAs to SFAs as indicator for total desaturation activity and the ratio of PUFAs to SFAs were generated. Data are presented as mean values ± SEM (n = 5-10). Two-way ANOVA with Tukey multiple comparisons test. WT vs. D4KO: *p < 0.05, **p < 0.01; Chow vs. HFD: #p < 0.05

In order to elucidate whether the deficiency of *Tbc1d4* leads to alterations in enzymatic activities of lipid desaturation, specific indices of fatty acid ratios were calculated as described in the method section (see 2.2.12). Interestingly, the HFD-intervention led to a decrease of the Δ9-desaturase index of C16:1/C16:0 ration in hearts of WT mice, indication a decrease of desaturase activity, while in D4KO samples no difference due to the diet intervention was observed (Figure 14C). For Δ5-desaturase index of C20:4/C18:2 (Figure 14A), Δ5-desaturase index of C18:3/C18:2 (Figure 14B)

and Δ9-desaturase index of C18:1/C18:0 (Figure 14D) neither genotype nor diet intervention led to alterations in ratio.

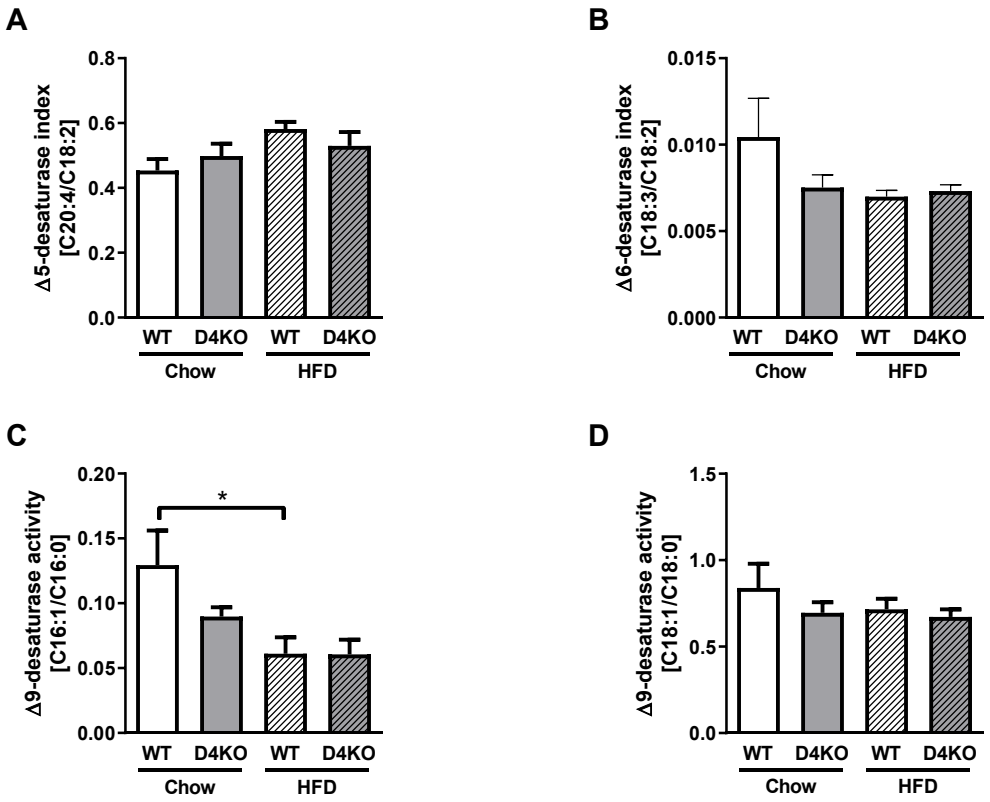

Figure 14: Desaturation activity indices of heart tissue from wild type and *Tbc1d4*-deficient mice. Based on the results of assessed fatty acid composition, activities of desaturases were calculated for 36 weeks old, male wild type (WT; white bars) and *Tbc1d4*-deficient (D4KO; grey bars) mice on a Chow or high-fat diet (HFD; hatched bars), respectively. Δ5- and Δ6- desaturase activity indexes (A, B) as well as Δ9-desaturase activity index specific for C16 and C18 fatty acids (C, D) were calculated. Data are presented as mean values ± SEM (n = 5-10). Two-way ANOVA with Tukey multiple comparisons test. *p < 0.05

Similar to the desaturase activity indices, also elongation processes and elongase activity can be assessed as ratio of specific fatty acid species. The elongase activity of the saturated fatty acids C18:0/C16:0 was unaltered due to genotype or diet intervention (Figure 15A). However, the elongase activity on the monounsaturated fatty acids C18:1/C16:1 (Figure 15B) as well as the C16:0 elongation index (Figure 15C) was increased due to HFD intervention in WT animals, indicating an increased elongase activity, but not in D4KO mice.

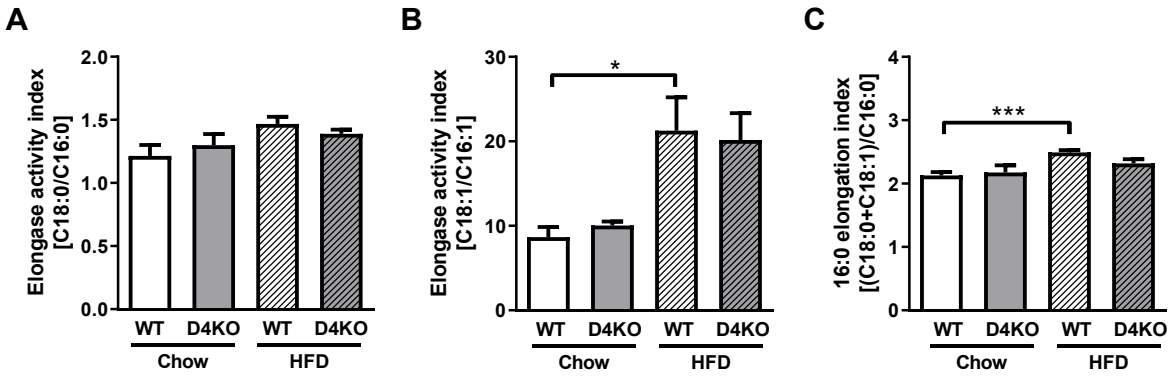

Figure 15: Elongase and elongation activity indices of heart tissue from wild type and *Tbc1d4*-deficient mice. Based on the results of assessed fatty acid composition, indices as estimates for elongase activity were calculated for 36 weeks old, male wild type (WT; white bars) and *Tbc1d4*-deficient (D4KO; grey bars) mice on a Chow or high-fat diet (HFD; hatched bars), respectively. Saturated fatty acid elongase activity (A), monounsaturated fatty acid elongase activity (B) and the palmitic acid-specific 16:0 elongation index (C) were assessed. Data are presented as mean values ± SEM (n = 5-10). Two-way ANOVA with Tukey multiple comparisons test. *p < 0.05; ***p < 0.001

As indicators for fatty acid synthesis, the thioesterase index (C16:0/C14:0) and de novo lipogeneses index (C16:0/C18:2) were calculated. Here, the thioesterase index was increased in D4KO animals under Chow diet conditions, compared to the corresponding WT situation, indicating an increase in thioesterase activity. At the same time, the diet intervention did not alter this parameter. (Figure 16A) The *de novo* lipogeneses index remained unaffected by genotype and diet (Figure 16B).

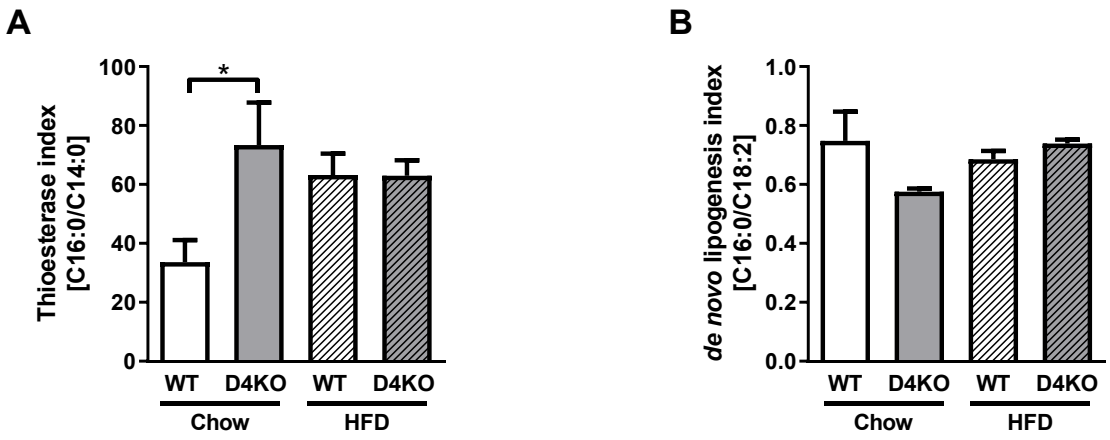

Figure 16: Lipid synthesis indices of heart tissue from wild type and *Tbc1d4*-deficient mice. Based on the results of assessed fatty acid composition, the thioesterase index (A) as well as the *de novo* lipogenesis index (B) were calculated as indicators of lipid synthesis for 36 weeks old, male wild type (WT; white bars) and *Tbc1d4*-deficient (D4KO; grey bars) mice on a Chow or high-fat diet (HFD; hatched bars), respectively. Thioesterase activity index (A) and *de novo* lipogenesis index (B) were assessed. Data are presented as mean values ± SEM (n = 5-10). Two-way ANOVA with Tukey multiple comparisons test. *p < 0.05

3.4 Effect of *Tbc1d4*-deficiency on mitochondrial function, morphology and distribution in mouse hearts

Cardiac energy supply is mainly regulated by the mitochondria. Since the loss of *Tbc1d4* leads to gradual impairments in cardiac function and morphology, the role of the mitochondria in the *Tbc1d4*-deficient situation was assessed.

3.4.1 Impact of *Tbc1d4*-deficiency on cardiac mitochondrial mass and copy number

In order to investigate the effect of cardiac *Tbc1d4*-deficiency on mitochondrial level, certain surrogate markers were measured using whole heart cell lysates from 36 weeks old male *Tbc1d4*-deficient animals and wild type littermates fed a Chow diet. The citrate synthase activity was assessed as an estimate for mitochondrial mass and

measured via an enzymatic *in vitro* assay. The abundance of the mitochondrial mt-Nd2 gene copy number was measured by qPCR as an estimation of mitochondrial copy number. Based on the results shown in Figure 17, the deficiency of *Tbc1d4* does not alter citrate synthase activity or mt-Nd2 gene abundance.

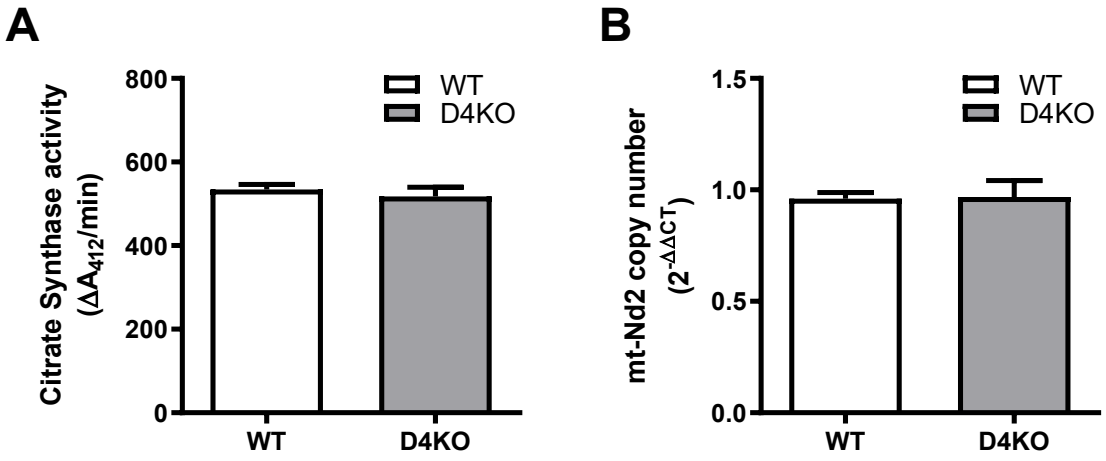

Figure 17: Measurement of markers for mitochondrial activity and copy number in cardiac tissue of wild type and *Tbc1d4*-deficient mice. Estimations of mitochondrial activity via citrate synthase activity and mitochondrial DNA copy number via PCR of mt-Nd2 was assessed in cardiac tissue of wild type (WT; white bars) and *Tbc1d4*-deficient (D4KO; grey bars) mice on a Chow-diet at 36 weeks of age. Data are presented as mean values ± SEM (n = 6-10). Two-tailed unpaired Student´s t-test with Welch´s correction.

3.4.2 Impact of *Tbc1d4*-deficiency on cardiac mitochondrial respiration

While parameters of mitochondrial mass and apparent copy number remained unaltered due to the loss of *Tbc1d4*, the mitochondrial function remained to be elucidated as parameter of mitochondrial efficiency. For this, mitochondrial high-resolution respiration at the different steps of the electron transport chain was analyzed as described in the methods section (Chapter 2.2.15). Briefly, this was performed by using different substrates of the TCA-cycle and β-oxidation respectively in isolated mitochondria of WT and D4KO hearts of male mice at 36 weeks of age on a Chow diet. Moreover, FCCP as

mitochondrial uncoupling agent and rotenone as complex I inhibitor and antimycin A as inhibitor of complex III of the electron transport chain were assessed.

The loss of *Tbc1d4* is associated with a decrease in mitochondrial oxygen flux in the TCA-cycle at the addition of malate, rotenone and antimycin A (Figure 18A) compared to WT controls, while at the same time the H_2O_2 emission as indicator for ROS production was also decreased after addition of antimycin A (Figure 18B). Interestingly, mitochondrial respiration and ROS production for substrates in β-oxidation were not altered due to *Tbc1d4* deficiency (Figure 18C, D). Similarly, the respiratory control ratio (RCR) as well as the leak control ratio (LCR) as indicators of mitochondrial coupling and efficiency are not altered due to the loss of *Tbc1d4*, regardless of TCA-cycle or β-oxidation substrates (Figure 18E, F).

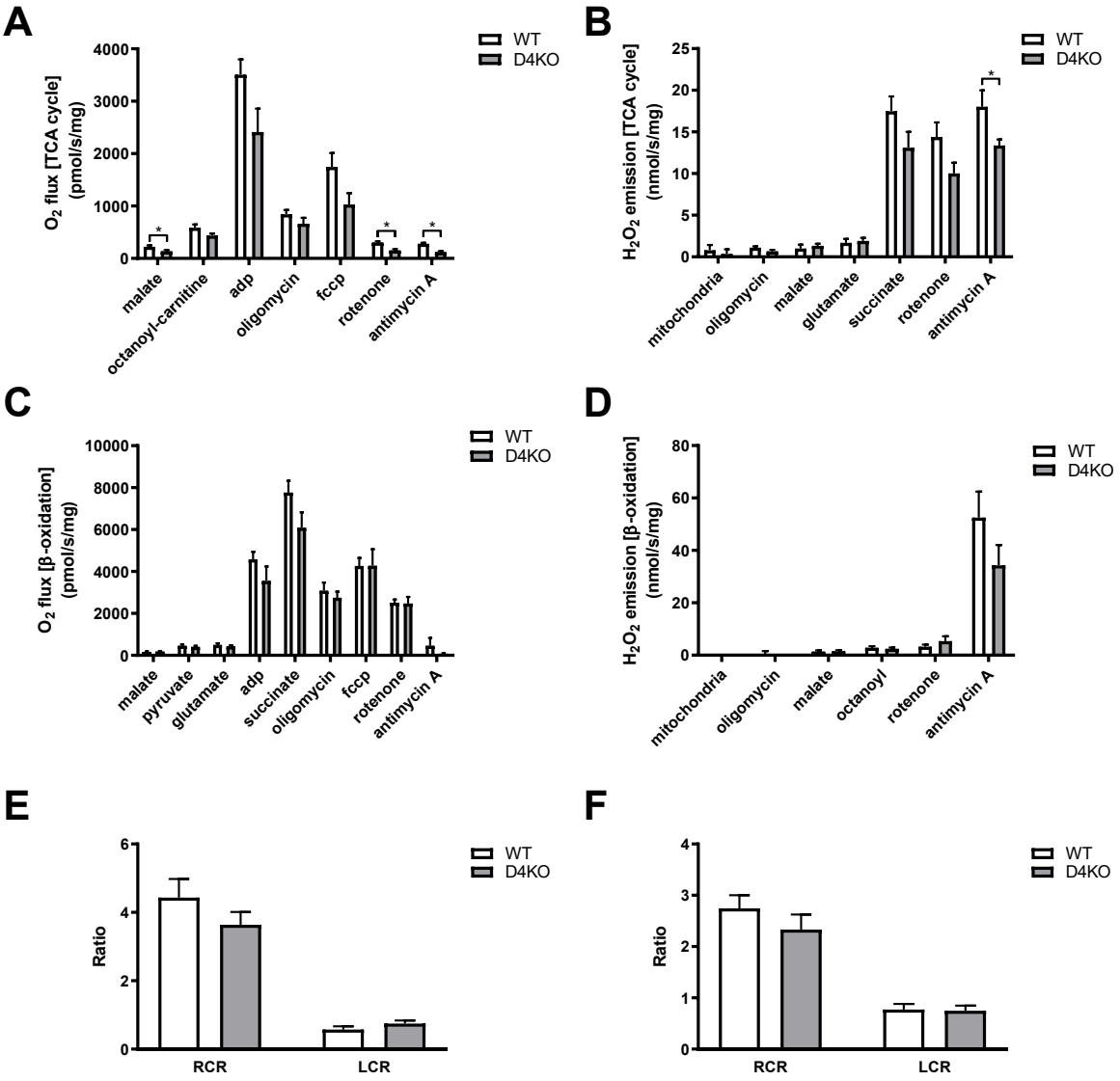

Figure 18: High-resolution mitochondrial respiration profile of isolated cardiac mitochondria from wild type and *Tbc1d4*-deficient mice. Mitochondrial oxygen flux and hydrogen peroxide emission were assessed using substrates for the tricarboxylic acid (TCA) cycle (A, B) and β-oxidation (C, D), as well as trifluoromethoxy carbonylcyanide phenylhydrazone (FCCP) for mitochondrial uncoupling, rotenone as complex I inhibitor and antimycin A as inhibitor of complex III of the electron transport chain for 36 weeks old, male wild type (WT; white bars) and *Tbc1d4*-deficient (D4KO; grey bars) mice. Based on these results, the respiratory control ratio (RCR) and leak control ratio (LCR) were calculated. Data are presented as mean values ± SEM (n = 8). Two-tailed unpaired Student´s t-test with Welch´s correction. *p < 0.05

3.4.3 Impact of *Tbc1d4*-deficiency on cardiac mitochondrial density and morphology

While total mitochondrial mass and copy number are unaltered due to the knockout of *Tbc1d4*, the morphology of mitochondria and size distribution remained to be elucidated. For this, the left ventricle of WT and D4KO hearts of male mice at 50 weeks of age on a Chow diet were dissected and sections were analyzed using transmission electron microscopy (TEM). Here, mitochondria were counted and morphologically measured in terms of size. The results in Figure 19 indicate no statistically significant difference in average mitochondrial number, area and size due to the loss of *Tbc1d4* (Figure 19A-D). In addition, the clustering of mitochondrial sizes as indicator for size distribution did not show any statistically significant size differences between D4KO and WT samples (Figure 19E), indicating no affection of mitochondrial morphology and distribution due to *Tbc1d4*-deficiency.

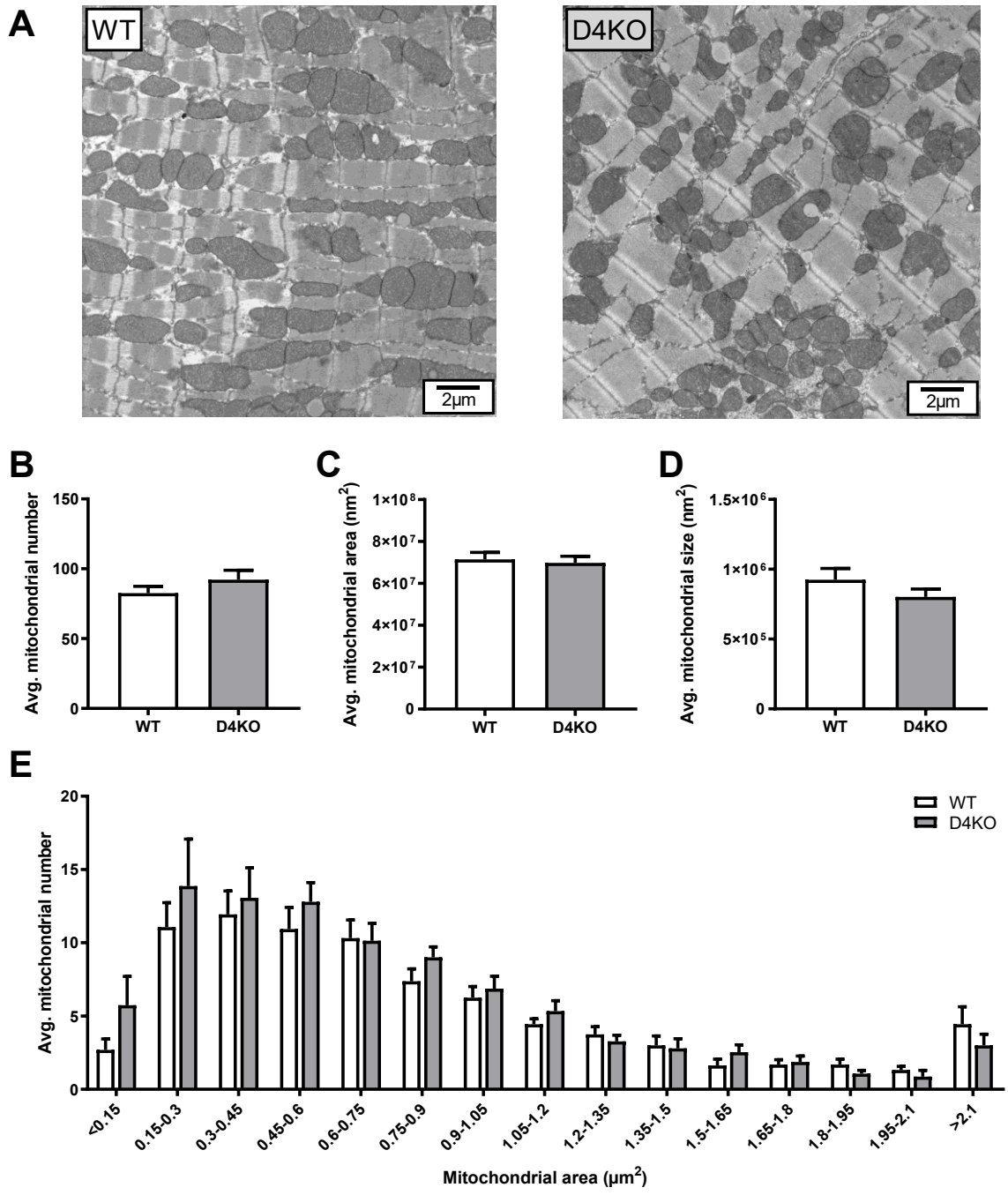

Figure 19: Analysis of mitochondrial density and number distribution in left-ventricular heart tissue of wild type and *Tbc1d4*-deficient mice. Mitochondrial area and number were investigated on histological ultrastructure level using transmission electron microscopy of left ventricular heart tissue of 50 weeks old, male wild type (WT) and *Tbc1d4*-deficient (D4KO) mice (A). Parameters of average mitochondrial number (B) as well as average mitochondrial area (B) were determined and average mitochondrial size (C) was calculated consequently. Average distribution of mitochondrial area was calculated for different size clusters (E) for wild type (WT; white bars) and *Tbc1d4*-deficient (D4KO; grey bars) mice. For each sample, ~1300 mitochondria were measured. Data are presented as mean values ± SEM (n=3). Two-tailed unpaired Student´s t-test with Welch´s correction.

3.5 Effects of *Tbc1d4*-deficiency and ischemia/reperfusion intervention on cardiac transcriptome

In order to investigate the molecular mechanisms which lead to the impaired post-I/R phenotype of *Tbc1d4*-deficient hearts, the cardiac transcriptome of WT and D4KO animals at 36 weeks of age on a Chow diet was analyzed in the pre-I/R state as well as the 3 week post-I/R state. For this, total cardiac RNA was extracted for whole hearts of WT and D4KO mice of the respective experimental groups. Following a polyA pre-selection step, the cardiac mRNA was sequenced using Illumina Next-Gen RNA-sequencing technique and bioinformatically prepared for analysis of differential gene regulation.

3.5.1 Alterations in cardiac transcriptome due to *Tbc1d4*-deficiency and I/R intervention

The adaptation of the heart to the *Tbc1d4*-deficiency and I/R-intervention was assessed by conducting unbiased transcriptome analysis, revealing various differentially regulated genes ($P < 0.05$) comparing the different tested conditions in regards to genotype and I/R-intervention (Figure 20). A comparable number of genes is differentially regulated due to the I/R-intervention in both genotypes (Figure 20A) with 4832 genes in the WT state and 4299 genes in the D4KO state. Comparing the genotypes a smaller number of genes is differentially regulated, i.e. at pre-I/R state 738 transcripts were differentially expressed between WT and *Tbc1d4*-deficient mice (Figure 20A-C), while 3 weeks after I/R intervention, only a number 113 genes were differentially regulated (Figure 20A,B, D). Surprisingly, the overlap of differentially regulated genes between WT and D4KO in pre- and post-I/R state is relatively small with a total of 10 genes, indicating

a distinct alteration of cardiac transcriptome in the hearts of D4KO animals due to the I/R intervention compared to WT mice (Figure 20B).

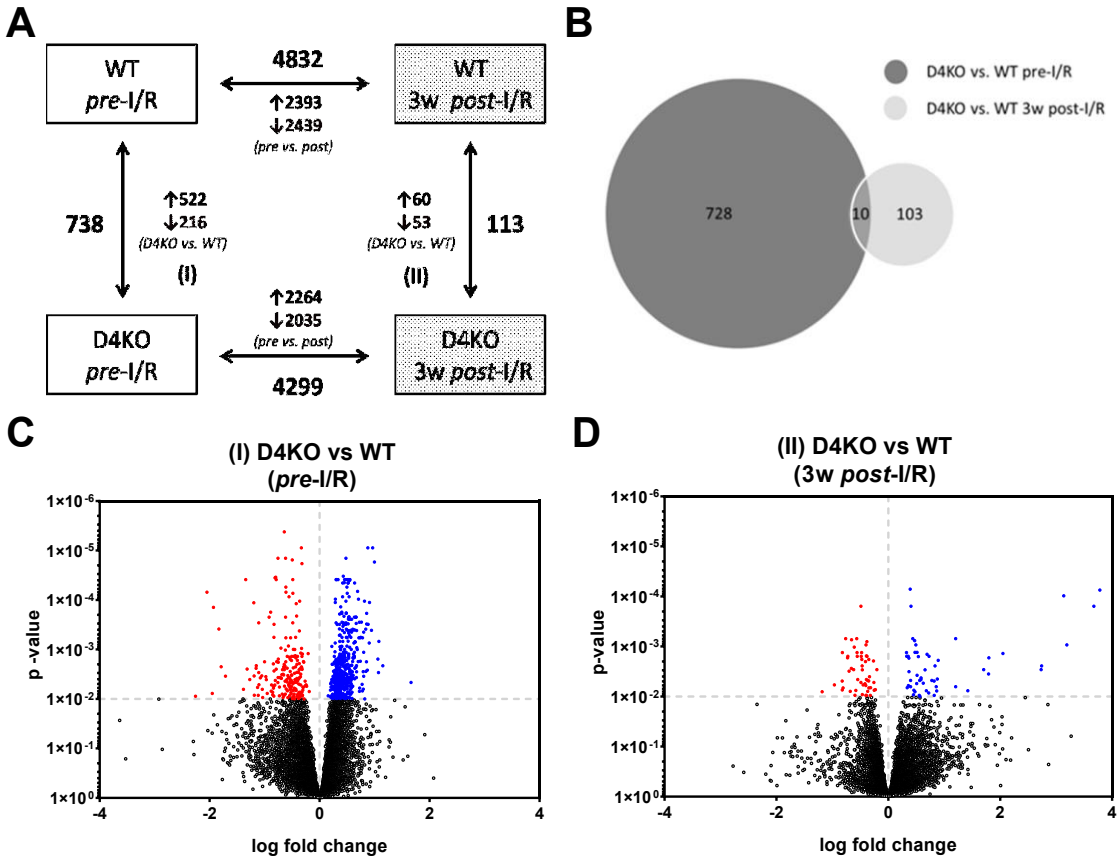

Figure 20: Alterations of cardiac transcriptome and gene regulation due to *Tbc1d4*-deficiency and/or I/R intervention. Cardiac transcriptome of wild type (WT) and *Tbc1d4*-deficient (D4KO) hearts from pre-I/R and 3 weeks post-I/R samples respectively were sequenced using RNASequencing and subsequently tested for differential gene expression. (A) Numbers of differentially expressed genes between the different experimental conditions (B) Overlap of differentially regulated genes due to the I/R-intervention between the genotypes and (C, D) corresponding volcano plots displaying the size of differential regulation and size of significance. Significance threshold was set at $p<0.01$ (n=4).

3.5.2 Analysis of differentially regulated canonical pathways and upstream regulators

Differentially regulated genes were analyzed using ingenuity pathway analysis (IPA) software for analysis of distinct canonical pathway regulation and potential upstream regulators due to the loss of *Tbc1d4* and/or I/R-intervention. The results in

Figure 21 show that comparing the pre-I/R situation (Figure 21A, B) and the 3 weeks post-I/R situation (Figure 21C, D), the canonical pathways (Figure 21A, C) and potential upstream regulators (Figure 21C, D) are distinct for each condition with no major overlap. This observation is in accordance with the individual expression patterns visualized in Figure 21A, B). Interestingly, already in the pre-I/R state without any kind of intervention, the knockout of *Tbc1d4* impacts molecular canonical pathways involved in CVD and diabetes associated pathways. In this course, *Tbc1d4*-deficiency is associated with alterations in the transcriptome, affecting genes involved in insulin receptor signaling and cardiac hypertrophy signaling (Figure 21A). However, this pathways are not affected 3 weeks after the I/R intervention.

Surprisingly, Ingenuity pathway analysis of the differentially expressed genes revealed coordinated changes in other pathways, which have not been directly linked to *Tbc1d4*-action. In both pre-I/R and 3 weeks post-I/R states, the lack of *Tbc1d4* leads to alterations in EIF2 and eIF4 signaling pathways (Figure 21A). These pathways are involved in translational control, the unfolded protein response (UPR) or ER-stress response. Moreover, the 3 weeks post-I/R analysis reveals the impairments of pathways associated with fibrosis (Figure 21C) due to the deficiency of *Tbc1d4*. This pathway is associated with extra cellular matrix (ECM)-related processes between the genotypes and the I/R intervention conditions well as corresponding canonical pathway and upstream target candidates.

A

pre-I/R state

Canonical pathway	p-value	overlap
Molecular Mechanisms of Cancer	4.75E-08	8.9 % (35/394)
EIF2 Signaling	1.66E-07	10.9 % (24/221)
mTOR Signaling	4.71E-07	10.9 % (22/201)
Regulation of eIF4 and p70S6K Signaling	6.10E-07	12.1 % (19/157)
Cardiac Hypertrophy Signaling	2.23E-05	8.9 % (21/236)
SAPK/JNK Signaling	2.53E-05	12.5 % (13/104)
Insulin Receptor Signaling	4.31E-05	10.6 % (15/141)

B

Upstream Regulator	Activation z-score	p-value of overlap
TP53	2,944	1,42E-03
PGR	2,421	8,76E-04
MAP4K4	-2,111	1,70E-03
mir-25	-2,396	1,97E-04
mir-19	-2,401	4,26E-05
miR-124-3p	-2,89	1,41E-03
miR-16-5p	-2,904	1,37E-04
miR-30c-5p	-3,162	3,26E-03

C

3 weeks post-I/R state

Canonical pathway	p-value	Overlap
Calcium Signaling	9.07E-06	3.9 % (8/206)
Hepatic Fibrosis	4.25E-05	3.7 % (7/187)
ILK Signaling	5.92E-05	3.6 % (7/197)
Tight Junction Signaling	1.91E-04	3.6 % (6/167)
Regulation of eIF4 and p70S6K Signaling	1.14E-03	3.2 % (5/157)

D

Upstream Regulator	Activation z-score	p-value of overlap
TGFB1	2,647	8,32E-05
SMTNL1	-2,000	1,45E-05
RUNX3	-2,000	3,29E-03
MYC	-2,315	4,21E-03
MYCN	-2,433	3,46E-03
KDM5A	-2,449	5,86E-05

Figure 21: Ingenuity pathway analysis for canonical pathways and upstream regulators of differentially regulated genes due to the I/R- intervention between the genotypes (D4KO vs WT). Cardiac transcriptome of 36 weeks old, male wild type and *Tbc1d4*-deficient mice on Chow diet in form of mRNA was sequenced using Illumina sequencing. Subsequently, the gained data was bioinformatically analyzed for differential gene expression due to genotype and I/R-intervention. Genes with a p-value of $p<0.01$ after multiple testing were taken into analysis with other measured genes as background control (see methods section 2.2.14). Significance threshold was set at $p<0.01$ for differentially regulated genes (n=4).

3.6 Effects of *Tbc1d4*-deficiency on cardiac unfolded protein response (UPR) and endoplasmic reticulum (ER) stress

The results of the transcriptome analysis revealed alterations of canonical pathways regarding endoplasmic reticulum (ER) stress and the unfolded protein response (UPR). Therefore, cardiac gene expression and protein abundance for specific marker genes and proteins for ER stress and the UPR were investigated via qPCR and Western Blotting using cardiac tissue of 36 weeks old, male WT and D4KO mice on a chow diet from pre- and post-I/R state.

3.6.1 Expression profile of marker genes for ER-stress response in WT and *Tbc1d4*-deficient hearts

Gene expression analysis for different markers of ER-stress response were measured heart tissue of WT and D4KO mice. Interestingly, only at level of *activating transcription factor 4* (*Atf4*) a significant alteration in gene expression due to the knockout of *Tbc1d4* in both pre-/R (Figure 22A) and post-I/R (Figure 22D) was detectable. Other markers like *X-box binding protein 1* (*Xbp1*) mRNA splicing ratio (Figure 22B, E) and *activating transcription factor 6* (*Atf6*) expression (Figure 22C, F) was unaltered regardless of the I/R intervention. Interestingly, without I/R intervention the lack of *Tbc1d4* leads to a decrease in *Atf4* expression (Figure 22A), while 3 weeks following reperfusion, an increase in the same parameter was detected (Figure 22D).

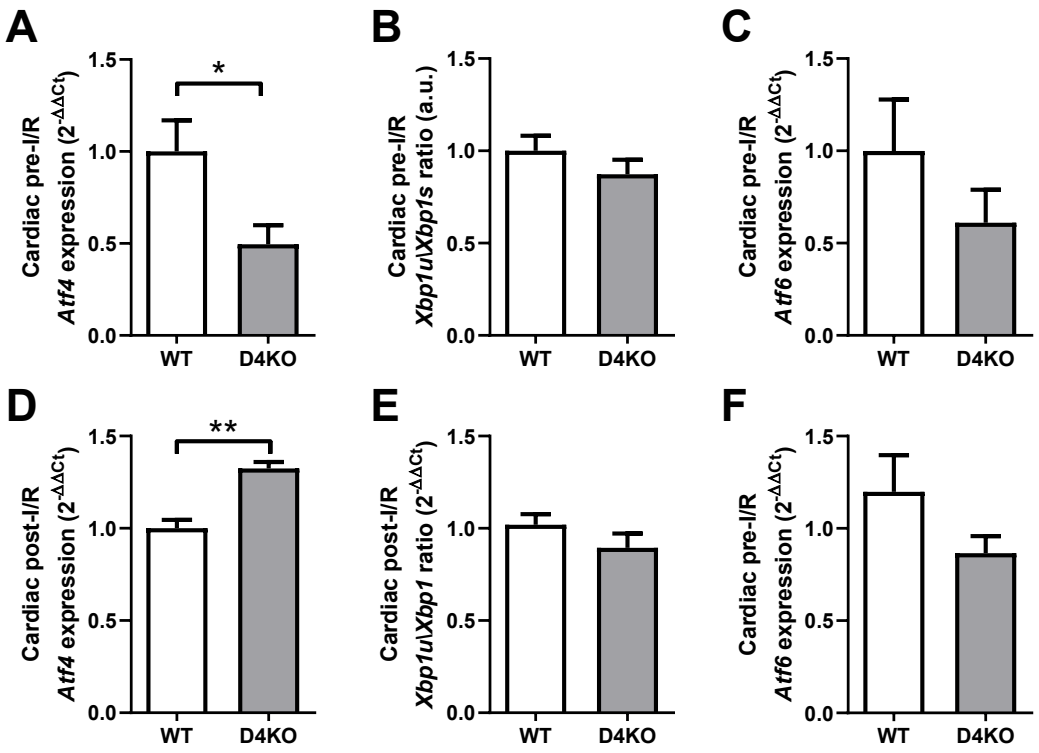

Figure 22: Gene expression of cardiac *Atf4*, *Atf6* and *Xbp1* splicing ratio as markers for ER stress in wild type and *Tbc1d4*-deficient mice 3 weeks post-I/R. Cardiac gene expression was measured in heart tissue of 36 weeks old, male wild type (WT; white bars) and *Tbc1d4*-deficient (D4KO; grey bars) mice on a Chow diet for pre I/R state (A-C) and 3 weeks post-I/R state (D-F), respectively. For this, marker genes for different pathways of ER stress response have been measured in form of *Atf4* expression (A, D), *Xbp1* splicing ratio (B, E) and *Atf6* expression (C, F). Data are presented as mean values ± SEM (n = 58). Two-tailed unpaired Student´s t-test with Welch´s correction. *p < 0.05, **p< 0.01

3.6.2 Protein content and phosphorylation of marker proteins for ER-stress response in WT and *Tbc1d4*-deficient hearts

Next to the situation on mRNA level, several marker proteins for ER-stress were investigated via Western Blot in heart tissues of WT and D4KO mice in 3 weeks post-I/R state. Interestingly, similar to the situation, only a distinct part of the ER-stress response was affected due to *Tbc1d4*-deficiency. While total protein abundance and phosphorylation at Ser51 of eukaryotic translation initiation factor 2α (eIF2α) was not affected due to the lack of *Tbc1d4*, the phosphorylation ratio revealed an increased phosphorylation status of eIF2α in *Tbc1d4*-deficient hearts compared to wild type controls

(Figure 23A). At the same time, Stress-activated protein kinase (SAPK) was not affected due to the lack of *Tbc1d4* on any of these parameters (Figure 23B).

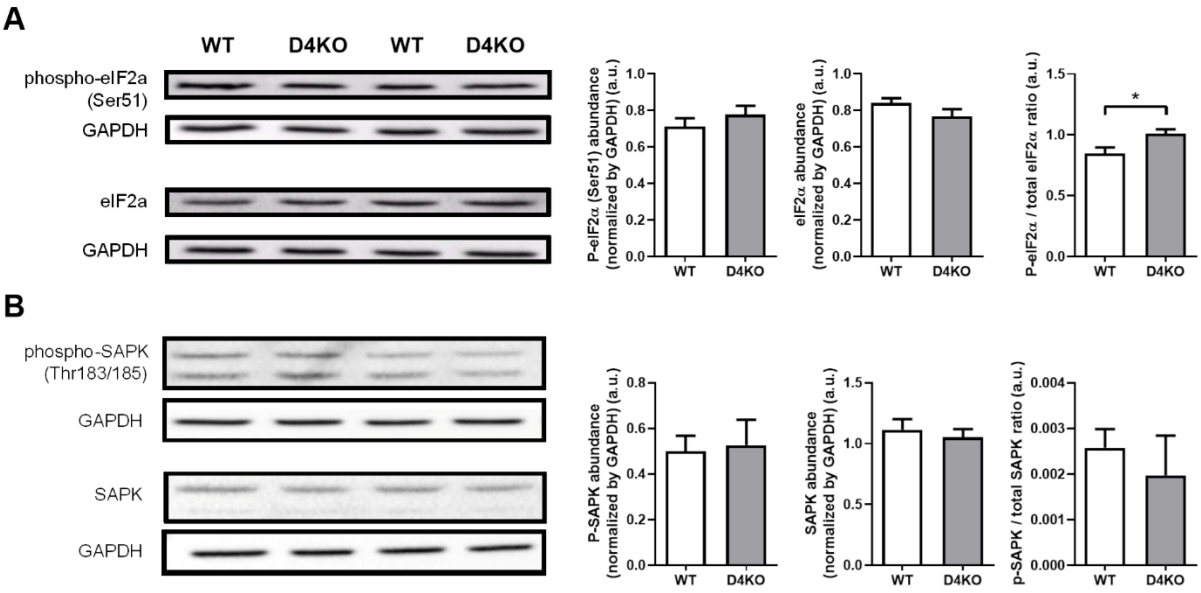

Figure 23: Protein abundance and phosphorylation of cardiac eIF2α and SAPK as markers for ER stress in wild type and *Tbc1d4*-deficient mice 3 weeks post-I/R. Cardiac protein content and phosphorylation was measured in heart tissue of 36 weeks old, male wild type (WT; white bars) and *Tbc1d4*-deficient (D4KO; grey bars) mice on a Chow diet for post-I/R state. For this, marker genes for different pathways of ER stress response have been measured in form of total abundance, ER-stress induced phosphorylation and the ratio of (A) eIF2α and (B) SAPK. Data are presented as mean values ± SEM (n = 5-8). Two-tailed unpaired Student´s t-test with Welch´s correction. *p < 0.05

3.7 Impact of *Tbc1d4*-deficiency on cardiac extracellular matrix (ECM) structure and remodeling

The results of the cardiac transcriptome analysis of WT and D4KO hearts revealed alterations of canonical pathways associated with extracellular matrix remodeling. Hence, extracellular matrix was analyzed in regards to its size on an ultrastructural histological level as well markers for potential ECM remodeling processes.

3.7.1 Assessment of extracellular matrix area via transmission electron microscopy (TEM)

Sections from the left ventricle of WT and D4KO hearts of mice on a chow diet were analyzed using transmission electron microscopy and morphometry as described in the methods section (chapter 2.2.8). In this, no gross alterations in cell morphology and organelle organization were observed. However, the images showed a markedly increased ECM area in D4KO samples (+43%) compared to the WT situation, indicating an altered remodeling of the cardiac ECM in D4KO mice (Figure 24).

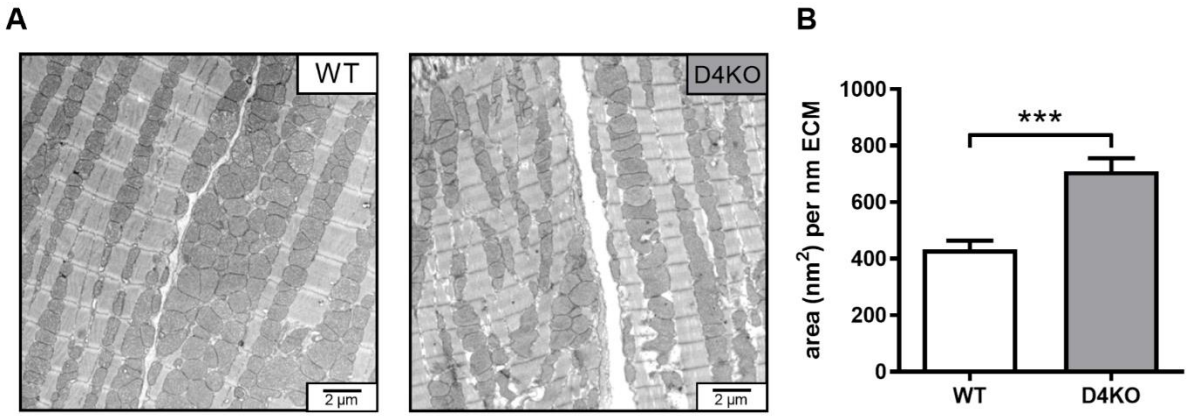

Figure 24: Transmission electron microscopy analysis of extracellular matrix area in cardiac left ventricle of wild type and *Tbc1d4*-deficient mice. (A) TEM-generated images were analyzed morphometrically for ECM area (white) and (B) subsequently quantified for 50 weeks old, male wild type (WT; white bars) and *Tbc1d4*-deficient (D4KO; grey bars) mice on a Chow-diet. Data are presented as mean values ± SEM (n = 3). Two-tailed unpaired Student´s t-test with Welch´s correction. ***p < 0.001

3.7.2 Gene expression of markers for ECM remodeling processes

The main regulators of ECM remodeling are the matrix metalloproteinases (MMPs) and the tissue inhibitors of metalloproteinases (TIMPs). The ratio of MMP/TIMPs is a marker for extracellular remodeling processes. In this course, elevated levels may indicate increased degradation of ECM, while lower levels indicate increased ECM generation and fibrosis. Therefore, cardiac *Mmp* and *Timp* expression profile was

assessed using qRT-PCR with whole heart mRNA from 36 week old and Chow-fed in WT and D4KO mice.

Interestingly, in *Tbc1d4*-deficient states the expression of certain *Mmp* genes is decreased. *Mmp13* expression is significantly reduced in D4KO hearts compared to the WT situation, while *Mmp2* and *Mmp9* show a tendency in the same direction (Figure 25A). speaking for a lower MMP content in hearts lacking *Tbc1d4*. Surprisingly, at the same time expression of *Timp1, Timp2, Timp3 and Timp4* is not altered by loss of *Tbc1d4* (Figure 25B).

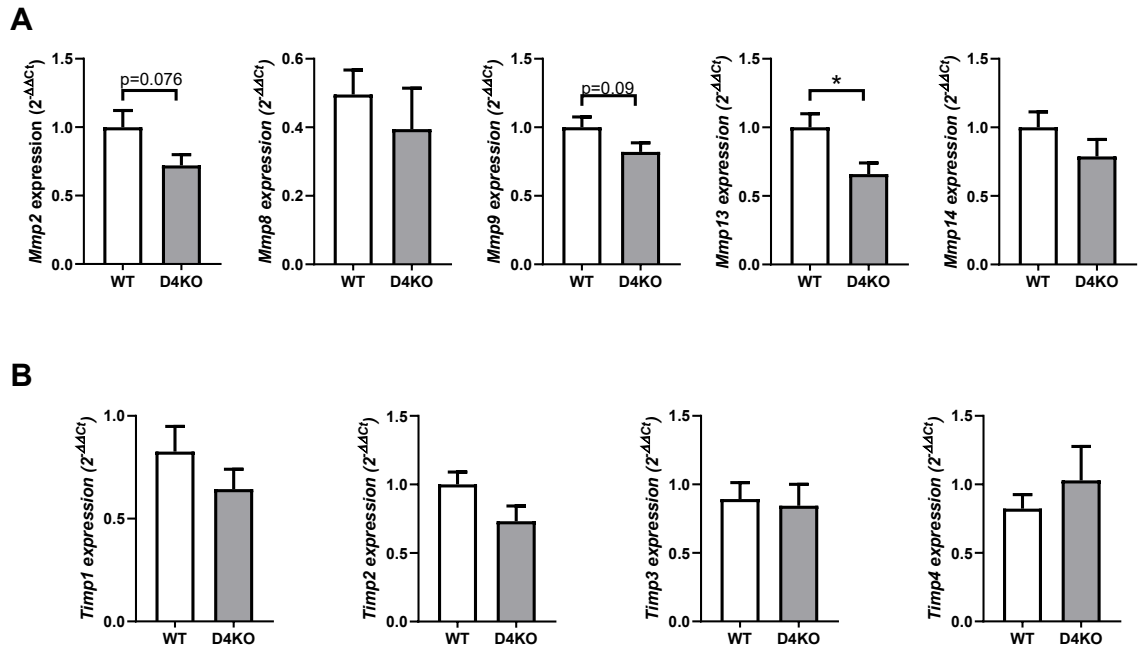

Figure 25: Cardiac expression of different matrix metalloproteinase (*Mmp*) and tissue inhibitors of metalloproteinases (*Timp*) as marker genes for ECM remodeling processes in pre-I/R state. Cardiac expression of various genes of the (A) *Mmp* and (B) *Timp* family was performed via qRT-PCR for 36 weeks old, male wild type (WT; white bars) and *Tbc1d4*-deficient (D4KO; grey bars) mice. Data are presented as mean values ± SEM (n = 9-10). Two-tailed unpaired Student´s t-test with Welch´s correction. *p < 0.05

Despite of this, the ratio of *Mmp2*/*Timp1* expression is decreased, indicating a decrease of MMP action in hearts of *Tbc1d4*-knockout mice compared to respective WT controls (Figure 26).

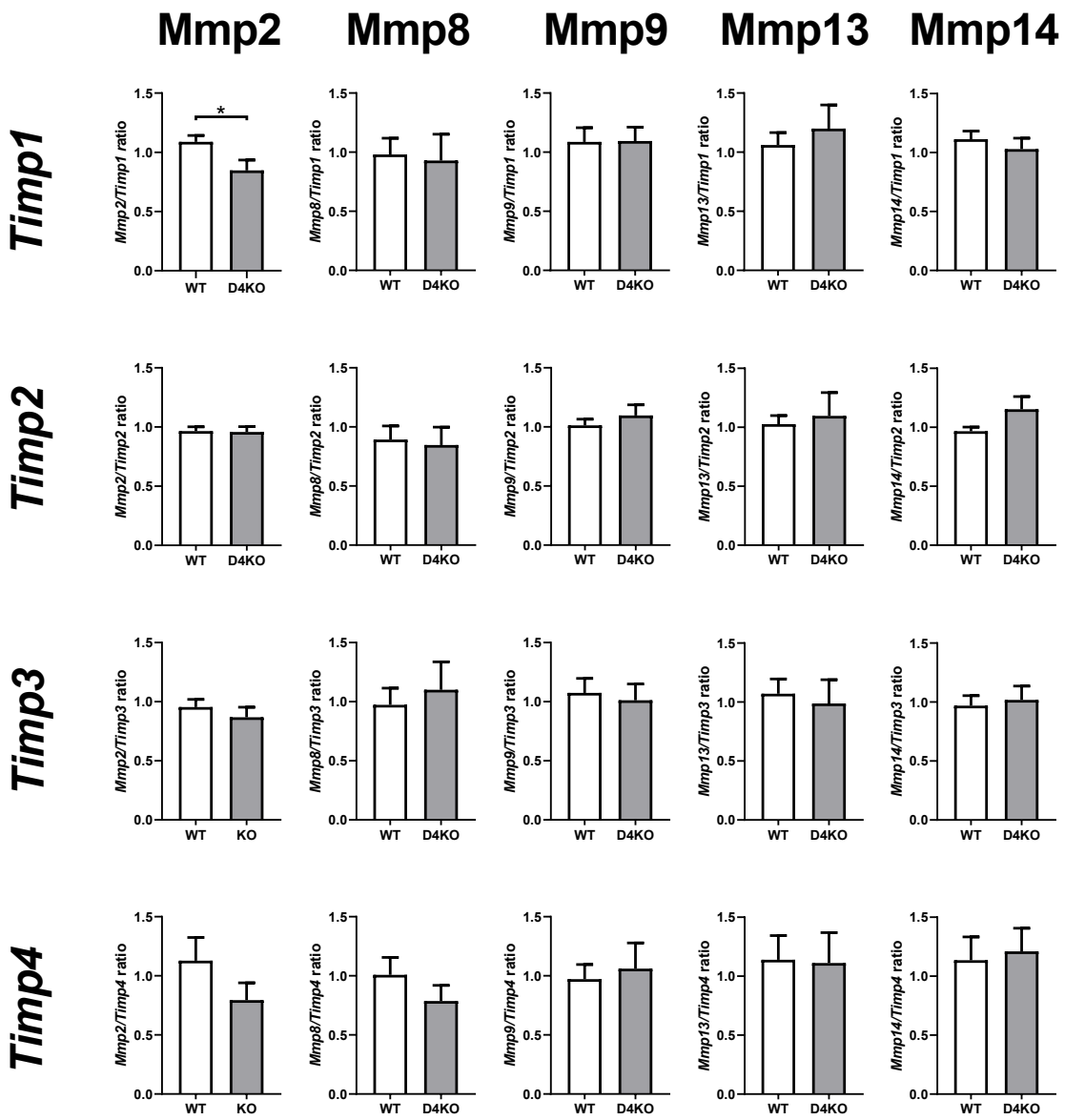

Figure 26: Ratios of cardiac *Mmp*/*Timp* expression as markers for extracellular matrix remodeling processes in pre-I/R state. Cardiac expression of various genes of the (A) *Mmp* and (B) *Timp* family was performed via qRT-PCR for 36 weeks old, male wild type (WT; white bars) and *Tbc1d4*-deficient (D4KO; grey bars) mice. Based on these results, individual *Mmp*/*Timp* expression rations were calculated as indicators for MMP activity. Data are presented as mean values ± SEM (n = 9-10). Two-tailed unpaired Student´s t-test with Welch´s correction. *p < 0.05

Interestingly, in contrast to the pre-I/R state, 3 weeks following the I/R-intervention *Mmp* expression (Figure 27) and *Mmp/Timp* ratio (Figure 28) were not altered.

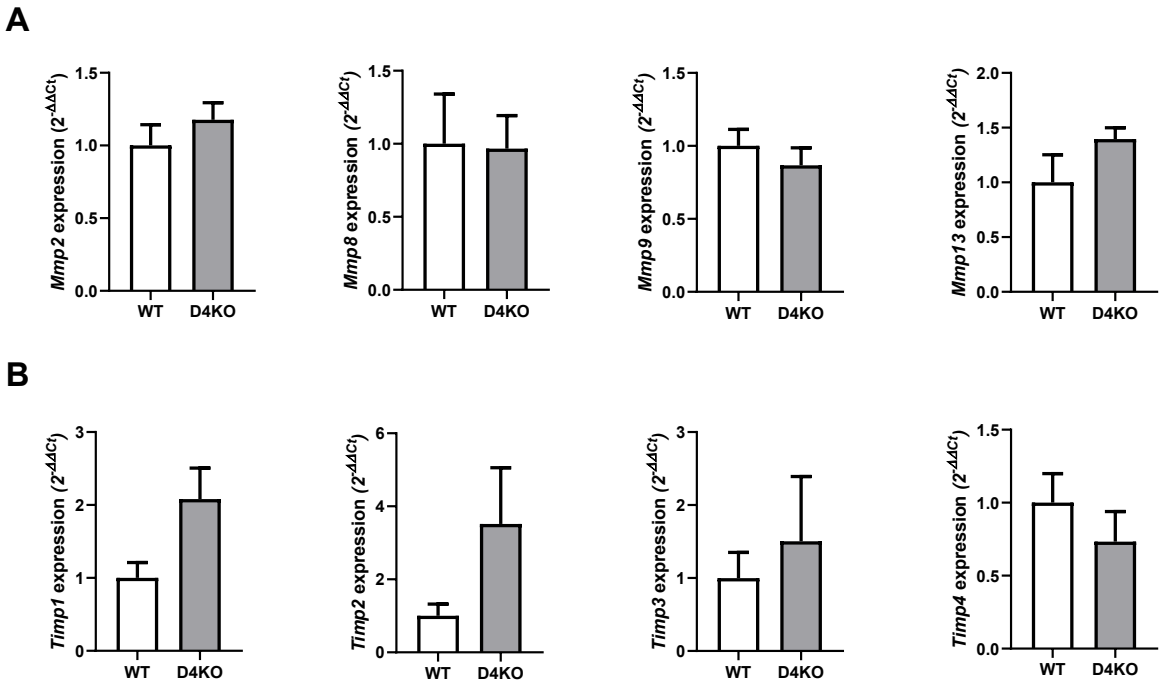

Figure 27: Cardiac expression of different matrix metalloproteinase (*Mmp*) and tissue inhibitors of metalloproteinases (*Timp*) as marker genes for ECM remodeling processes 3 weeks post-I/R. Cardiac expression of various genes of the (A) *Mmp* and (B) *Timp* family was performed via qRT-PCR for 36 weeks old, male wild type (WT; white bars) and *Tbc1d4*-deficient (D4KO; grey bars) mice 3 weeks post-I/R. Data are presented as mean values ± SEM (n = 5-6).

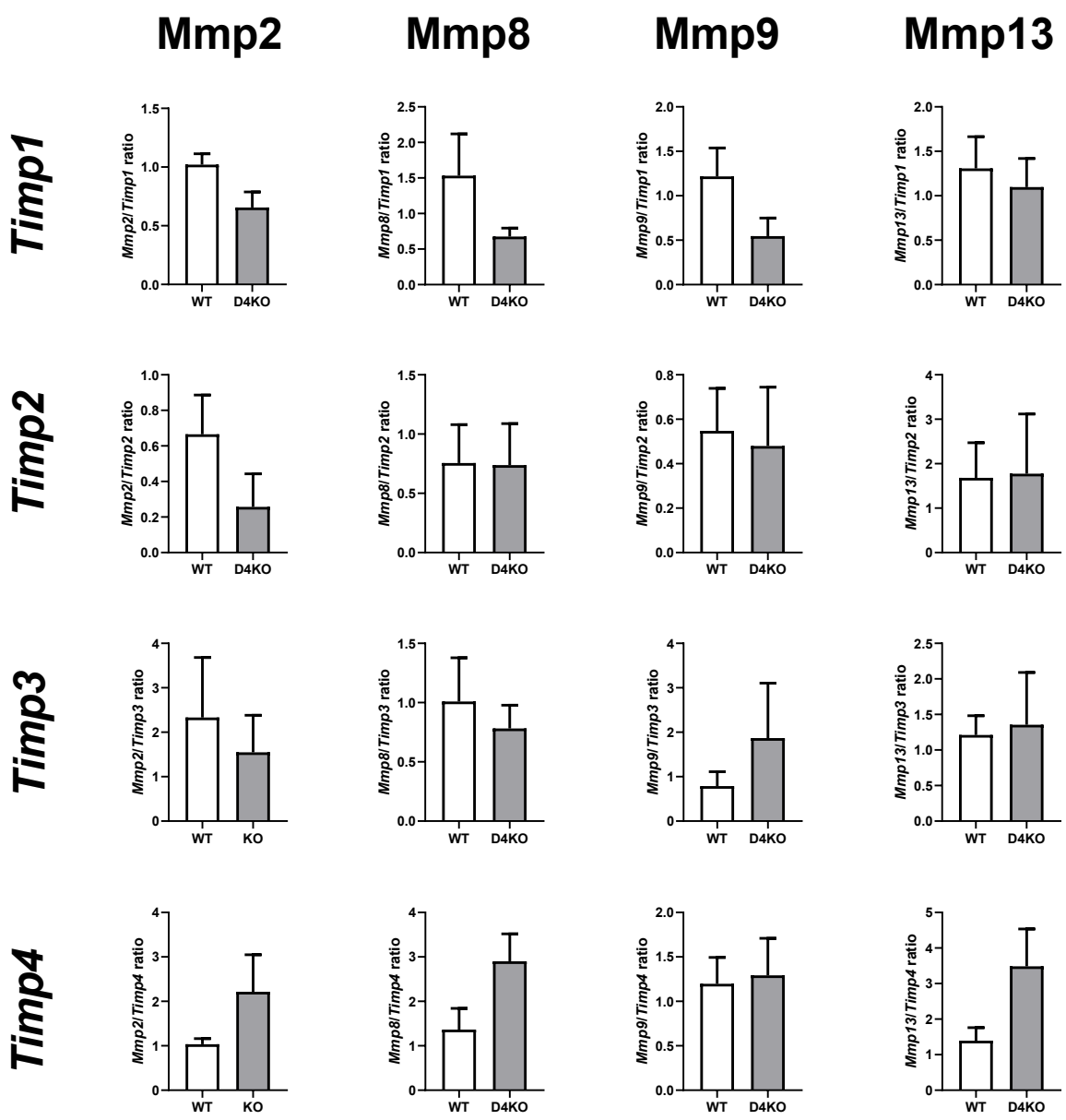

Figure 28: Ratios of cardiac *Mmp*/*Timp* expression as markers for extracellular matrix remodeling processes 3 weeks post-I/R. Cardiac expression of various genes of the (A) Mmp and (B) Timp family was performed via qRT-PCR for 36 weeks old, male wild type (WT; white bars) and *Tbc1d4*-deficient (D4KO; grey bars) mice 3 weeks post-I/R. Based on these results, individual *Mmp*/*Timp* expression rations were calculated as indicators for MMP activity. Data are presented as mean values ± SEM (n = 5-6).

4. Discussion

4.1. Deficiency of *Tbc1d4* leads to impaired cardiac insulin-stimulated glucose uptake

One aim of this study was to investigate the impact of *Tbc1d4*-deficiency on cardiac carbohydrate utilization and glucose uptake. In this course, ex vivo assays of [^{3}H]-deoxyglucose uptake in isolated intact papillary muscles of the cardiac left ventricle revealed that the loss of *Tbc1d4* leads to decreased responsiveness to insulin as stimulator of cardiac glucose uptake as well as reduced abundance of GLUT4 in the heart. Interestingly, at the same time the basal glucose uptake was not altered due to the knockout of *Tbc1d4*. *In vivo* 18-FDG-PET/CT scanning confirmed unchanged cardiac glucose flux in *Tbc1d4*-deficient mice whereas influx of labeled-glucose into the heart during a glucose bolus was substantially reduced compared to corresponding wild type controls

Therefore, TBC1D4 can be defined as a critical mediator of cardiac glucose homeostasis via regulation of cardiac insulin-stimulated glucose uptake. Interestingly, only a few studies focused on the role of TBC1D4 in in the heart in the heart. Similar to the results in the present study in *Tbc1d4*-knockout mice, a report on AS160-knockout rats showed decreased cardiac GLUT4 abundance due to the lack of AS160 (Arias et al., 2019). Paradoxically, AS160-knockout rats showed increased glucose uptake during hyperinsulinemic-euglycemic clamps (Arias et al., 2019). The authors speculated that this observation could be due to alterations in lipid composition, which was however not detectable (Arias et al., 2019). This is in accordance with the observation of unaltered lipid composition due to the knockout of *Tbc1d4* in the present study.

This observed impairment of glucose uptake in murine hearts is similar to the situation in other tissues of *Tbc1d4*-deficient mice such as skeletal muscle (Chadt et al., 2015) and adipose tissue (Lansey et al., 2012). Studies in the soleus skeletal muscle of

Tbc1d4-deficient mice show no difference in basal glucose uptake while the insulin-stimulated glucose uptake is markedly decreased compared to wild type controls. At the same time, the GLUT4 content in soleus muscle is reduced due to the knockout of *Tbc1d4* (Chadt et al., 2015). Thus, the findings on GLUT4-mediated glucose uptake in the heart in the present study are consistent with an important role of TBC1D4 in the regulation of glucose transport in other insulin-sensitive tissues.

Skeletal muscle contains both, TBC1D1 and TBC1D4 at variable ratios, depending on the muscle type (Chadt et al., 2015). In the present study, determination of *Tbc1d4*-abundance in the murine heart tissue via qRT-PCR identified *Tbc1d4* as the major expressed RabGAP gene compared to its close paralogue *Tbc1d1.* This observation is consistent with prior reports in which *Tbc1d4* action is associated with oxidative skeletal muscle types, whereas *Tbc1d1* is predominantly active in glycolytic muscle types (Chadt et al., 2015). Here, the glycolytic *extensor digitorum longus* (EDL) showed unaltered insulin-stimulated glucose uptake and GLUT4 content due to *Tbc1d4*-deficiency (Chadt et al., 2015). Interestingly, the same effects of *Tbc1d4*-deficiency observed in in soleus muscle were seen in EDL muscles lacking *Tbc1d1*. The similarity of the glucose homeostasis situation in the heart and the oxidative soleus muscle rather than the glycolytic EDL are consistent with the characterization of cardiomyocytes being mainly fueled by mitochondrial lipid oxidation (Martínez et al., 2017).

Interestingly, on a whole body level, the combined knockout of *Tbc1d1* and *Tbc1d4* has been shown to induce higher intolerance for glucose and insulin compared to the ablation of one RabGAP alone. This observation suggests a compensatory mechanism in case of singular RabGAP-deficiency on the level of the remaining functional RabGAP. Since the present study focused on *Tbc1d4* as the major RabGAP expressed in the heart, further assessment of the combined effects of *Tbc1d1* and *Tbc1d4* (e.g. using a double-

knockout mouse model for these genes) could be performed. By this, the combined role of these RabGAPs and their interplay could refine the image of RabGAP action in the heart and lead to new potential clinical intervention points for improved myocardial healing following MI.

The heart expresses mainly two GLUT-family glucose transporters, GLUT1 and GLUT4. While the former is expressed ubiquitously, the latter is expressed almost exclusively in skeletal muscle, the heart and adipose cells (Shao & Tian, 2015). In order to investigate whether *Tbc1d4*-deficiency alters the abundance of specific GLUTs, Western Blot analysis of glucose transporters GLUT1 and GLUT4 was performed, since these are the main proteins responsible for cardiac glucose uptake (Shao & Tian, 2015). Based on this approach, a substantial decrease in cardiac GLUT4 abundance due to the knockout of *Tbc1d4* was observed.

Interestingly, at the same time the abundance of GLUT1 remains unaffected and thereby excludes its involvement in potential compensatory effects on cardiac glucose uptake at this level. Although it has to be noted, that in the present study the focus was set on protein abundance of glucose transporters that do not directly reflect the situation of their actual presence at the plasma membrane. Studies from glycolytic EDL skeletal muscle of *Tbc1d1*-deficient mice report a decrease of GLUT4 at the cell surface after insulin stimulation (Chadt et al., 2015). Since the situation on glucose homeostasis in *Tbc1d1*-deficient glycolytic muscle is comparable to the *Tbc1d4*-deficient oxidative muscle, a similar effect on the level of the heart can be assumed. However, whether this observation is due to impaired trafficking of GLUT4-vesicles towards the cell surface or due to the already reduced total GLUT4 content in the muscle remains to be elucidated.

This observation however is in accordance with the observed phenomenon of unaltered basal glucose uptake but inhibited insulin-responsive glucose uptake.

Since GLUT1 is seen as responsible for the main part of basal glucose uptake while GLUT4 is predominantly attributed to the glucose uptake upon insulin stimulation (Shao & Tian, 2015), the reduction of cardiac GLUT4 content in *Tbc1d4*-deficient mice explains the observed impairment of insulin-stimulated glucose uptake. At the same time, due to the unaltered GLUT1 abundance in the heart, the basal glucose uptake remains unaffected. Therefore, partially, these impaired insulin-stimulated glucose uptake due to*Tbc1d4*-deficiency in the heart might be explained due to a secondary effect of GLUT4 reduction in the heart. Other studies identified the lysosome as source of GLUT4 degradation under condition of TBC1D4 deficiency or inactivation of its RabGAP function (Xie et al., 2016). The authors speculate on either a direct role of *Tbc1d4* on lysosomal degradation processes or a secondary effect of accelerated lysosomal degradation due to higher subcellular activity of GLUT4-vesicles (Xie et al., 2016). The impaired glucose uptake in the hearts of *Tbc1d4*-defiencient mice might also explain the impaired phenotype of impaired cardiac function and morphology following I/R. Especially under conditions of oxygen deprivation, the switch towards glucose as cardiac fuel is of importance, since it requires less oxygen for metabolization compared to lipids.

However, other studies on the role of GLUT4 in cardiac metabolism suggest another role of *Tbc1d4* action in the course if I/R-induced injury in the heart. A study in mice with a cardiac-specific knockout of GLUT4 reports decreased utilization of glucose accompanied by dysfunctions in heart function during ischemia (Tian & Abel, 2001), similar to the situation in *Tbc1d4*-deficient mice. However, interestingly, these GLUT4-deficient mice show an already elevated glucose cardiac uptake at basal state (Tian & Abel, 2001), which is not observed in mice with *Tbc1d4*-deficiency, despite of decreased

levels of cardiac GLUT4 abundance. This difference in basal glucose uptake between these two knockout mouse models is crucial. It reveals that *Tbc1d4*-deficiency affects only the insulin-stimulated response and does not lead to alterations in glucose uptake at basal level. Supporting this, other studies of GLUT4-deficient hearts revealed an increase in GLUT1 levels (Katz et al., 1995) as potential compensatory mechanism. However the heterozygous knockout of GLUT 4, which led to reductions in GLUT4 content comparable to the ones seen in *Tbc1d4*-deficient hearts did not alter GLUT1 content (Zisman et al., 2000). In an additional study, hearts of cardiac GLUT4-deficient mice showed maladaptive hypertrophy (Wende et al., 2017), which is different from the *Tbc1d4*-knockout situation of no differences in body to heart weight ratios independent of genotype and analyzed diets.

Collectively, *Tbc1d4* is a crucial regulator of insulin-stimulated cardiac glucose uptake. Although the main site of glucose disposal in response to insulin is skeletal muscle with 60-80% (Ng et al., 2012), the specific need of steady energy supply in the heart underlines the need for proper cardiac glucose supply. Especially under stress conditions, such as ischemia, the adequate switch between lipids and glucose as fuel is crucial for proper cardiac function. Therefore, the proper function of GLUT4-trafficking upon insulin-stimulation could be a vital process for adaptation towards ischemia. The reduction of cardiac GLUT4 content due to the loss of *Tbc1d4* provides one explanation for the phenotype of impaired glucose cardiac homeostasis, but cannot be the sole source. Especially due to the differences in heart morphology and basal glucose uptake between mice lacking GLUT4 and *Tbc1d4*-deficient mice, it can be suggested that *Tbc1d4* might have another GLUT4-independent function on cardiac post-infarction healing.

4.2. Deficiency of *Tbc1d4* impairs cardiac function and morphology following ischemia/reperfusion-induced injury

Next to the role of *Tbc1d4* on cardiac glucose metabolism, the aim was to determine its impact on ischemia and reperfusion mediated injury in the heart. Since the healthy heart adapts to environmental circumstances in switching of substrates for optimal energy production, the impairments of glucose uptake can be a limiting factor, especially under circumstances of oxygen depletion and the thereby triggered reduced efficiency of lipids as cardiac fuel.

Under normal conditions, the heart relies mainly on lipids for energy production, since the amount of generated energy in form of ATP gained from one lipid molecule is higher than from one glucose molecule. For example, the complete oxidation of one palmitate (C16) molecule delivers 105 molecules ATP, while the oxidation of glucose only produces 31 molecules of ATP (Jaswal, Keung, Wang, Ussher, & Lopaschuk, 2011). Although the ATP gain form lipids is higher, it also requires more oxygen than the oxidation of glucose. Hence, the phosphorous/oxygen (P/O) ratio, as indicator for the number of molecules ATP produced per atom of oxygen, of palmitate is lower than the one of glucose, making palmitate less efficient based on oxygen demand (Jaswal et al., 2011),. Since the human heart requires 70-80% of the molecular oxygen (O_2) delivered by the blood (Cunha, Poole, Lorenzetti, & Ferreira, 1992), circumstances of insufficient oxygen supply (e.g. ischemia) make glucose the favorable substrate for energy production over lipids.

The assessment of cardiac function and morphology following I/R-intervention revealed a severe impairment of these parameters in hearts of *Tbc1d4*-deficient mice. While at basal state the cardiac function of *Tbc1d4*-deficient mice in terms of endsystolic volume is not altered compared to wild type controls, the development over a time course

of 3 weeks leads to a markedly increased endsystolic volume, indicating impaired heart function. This observation reveals that the knockout of *Tbc1d4* alone does not affect cardiac function in this parameter. Only after induction of I/R the deficiency of *Tbc1d4* leads to an impaired cardiac function. Therefore, it can be speculated that *Tbc1d4* has a role in cardiac adaptation to I/R-induced myocardial injury. Other typical echocardiographic parameters of cardiac function, such as ejection fraction and cardiac output do not reach statistical significant alterations during the time course of 3 weeks between the *Tbc1d4*-deficient and wild type situation.

Three weeks post-I/R, Azan staining and morphometric analysis of heart sections uncovered a marked increase in infarction size associated with the lack of *Tbc1d4*. At the same time in *Tbc1d4*-deficient hearts, the left ventricular wall thickness is decreased, while the left ventricular lumen increased compared to corresponding wild type controls, indicating a reduction of myocardial muscle mass. Due to unaltered cardiac function at basal, i.e. non-infarcted state and the consecutive progressive impairments over the time course of 3 weeks, the data suggest that *Tbc1d4* may play a role in the long-term post-infarction healing and remodeling processes rather than in the acute response to MI. One possible effect of *Tbc1d4*-deficiency in this manner could be an increased apoptosis or necrosis of cardiomyocytes during this time, which could be indicating a *Tbc1d4*-dependent mechanism in regards to ROS-induced oxidative damage. Another possibility is an impaired recovery from the I/R-intervention, which would indicate a role of *Tbc1d4* in post-MI remodeling processes, e.g. regarding fibrosis or ECM remodeling.

At the same time, immunohistochemical staining for platelet endothelial cell adhesion molecule 1 (PECAM-1) and vascular cell adhesion molecule 1 (VCAM-1), as markers for angiogenesis and inflammatory processes, revealed no differences in their abundance or localization due to the loss of *Tbc1d4*. This observation suggest no

alterations in regards to-revascularization or angiogenesis, as well as inflammatory migration processes from the blood stream at this time point.

A previous study investigated the impact of *Tbc1d4* on cardiac physiology in a different approach (Quan et al., 2015). For this, the authors analyzed a knock-in mouse model in which the phosphorylation of TBC1D4 via the AKT-pathway was blunted. In the described mouse model, an amino acid substitution of Thr649 for Ala (TBC1D4^{Thr649Ala}) leads to an inhibition of TBC1D4 phosphorylation by AKT at this site. Thereby, TBC1D4 remained functional in this experiment, while specifically the AKT-mediated response to insulin was interrupted. Interestingly, when these mice were subjected to myocardial infarction, no impairments in the outcome could be detected due to the loss of the AKT signal of TBC1D4, which is in contrast to the observed phenotype of diminished cardiac function and structure found *Tbc1d4*-deficient mice. At this point, it has to be noted, that the kind of ischemic intervention differed between the present study and the work of Quan et al. While in both compared studies the LAD of was occluded the study of Quan at al contained a permanent occlusion without reperfusion.

Interestingly, TBC1D4^{Thr649Ala} mice showed leading to an increase in R-wave amplitude in ECG, which was discussed as a potential role of TBC1D4 in the cardiac electrical conduction system (Quan et al., 2015). An elevation in R-Wave may suggest a cardiac hypertrophy, but neither in the study of Quan et al. nor in the present study cardiac hypertrophy in the pre-infarcted state was detected. In fact, the transcriptome analyses of whole heart tissue pre-I/R revealed differential expression of genes associated with cardiac hypertrophy, indicating a potential susceptibility of *Tbc1d4*-deficient hearts compared to hearts from wild type littermates. Interestingly, mice containing a mutation for TBC1D4^{Thr649Ala} show an increased heart to body weight ratio (S. Chen, Wasserman, MacKintosh, & Sakamoto, 2011), which might be an indicator for cardiac hypertrophy.

This finding however could not be replicated in the present study, where body weight to heart weight ratio of *Tbc1d4*-deficient mice was unaltered. Combined, these results suggest a potential role of TBC1D4 in post-infarction healing that might be at least partially independent of AKT-signaling (Quan et al., 2015), since effects on cardiac function and morphology following ischemic intervention were only present under knockout conditions of TBC1D4 and not inhibition of phosphorylation through AKT.

Alteration of ECG in terms of R-wave amplitude was also observed in the present study in our *Tbc1d4*-deficient mice. Although no differences in basal R-Wave pattern like in TBC1D4^{Thr649Ala} mice was detected, the relative R-Wave amplitude during acute reperfusion phase was elevated due to the loss of *Tbc1d4*.

This finding may suggest a potential role of *Tbc1d4* in cardiac electrical conduction system. Interestingly, the R-Wave amplitude is not only a marker for cardiac hypertrophy (Mazzaro Cdo et al., 2008), but a has also been described to be an indicator for cardiac ischemia (Ribeiro, Louie, Hillis, Davis, & Maroko, 1979). The exact role of *Tbc1d4* on the cardiac electrical conduction system remains to be elucidated. A potential mechanism could be the regulation of ion homeostasis in cardiomyocytes by TBC1D4, since it has already been described to be involved in sodium channel and ATPase trafficking in kidneys (Comellas et al., 2010; Liang, Butterworth, Peters, & Frizzell, 2010).

Another interesting finding in the work of Quan et al is the observation of increased TBC1D1 abundance in the infarcted heart (Quan et al., 2015). This would suggest a compensatory mechanism of the lack of TBC1D4 action through its close orthologue TBC1D1. However, since the in *Tbc1d4*-deficient hearts as presented in this study, the myocardial damage is increased compared to WT controls, a potential compensatory mechanism at the level of *Tbc1d1* is not present or nut sufficient enough to rescue the phenotype.

Collectively, TBC1D4 is necessary for adequate adaptation to I/R-induced injury in the heart in terms of heart function and structure. The action of TBC1D4 in this course might be independent of AKT signaling and may also affect cardiac electrical physiology.

4.3. Deficiency of *Tbc1d4* does not affect mitochondrial function/morphology and lipid profile in the heart

As an organ, which uses mainly lipids as energy source under normal conditions, the heart relies on the mitochondria and their function for cardiac energy supply and metabolic switching upon environmental factors. Since the uptake of glucose is disturbed under circumstances of *Tbc1d4*-deficiency, one aim of this study was to elucidate the role of mitochondria in hearts lacking *Tbc1d4*.

Although especially the reperfusion phase of cardiac I/R-injury has been described to be particularly injurious to the mitochondria (Ramachandra, Hernandez-Resendiz, Crespo-Avilan, Lin, & Hausenloy, 2020; Siasos et al., 2018; Walters, Porter, & Brookes, 2012), the unaltered mitochondrial function and mass in the heart of *Tbc1d4*-knockout animals suggest, that the observed worse outcome of *Tbc1d4*-deficient hearts following I/R is unlikely to be explained at the level of mitochondria. Conversely, a study of cardiac GLUT4-deficient mice showed disturbances in mitochondrial metabolism (Wende et al., 2017). This is another indicator for an additional role of *Tbc1d4* as a mediator of the observed worse outcome after I/R-intervention, other than the impaired glucose metabolism due to reduction in cardiac GLUT4 abundance.

Another aim was to elucidate the potential role of lipid composition in the heart as an indicator for potential differences in cardiac fuel supply due to the knockout of *Tbc1d4*. Prior studies have linked silencing of *Tbc1d4* in L6 myotubes to alterations in intracellular

lipid milieu (Miklosz et al., 2017). Further studies revealed TBC1D4 and TBC1D1 as regulators of long-chain fatty acid uptake (Benninghoff et al., 2020). The cardiac lipid profile does not only affect the risk for development of CVD (Tomczyk & Dolinsky, 2020) but also influence post-MI remodeling processes (Ji et al., 2017). Therefore, TBC1D4 might be a regulator of cardiac lipid content and composition, which may be affecting post-MI healing processes. The result showed that knockout of *Tbc1d4* led to a reduction in cardiac content of C14:0 and C18:1 lipid species. Moreover, for C14:0 also the feeding of a HFD led to reduction of its abundance in wild type hearts. Interestingly, C14:0 intake was associated with a lower risk for MI in a human cohort study (Praagman et al., 2019). However, in another study C14:0 intake was associated with increase in risk for MI (Kabagambe, Baylin, Siles, & Campos, 2003). Hence, the exact role of fatty acid consumption and their cardiac abundance remains to be elucidated.

Moreover, in clusters of lipid species in terms of their saturation status alterations due to the loss of *Tbc1d4* were observed. However, certain activity indices for enzymatic function regulating the length or saturation on specific lipid species, revealed impairments in *Tbc1d4*-deficient hearts. Although elongase and desaturase activity was only altered in wild type animals due to the diet intervention (Figure 15), *Tbc1d4*- animals showed an elevated thioesterase index on a Chow diet compared to corresponding WT controls. Interestingly, thioesterases have been associated with cardio-protective effects in diabetes models (Yang et al., 2012).

In conclusion, *Tbc1d4*-deficiency does not affect the cardiac mitochondria in terms of function, size and distribution. Moreover, the abundance and composition of cardiac lipids is due to the presence of TBC1D4 needs to be elucidated despite of alterations of some lipid species and indices for enzymatic activity in regards to lipid remodeling.

However, these results indicate an additional role of *Tbc1d4* in post-MI healing apart from the accompanied reduction in GLUT4 content.

4.4. Deficiency of *Tbc1d4* alters cardiac transcriptome

In order to identify molecular mechanisms mediate the effects of TBC1D4 in post-I/R healing processes the cardiac transcriptome of *Tbc1d4*-deficient and wild type mice was analyzed using Next Generation RNA Sequencing technology (RNASeq). In addition to the two genotypes, *Tbc1d4* knockout and wild type, also the pre-I/R and the 3 week post-I/R states were compared. Interestingly, the results revealed not only a different number of genes affected comparing the pre-I/R and post-I/R situation between *Tbc1d4*-deficient animals and corresponding wild types, but also quite different sets of differentially regulated genes with only small overlap. This indicates that *Tbc1d4* has a distinct part in the processes of post-I/R molecular events of remodeling.

Consequently, different pathways and potential upstream regulators were revealed trough ingenuity Pathway analysis (IPA). Interestingly, already without any kind of I/R intervention, the lack of *Tbc1d4* leads to the alteration of pathways associated with insulin receptor signaling. This supports the importance of *Tbc1d4* in cardiac glucose homeostasis similar to its role in skeletal muscle (Chadt et al., 2015). This observation, along with the impairment of insulin-stimulated glucose uptake and reduction of GLUT 4 content in this study, strengthen the suggested role of *Tbc1d4* as an important regulator of cardiac glucose uptake. Moreover, the alterations of gene expression regarding pathways of myocardial hypertrophy suggests an important role of proper *Tbc1d4*-function for normal heart physiology. This is also in accordance with an observation of cardiac increased heart to body weight ratio in prior studies on TBC1D4^{Thr649Ala} mice (Quan et al., 2015). Although this cardiac hypertrophy pathway is affected due to the

knockout of *Tbc1d4*, neither in *Tbc1d4*-deficient nor in TBC1D4^{Thr649Ala} mice, cardiac hypertrophy was detectable or reported (Quan et al., 2015), respectively.

Another interesting finding relates to the 3 weeks post-I/R transcriptome analysis. At this time-point, a large portion of the myocardium has already been replaced by fibrotic tissue, as shown in the Azan staining of the present study. The fibrotic expansion of the wound is likely required to maintain cardiac stability and function and could explain the lower number of differentially expressed genes in the 3 weeks post-I/R state compared to pre-I/R situation. However, surprisingly, alterations in pathways involving the activity of genes associated with fibrosis are apparent at this time point. This indicates a possible role of *Tbc1d4* the transcriptional regulation of wound healing regarding post-MI remodeling processes in the heart.

4.5. Deficiency of *Tbc1d4* is associated with distinct activation of ER-Stress response

The result of cardiac transcriptome analysis linked *Tbc1d4*-deficiency to alterations in ER-stress and the unfolded protein response. Especially in myocardial infarction, the generation of reactive oxygen species and oxidative stress lead to a response of the endoplasmic reticulum. Disruption of ER function by various stimuli have been reported to lead to accumulation of misfolded proteins and consequently to ER stress (S. Wang et al., 2018). Especially under conditions of cardiac ischemia and reperfusion events, the ER stress response has been shown to be critical for the myocardial damage following I/R (Zhang et al., 2017). However, the kind of response is highly dependent on the time of ER-stress (M. Liu & Dudley, 2015). Depending on the time, the response can either be protective and focusing on cell survival or triggering apoptotic processes and inducing cell death (M. Liu & Dudley, 2015).

Briefly, in eukaryotic cells, ER-stress can be mediated via three signaling pathways (Lenna & Trojanowska, 2012) (Figure 29). One of them is initiated via protein kinase RNA-like endoplasmic reticulum kinase (PERK). Consequently, PERK phosphorylates eukaryotic initiation factor 2α (eIF2α), which leads to an reduction of global protein synthesis (Hughes & Mallucci, 2019) as well as the phosphorylation of activating transcription factor 4 (ATF4). While ATF4 can induce cell-protective responses, it also induces transcription of CCAAT-enhancer-binding protein homologous protein (CHOP), which triggers an apoptotic response.

Another pathway of the ER-stress response is mediated through Inositol-Requiring Enzyme 1 (IRE1), which induces splicing of X box binding protein 1 (XBP1) mRNA in order to allow translation of the active form of XBP1. The ratio of spliced and unspliced *Xbp1* mRNA is a surrogate marker for ER-response. While XBP1 induces cell survival processes, e.g. through Chaperones, another downstream target of XBP1, the stress activated protein kinase (SAPK/JNK) triggers apoptotic response (Kadowaki & Nishitoh, 2013).

A third pathway of ER-Stress response is mediated via Activating transcription factor 6 (ATF6). Similar to XBP1, activation of ATF6 can lead on to cell-protective ER-stress response.

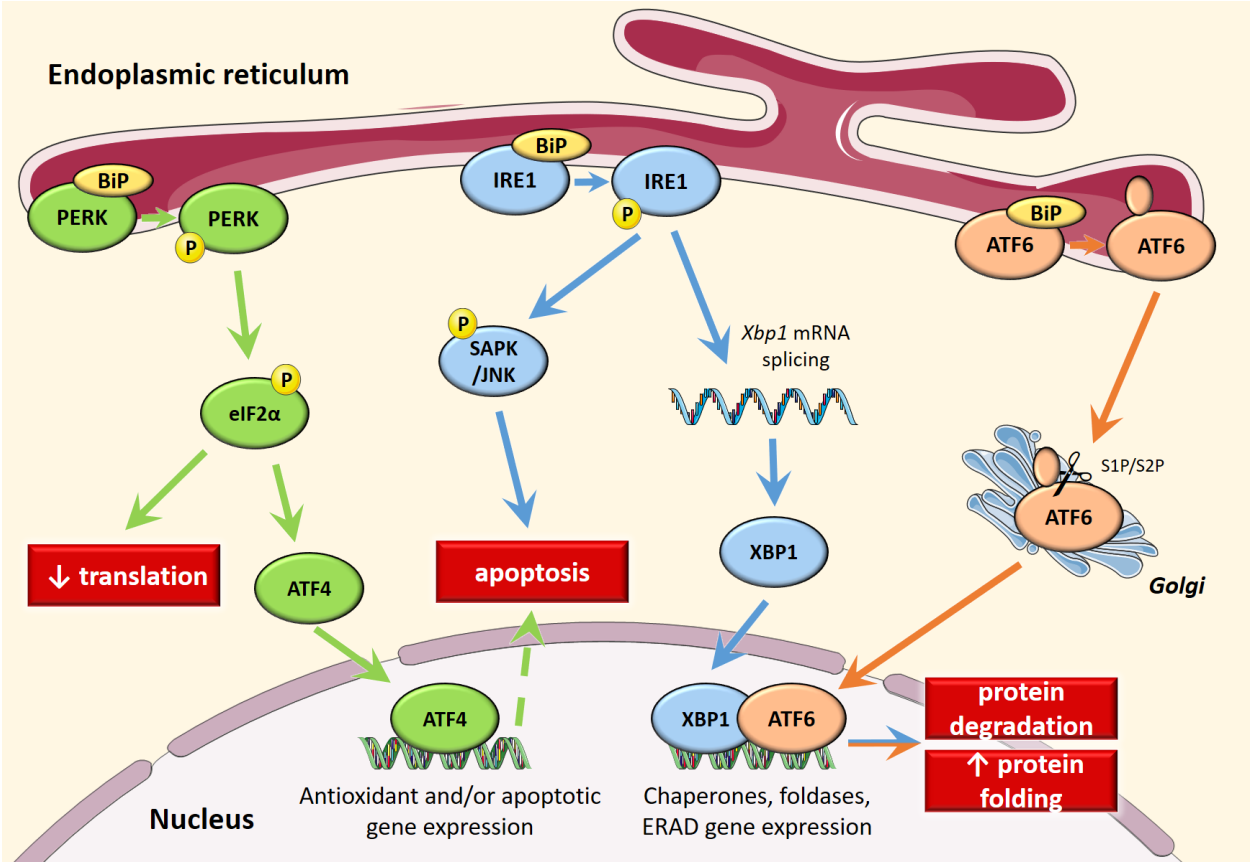

Figure 29: Overview of the different pathways of the unfolded protein response (UPR). Due to severe or prolonged ER stress and unfolded or misfolded proteins, the ER stress response is triggered via three different pathways. The first pathway is mediated via PKR-like endoplasmic reticulum kinase (PERK), eukaryotic translation initiation factor 2α (eiF2α) and activating transcription factor 4 (ATF4) and leads to antioxidant response and/or expression of apoptotic genes. A second pathway is mediated via inositol-requiring enzyme 1 (IRE1), c-Jun N-terminal kinase (JNK) and the splicing of X-box binding protein 1 (XBP1), triggering apoptotic processes and/or the expression of chaperones and foldases. A third pathway is mediated via activating transcription factor 6 (ATF6), leading also to expression of Chaperones, foldases and ERAD genes, resulting in Protein degradation and folding processes. Adapted from (Flamment, Hajduch, Ferre, & Foufelle, 2012).

Due to the reported importance of the ER-stress response on I/R-induced myocardial damage, various markers for UPR activity were assessed on qRT-PCR and Western Blot level. Results revealed that alterations induced by deficiency of *Tbc1d4* were directed to a very distinct ER-stress response via the ATF4/eIF2α pathway. This observation was quite surprising, since already 3 weeks have been passed since the surgical intervention. The changes in ER-stress response this late underline the

importance of *Tbc1d4* in long-term cardiac healing processes following MI. However, other arms of the ER-stress response via *Atf6* or *Xbp1* and SAPK/JNK appeared to be unaffected due to the loss of *Tbc1d4,* at least at the time points investigated. In the literature, ATF4 as a transcription factor has been shown to regulate various stress genes involved in cardiomyocytes death (Freundt et al., 2018). On the other hand, ATF4 action is important in order to restore ER homeostasis in cardiomyocytes following ischemia (Azfer, Niu, Rogers, Adamski, & Kolattukudy, 2006).

Reports of cardiac I/R-intervention in rats show an increase in ER-stress response at the level of *Chop* and *Xbp1* expression. These observations were not made with the mouse model in the present study. However, the differences in animal model as and the fact that animals were pre-treated with UPR-inhibitors and stimulators prior to the I/R intervention, a comparison between the results of these two studies is complicated.

In literature, the impact of ER-stress response has been linked with cardiac hypertrophy and fibrotic processes (Dickhout, Carlisle, & Austin, 2011; Lenna & Trojanowska, 2012). This observation links the cardiac ER-stress response to myocardial remodeling. Therefore, the impairments in cardiac ER-stress response due to the knockout of *Tbc1d4* could contribute to the phenotype of increased infarction size of D4KO hearts 3 weeks after the I/R intervention.

In conclusion, cardiac ER-stress response is associated with expression of *Tbc1d4*. However, the exact molecular mechanisms of *Tbc1d4* action remain to be elucidated. One possible connection could be found in the Rab proteins. Since TBC1D4 is a regulator of Rab proteins, its role on cardiac ER-stress response might be found on this level. For example, absence of Rab7a has been shown to be enhancing basal ER Stress and also causing expansion of the ER membranes (Mateus, Marini, Progida, & Bakke, 2018). Interestingly, Rab7 is also involved in GLUT4 vesicle trafficking (Miinea et

al., 2005), which is regulated by TBC1D4 activity. Therefore, it can be speculated, that TBC1D4 might influence the cardiac ER-Stress response via Rab proteins.

4.6. Deficiency of *Tbc1d4* is associated with impaired ECM remodeling

The extracellular matrix (ECM) has an important role in myocardial adaptation to heart diseases, such as myocardial infarction. The ECM serves as a scaffold and provides structural support but also for storage of cytokines and growth factors. Consequently, alterations and disturbances in ECM structure might result in cardiac fibrosis, hypertrophy and apoptosis. (Moore, Fan, Basu, Kandalam, & Kassiri, 2012)

Analysis of *Tbc1d4*-deficient and wild type hearts using transmission electron microscopy (TEM) and morphometric measurement revealed an increase in extracellular matrix (ECM) area due to the lack of *Tbc1d4*. This observation suggests alterations in ECM-remodeling processes, which control degradation, and construction, which is a highly dynamic entity (Moore et al., 2012; Vanhoutte, Schellings, Pinto, & Heymans, 2006). The major protein family involved in this process is the matrix metalloproteinases (MMPs) and the tissue inhibitors of metalloproteinases (TIMPs). Especially the balance between MMP and TIMP has been described to be essential for normal ECM remodeling and function (Fan, Takawale, Lee, & Kassiri, 2012; Moore et al., 2012; Vanhoutte et al., 2006). In this course, a high activity of MMPs indicates ECM degradation, while lower MMP activity speaks for increased ECM area that ultimately may result in cardiac fibrosis, myocardial stiffness and cardiac dysfunction (Jugdutt, 2014). In accordance with these observations, qRT-PCR revealed a significant decrease in *Mmp13* expression and *Mmp2/Timp1* ratio (and in tendential decreased expression of *Mmp2* and *Mmp9* expression), linking this observation to the phenotype of increased ECM area. Indeed,

the altered MMPs have been shown to be active cardiac post-MI remodeling and alterations of MMPs lead to impairments of heart structure and heart functions (Chakraborti & Dhalla, 2016). Interestingly, a similar study in *Timp2*-deficient mice revealed an increased infarction size, left ventricular dilation and cardiac dysfunction after MI (Kandalam, Basu, Abraham, Wang, Awad, et al., 2010; Kandalam, Basu, Abraham, Wang, Soloway, et al., 2010) similar to the observed *Tbc1d4*-phenotype presented in the present study.

Conversely, the observations of impaired *Mmp* expression and *Mmp/Timp* ratios seen while comparing wild type and *Tbc1d4*-deficient hearts in pre-I/R state could not be made in hearts 3 weeks after the I/R intervention. This might be due to the lower number of biological replicates available, since the number of surgeries was a limiting step.

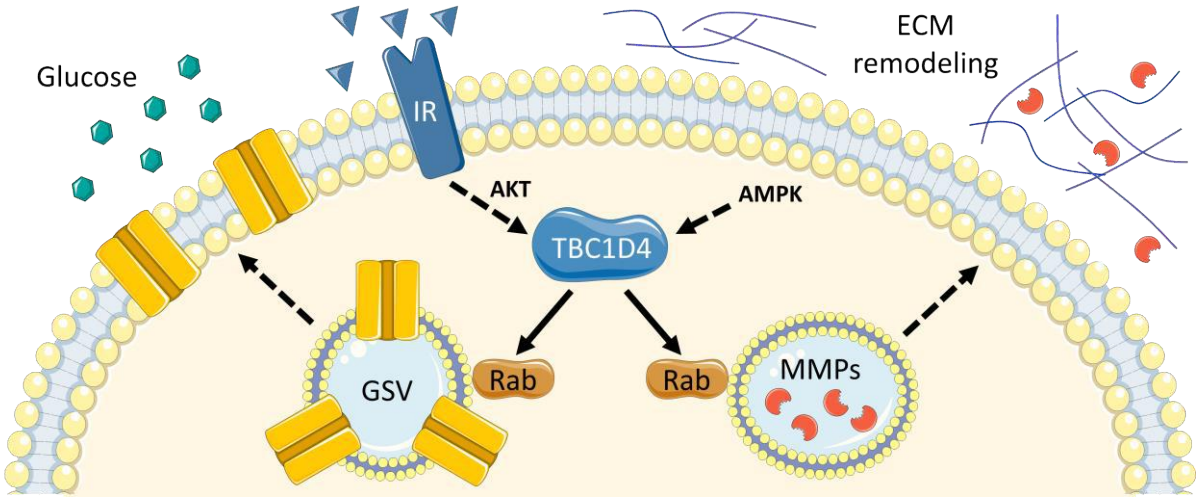

Figure 30: Hypothetical model of TBC1D4 action on cardiac glucose uptake and extracellular matrix remodeling. TBC1D4 action on glucose uptake via translocation of glucose transporter containing vesicles (GSV) from cytosolic storage to plasma membrane and putative TBC1D4 action on extracellular matrix (ECM) remodeling via regulation of trafficking control of matrix metalloproteinase (MMP) for exocytosis into extracellular space.

However, at this point the actual molecular role of *Tbc1d4* remains to be elucidated. One link between *Tbc1d4* action and MMP/TIMP-driven ECM remodeling event could be found in the Rab proteins. Multiple studies have identified Rab proteins as a crucial initiator of MMP exocytosis from intracellular storage vesicles towards the extracellular space of various tissues. MMP14 activity in exocytosis is dependent on Rab8 (Bravo-Cordero et al., 2007) as well as Rab5a, Rab8a and Rab14 action (Wiesner, El Azzouzi, & Linder, 2013). Moreover, Rab4 has been shown to be responsible for ECM secretion of fibronectin in mesangial cells (Hu et al., 2015). Besides, Rab11a was shown to be responsible for secretion of multiple soluble MMPs by regulation of vesicular traffic (Yu et al., 2014).

The activity of the Rab proteins themselves is directly mediated via RabGAP proteins, such as *Tbc1d4*. Therefore, a putative role of *Tbc1d4* might be in the mediation of MMP trafficking events via the *Rab* proteins in a similar manner to the well-described translocation of GLUT4 (Figure 30). In order to answer this question, further functional studies are needed, for example in a cell culture model using primary cardiomyocytes or HL1-cells.

4.7. Outlook

4.7.1 Translational studies

The present study reveals that *Tbc1d4* is more abundant in murine hearts compared to its orthologue *Tbc1d1*. Moreover, the so-called “long”- isoform of *Tbc1d4*, which is specific for skeletal muscle, is also expressed in the heart. A recent report identified a common mutation in *TBC1D4* in the Greenlandic Inuit and other arctic populations (Moltke et al., 2014). This nonsense p. variant in the *TBC1D4* gene (Arg684Ter) maps to the alternatively spliced exon 11, which is only expressed in the

long muscle form, leading to a muscle-specific knockout of *TBC1D4* in affected homozygous carriers of the allele. Importantly, in their study, Moltke et al, discovered that p.Arg684Ter in the *TBC1D4* gene, leads to increased plasma glucose and insulin levels as well as increased risk for T2DM. Moreover, similar to the situation of *Tbc1d4*-deficient mice, muscle GLUT4 and *TBC1D4* mRNA content were reduced in p.Arg684Ter allele carriers. The similarity of impaired glucose homeostasis of in p.Arg684Ter allele carriers and the situation in *Tbc1d4*-deficient mice suggest a similar situation in the hearts of these Greenlandic Inuit. The risk for incidence of CVD in these allele carriers has been reported to be tendentially increased (JØRGENSEN et al., 2018), however this did not reach statistical significance. Among 273 patients with CVD events there were 13 homozygous and 78 heterozygous carriers of p.Arg684Ter allele reported (JØRGENSEN et al., 2018) Therefore, the risk for CVD incidence remains to be further investigated, since studies showed no or only slight increases for CVD risk in these Greenlandic Inuit populations and comparable ones (Bjerregaard et al., 2003; Ronn et al., 2017). Extensive studies with larger number of participants or longer follow up would be needed. Nevertheless, since these studies only describe the incidence of CVD events and not the recovery following myocardial infarction, the proximity to the human situation makes TBC1D4 a potential target for medical intervention studies.

The results of the present study identify TBC1D4 as a potential target for clinical intervention studies in the course of myocardial infarction. The observation, that the loss of *Tbc1d4* affects cardiac function over the time course of 3 weeks displays a potential time frame for therapeutically intervention. Following the principle of “time is muscle” (Abreu, 2019), meaning the earlier the blood flow is restored the more viable tissue can be saved, the action of TBC1D4 over a time course of weeks might offer an interventional point also for undiagnosed or later stages of myocardial infarction.

Consequently, a potential leverage point for father molecular studies in order to elucidate the role of *Tbc1d4* in post MI healing can be found in high throughput proteomic and transcriptomic profiling of human heart samples from TBC1D4 p.Arg684Ter allele carriers in Greenlandic Inuit to validate defects in MMP expression/secretion and RabGAP signaling.

4.7.2 The role of *Tbc1d4* in cardiac subcellular transportation processes

Another interesting aspect of *Tbc1d4* action in the heart might also be found at the level of inflammatory processes. Especially in the acute phases of myocardial infarction, the pro-inflammatory and also anti-inflammatory response is crucial for the outcome following MI (J. Liu, Wang, & Li, 2016). The link of the cardiac inflammatory response to *Tbc1d4* action might be found in the dendritic cells, which are responsible for antigen cross-presentation. In this, TBC1D4 was identified as a crucial regulator of endosome trafficking in dendritic cells via regulation of Rab14 (Weimershaus et al., 2018). Therefore, another leverage point for further studies is found at the cardiac inflammatory response to I/R injury, especially on the level of dendritic cells.

In this study, it was shown that lack of *Tbc1d4* causes alterations in ECM area, presumably via remodeling processes through MMP. For this, functional assays are needed in order to determine whether this observation is due to a decrease in total cardiac MMP abundance or an impaired trafficking of MMPs towards the extracellular space. One possibility model to elucidate this point is primary cardiomyocyte of *Tbc1d4*-deficient murine hearts and corresponding controls. In this course, the protein abundance of MMPs as well as their secretion could be measured. Alternatively, a similar approach could be performed using immortalized cardiac cell lines, like HL-1 cells (Claycomb et al., 1998) with a corresponding knockdown of *Tbc1d4* through siRNA.

Another interesting point for further research could be the involvement of TBC1D4 in Ca^{2+}-stimulated glucose transport. A study in insulin-deficient diabetic transgenic mice expressing the sarcoplasmic reticulum calcium ATPase (SERCA1a) in the heart reported a decrease in basal and increase in calmodulin bound AS160, paralleling increases GLUT4 presence at the membrane (Waller, Kalyanasundaram, Hayes, Periasamy, & Lacombe, 2015). This suggests TBC1D4 to be a regulator glucose uptake via GLUT4 in a Ca^{2+}/calmodulin dependent manner. Further studies could elucidate the role of TBC1D4 in I/R-induced changes in Ca^{2+} homeostasis and cardiac recovery processes.

Moreover, TBC1D4 action could be further investigated regarding processes in adaptation to ischemia and states of hypoxia. A study in skeletal muscle revealed the importance of the hypoxia-inducible factor 1α (HIF-1α) on glucose metabolism and insulin action in skeletal muscle (Gorgens et al., 2017). In this, HIF-1α was identified as a regulator of Rab20 transcription and the loss of Rab20 led to impairments of insulin-stimulated glucose uptake in skeletal muscle (Gorgens et al., 2017). Since TBC1D4 is a regulator of Rab protein activity, its role on the hypoxia driven effects on glucose uptake could be an interesting approach in investigation of cardiac events of ischemia and I/R-induced injury.

4.7.3 Interventional studies and *Tbc1d4*-overexpression

This study was able to show that *Tbc1d4*-deficiency leads to impairments in cardiac glucose metabolism as well as post myocardial infarction healing. Consequently, an analogous study using a mouse model of *Tbc1d4* overexpression could be investigated for a possible opposite effect following I/R induced injury. Based on the results of this study, the overexpression of *Tbc1d4* could lead to a cardio-protective effect following I/R induced injury.

Moreover, it has to be stated, that the mouse model used in the present study carried a global knockout for *Tbc1d4*. Therefore, possible interferences form other TBC1D4-dependent organs and processes as well as organ crosstalk cannot be out ruled to be affecting the observed phenotype. In order to elucidate this, a cardiac specific knockout mouse model (e.g. expressed under the cardiac α-myosin heavy chain αMHC promoter) displays an interesting starting point in order to distinguish between cardiac exclusive and whole body-driven contributions to the phenotype.

Additionally, the control mice used in the I/R-intervention experiments were age-matched mice without any surgical intervention. In the course of this study, due to animal ethics a sham control was not possible to be generated.

Considering all aspects, this study for the first time has identified TBC1D4 as a crucial mediator of the response to cardiac I/R-induced injury and as a potential target for therapeutically intervention in clinical trials.

5. References

Abreu, L. M. (2019). Time is Muscle. *Arq Bras Cardiol, 112*(4), 408-409. doi: 10.5935/abc.20190059

Arias, E. B., Zheng, X., Agrawal, S., & Cartee, G. D. (2019). Whole body glucoregulation and tissue-specific glucose uptake in a novel Akt substrate of 160 kDa knockout rat model. *PLoS One, 14*(4), e0216236. doi: 10.1371/journal.pone.0216236

Azfer, A., Niu, J., Rogers, L. M., Adamski, F. M., & Kolattukudy, P. E. (2006). Activation of endoplasmic reticulum stress response during the development of ischemic heart disease. *Am J Physiol Heart Circ Physiol, 291*(3), H1411-1420. doi: 10.1152/ajpheart.01378.2005

Benjamini, Y., & Hochberg, Y. (1995). Controlling the False Discovery Rate: A Practical and Powerful Approach to Multiple Testing. *Journal of the Royal Statistical Society. Series B (Methodological), 57*(1), 289-300.

Benninghoff, T., Espelage, L., Eickelschulte, S., Zeinert, I., Sinowenka, I., Muller, F., . . . Al-Hasani, H. (2020). The RabGAPs TBC1D1 and TBC1D4 Control Uptake of Long-Chain Fatty Acids Into Skeletal Muscle via Fatty Acid Transporter SLC27A4/FATP4. *Diabetes, 69*(11), 2281-2293. doi: 10.2337/db20-0180

Bjerregaard, P., Young, T. K., & Hegele, R. A. (2003). Low incidence of cardiovascular disease among the Inuit--what is the evidence? *Atherosclerosis, 166*(2), 351-357. doi: 10.1016/s0021-9150(02)00364-7

Braunwald, E., & Kloner, R. A. (1985). Myocardial reperfusion: a double-edged sword? *J Clin Invest, 76*(5), 1713-1719. doi: 10.1172/JCI112160

Bravo-Cordero, J. J., Marrero-Diaz, R., Megias, D., Genis, L., Garcia-Grande, A., Garcia, M. A., . . . Montoya, M. C. (2007). MT1-MMP proinvasive activity is regulated by a novel Rab8-dependent exocytic pathway. *EMBO J, 26*(6), 1499-1510. doi: 10.1038/sj.emboj.7601606

Brewer, P. D., Romenskaia, I., Kanow, M. A., & Mastick, C. C. (2011). Loss of AS160 Akt substrate causes Glut4 protein to accumulate in compartments that are primed for fusion in basal adipocytes. *J Biol Chem, 286*(30), 26287-26297. doi: 10.1074/jbc.M111.253880

Chadt, A., Immisch, A., de Wendt, C., Springer, C., Zhou, Z., Stermann, T., . . . Al-Hasani, H. (2015). "Deletion of both Rab-GTPase-activating proteins TBC1D1 and TBC1D4 in mice eliminates insulin- and AICAR-stimulated glucose transport [corrected]. *Diabetes, 64*(3), 746-759. doi: 10.2337/db14-0368

Chadt, A., Leicht, K., Deshmukh, A., Jiang, L. Q., Scherneck, S., Bernhardt, U., . . . Al-Hasani, H. (2008). Tbc1d1 mutation in lean mouse strain confers leanness and protects from diet-induced obesity. *Nat Genet, 40*(11), 1354-1359. doi: 10.1038/ng.244

Chakraborti, S., & Dhalla, N. S. (2016). *Role of proteases in cellular dysfunction*.

Chen, Q., & Lesnefsky, E. J. (2018). A new strategy to decrease cardiac injury in aged heart following ischaemia-reperfusion: enhancement of the interaction between AMPK and SIRT1. *Cardiovasc Res, 114*(6), 771-772. doi: 10.1093/cvr/cvy062

Chen, S., Wasserman, D. H., MacKintosh, C., & Sakamoto, K. (2011). Mice with AS160/TBC1D4-Thr649Ala knockin mutation are glucose intolerant with reduced insulin sensitivity and altered GLUT4 trafficking. *Cell Metab, 13*(1), 68-79. doi: 10.1016/j.cmet.2010.12.005

Claycomb, W. C., Lanson, N. A., Jr., Stallworth, B. S., Egeland, D. B., Delcarpio, J. B., Bahinski, A., & Izzo, N. J., Jr. (1998). HL-1 cells: a cardiac muscle cell line that contracts and retains phenotypic characteristics of the adult cardiomyocyte. *Proc Natl Acad Sci U S A, 95*(6), 2979-2984. doi: 10.1073/pnas.95.6.2979

Colberg, S. R., Albright, A. L., Blissmer, B. J., Braun, B., Chasan-Taber, L., Fernhall, B., . . . American Diabetes, A. (2010). Exercise and type 2 diabetes: American College of Sports Medicine and the American Diabetes Association: joint position statement. Exercise and type 2 diabetes. *Med Sci Sports Exerc, 42*(12), 2282-2303. doi: 10.1249/MSS.0b013e3181eeb61c

Collaboration, N. C. D. R. F. (2016). Worldwide trends in diabetes since 1980: a pooled analysis of 751 population-based studies with 4.4 million participants. *Lancet, 387*(10027), 1513-1530. doi: 10.1016/S0140-6736(16)00618-8

Comellas, A. P., Kelly, A. M., Trejo, H. E., Briva, A., Lee, J., Sznajder, J. I., & Dada, L. A. (2010). Insulin regulates alveolar epithelial function by inducing Na+/K+-ATPase translocation to the plasma membrane in a process mediated by the action of Akt. *J Cell Sci, 123*(Pt 8), 1343-1351. doi: 10.1242/jcs.066464

Cunha, F. Q., Poole, S., Lorenzetti, B. B., & Ferreira, S. H. (1992). The pivotal role of tumour necrosis factor alpha in the development of inflammatory hyperalgesia. *Br J Pharmacol, 107*(3), 660-664. doi: 10.1111/j.1476-5381.1992.tb14503.x

Dash, S., Sano, H., Rochford, J. J., Semple, R. K., Yeo, G., Hyden, C. S., . . . Savage, D. B. (2009). A truncation mutation in TBC1D4 in a family with acanthosis nigricans and postprandial hyperinsulinemia. *Proc Natl Acad Sci U S A, 106*(23), 9350-9355. doi: 10.1073/pnas.0900909106

Dickhout, J. G., Carlisle, R. E., & Austin, R. C. (2011). Interrelationship between cardiac hypertrophy, heart failure, and chronic kidney disease: endoplasmic reticulum stress as a mediator of pathogenesis. *Circ Res, 108*(5), 629-642. doi: 10.1161/CIRCRESAHA.110.226803

Dinesh Shah, A., Langenberg, C., Rapsomaniki, E., Denaxas, S., Pujades-Rodriguez, M., Gale, C. P., . . . Hemingway, H. (2015). Type 2 diabetes and incidence of a wide range of cardiovascular diseases: a cohort study in 1.9 million people. *Lancet, 385 Suppl 1*, S86. doi: 10.1016/S0140-6736(15)60401-9

Dobin, A., Davis, C. A., Schlesinger, F., Drenkow, J., Zaleski, C., Jha, S., . . . Gingeras, T. R. (2013). STAR: ultrafast universal RNA-seq aligner. *Bioinformatics, 29*(1), 15-21. doi: 10.1093/bioinformatics/bts635

Doenst, T., Nguyen, T. D., & Abel, E. D. (2013). Cardiac metabolism in heart failure: implications beyond ATP production. *Circ Res, 113*(6), 709-724. doi: 10.1161/CIRCRESAHA.113.300376

Dokas, J., Chadt, A., Nolden, T., Himmelbauer, H., Zierath, J. R., Joost, H. G., & Al-Hasani, H. (2013). Conventional knockout of Tbc1d1 in mice impairs insulin- and AICAR-stimulated glucose uptake in skeletal muscle. *Endocrinology, 154*(10), 3502-3514. doi: 10.1210/en.2012-2147

Eguez, L., Lee, A., Chavez, J. A., Miinea, C. P., Kane, S., Lienhard, G. E., & McGraw, T. E. (2005). Full intracellular retention of GLUT4 requires AS160 Rab GTPase activating protein. *Cell Metab, 2*(4), 263-272. doi: 10.1016/j.cmet.2005.09.005

Einarson, T. R., Acs, A., Ludwig, C., & Panton, U. H. (2018). Prevalence of cardiovascular disease in type 2 diabetes: a systematic literature review of scientific evidence from across the world in 2007-2017. *Cardiovasc Diabetol, 17*(1), 83. doi: 10.1186/s12933-018-0728-6

Espelage, L., Al-Hasani, H., & Chadt, A. (2020). RabGAPs in skeletal muscle function and exercise. *J Mol Endocrinol, 64*(1), R1-R19. doi: 10.1530/JME-19-0143

Fan, D., Takawale, A., Lee, J., & Kassiri, Z. (2012). Cardiac fibroblasts, fibrosis and extracellular matrix remodeling in heart disease. *Fibrogenesis Tissue Repair, 5*(1), 15. doi: 10.1186/1755-1536-5-15

Federation, I. D. (2019). *IDF Diabetes Atlas, 9th edn.* . Brussels, Belgium: International Diabetes Federation.

Flamment, M., Hajduch, E., Ferre, P., & Foufelle, F. (2012). New insights into ER stress-induced insulin resistance. *Trends Endocrinol Metab, 23*(8), 381-390. doi: 10.1016/j.tem.2012.06.003

Flowers, M. T. (2009). The delta9 fatty acid desaturation index as a predictor of metabolic disease. *Clin Chem, 55*(12), 2071-2073. doi: 10.1373/clinchem.2009.135152

Freundt, J. K., Frommeyer, G., Wotzel, F., Huge, A., Hoffmeier, A., Martens, S., . . . Lange, P. S. (2018). The Transcription Factor ATF4 Promotes Expression of Cell Stress Genes and Cardiomyocyte Death in a Cellular Model of Atrial Fibrillation. *Biomed Res Int, 2018*, 3694362. doi: 10.1155/2018/3694362

Gast, K. B., Tjeerdema, N., Stijnen, T., Smit, J. W., & Dekkers, O. M. (2012). Insulin resistance and risk of incident cardiovascular events in adults without diabetes: meta-analysis. *PLoS One, 7*(12), e52036. doi: 10.1371/journal.pone.0052036

Goodwin, G. W., & Taegtmeyer, H. (2000). Improved energy homeostasis of the heart in the metabolic state of exercise. *Am J Physiol Heart Circ Physiol, 279*(4), H1490-1501. doi: 10.1152/ajpheart.2000.279.4.H1490

Gorgens, S. W., Benninghoff, T., Eckardt, K., Springer, C., Chadt, A., Melior, A., . . . Eckel, J. (2017). Hypoxia in Combination With Muscle Contraction Improves Insulin Action and

Glucose Metabolism in Human Skeletal Muscle via the HIF-1alpha Pathway. *Diabetes, 66*(11), 2800-2807. doi: 10.2337/db16-1488

Gorressen, S., Stern, M., van de Sandt, A. M., Cortese-Krott, M. M., Ohlig, J., Rassaf, T., . . . Kelm, M. (2015). Circulating NOS3 modulates left ventricular remodeling following reperfused myocardial infarction. *PLoS One, 10*(4), e0120961. doi: 10.1371/journal.pone.0120961

Hargett, S. R., Walker, N. N., & Keller, S. R. (2016). Rab GAPs AS160 and Tbc1d1 play nonredundant roles in the regulation of glucose and energy homeostasis in mice. *Am J Physiol Endocrinol Metab, 310*(4), E276-288. doi: 10.1152/ajpendo.00342.2015

Hausenloy, D. J., & Yellon, D. M. (2013). Myocardial ischemia-reperfusion injury: a neglected therapeutic target. *J Clin Invest, 123*(1), 92-100. doi: 10.1172/JCI62874

Henning, S. L., Wambolt, R. B., Schonekess, B. O., Lopaschuk, G. D., & Allard, M. F. (1996). Contribution of glycogen to aerobic myocardial glucose utilization. *Circulation, 93*(8), 1549-1555. doi: 10.1161/01.cir.93.8.1549

Herwig, R., Hardt, C., Lienhard, M., & Kamburov, A. (2016). Analyzing and interpreting genome data at the network level with ConsensusPathDB. *Nat Protoc, 11*(10), 1889-1907. doi: 10.1038/nprot.2016.117

Holman, G. D., & Cushman, S. W. (1994). Subcellular localization and trafficking of the GLUT4 glucose transporter isoform in insulin-responsive cells. *Bioessays, 16*(10), 753-759. doi: 10.1002/bies.950161010

Hu, C., Sun, L., Xiao, L., Han, Y., Fu, X., Xiong, X., . . . Kanwar, Y. S. (2015). Insights into the Mechanisms Involved in the Expression and Regulation of Extracellular Matrix Proteins in Diabetic Nephropathy. *Curr Med Chem, 22*(24), 2858-2870. doi: 10.2174/0929867322666150625095407

Hughes, D., & Mallucci, G. R. (2019). The unfolded protein response in neurodegenerative disorders - therapeutic modulation of the PERK pathway. *FEBS J, 286*(2), 342-355. doi: 10.1111/febs.14422

Jaswal, J. S., Keung, W., Wang, W., Ussher, J. R., & Lopaschuk, G. D. (2011). Targeting fatty acid and carbohydrate oxidation--a novel therapeutic intervention in the ischemic and failing heart. *Biochim Biophys Acta, 1813*(7), 1333-1350. doi: 10.1016/j.bbamcr.2011.01.015

Jelenik, T., Kaul, K., Sequaris, G., Flogel, U., Phielix, E., Kotzka, J., . . . Roden, M. (2017). Mechanisms of Insulin Resistance in Primary and Secondary Nonalcoholic Fatty Liver. *Diabetes, 66*(8), 2241-2253. doi: 10.2337/db16-1147

Jelenik, T., Sequaris, G., Kaul, K., Ouwens, D. M., Phielix, E., Kotzka, J., . . . Roden, M. (2014). Tissue-specific differences in the development of insulin resistance in a mouse model for type 1 diabetes. *Diabetes, 63*(11), 3856-3867. doi: 10.2337/db13-1794

Jennings, R. B., & Ganote, C. E. (1974). Structural changes in myocardium during acute ischemia. *Circ Res, 35 Suppl 3*, 156-172.

Ji, R., Akashi, H., Drosatos, K., Liao, X., Jiang, H., Kennel, P. J., . . . Schulze, P. C. (2017). Increased de novo ceramide synthesis and accumulation in failing myocardium. *JCI Insight, 2*(9). doi: 10.1172/jci.insight.82922

Jia, G., Hill, M. A., & Sowers, J. R. (2018). Diabetic Cardiomyopathy: An Update of Mechanisms Contributing to This Clinical Entity. *Circ Res, 122*(4), 624-638. doi: 10.1161/CIRCRESAHA.117.311586

JØRGENSEN, M. E., TVERMOSEGAARD, M., RØNN, P. F., BJERREGAARD, P., DAHL-PETERSEN, I. K., LARSEN, C. V., . . . HANSEN, T. (2018). Do Greenlandic Carriers of the TBC1D4 p.Arg684Ter Variant Have Increased Risk of Cardiovascular Disease? *Diabetes, 67*(Supplement 1), 439-P. doi: 10.2337/db18-439-P

Jugdutt, B. I. (2014). Aging and heart failure : mechanisms and management. from http://public.ebookcentral.proquest.com/choice/publicfullrecord.aspx?p=1698082

Kabagambe, E. K., Baylin, A., Siles, X., & Campos, H. (2003). Individual saturated fatty acids and nonfatal acute myocardial infarction in Costa Rica. *Eur J Clin Nutr, 57*(11), 1447-1457. doi: 10.1038/sj.ejcn.1601709

Kadowaki, H., & Nishitoh, H. (2013). Signaling pathways from the endoplasmic reticulum and their roles in disease. *Genes (Basel), 4*(3), 306-333. doi: 10.3390/genes4030306

Kalofoutis, C., Piperi, C., Kalofoutis, A., Harris, F., Phoenix, D., & Singh, J. (2007). Type II diabetes mellitus and cardiovascular risk factors: Current therapeutic approaches. *Exp Clin Cardiol, 12*(1), 17-28.

Kamburov, A., Wierling, C., Lehrach, H., & Herwig, R. (2009). ConsensusPathDB--a database for integrating human functional interaction networks. *Nucleic Acids Res, 37*(Database issue), D623-628. doi: 10.1093/nar/gkn698

Kandalam, V., Basu, R., Abraham, T., Wang, X., Awad, A., Wang, W., . . . Kassiri, Z. (2010). Early activation of matrix metalloproteinases underlies the exacerbated systolic and diastolic dysfunction in mice lacking TIMP3 following myocardial infarction. *Am J Physiol Heart Circ Physiol, 299*(4), H1012-1023. doi: 10.1152/ajpheart.00246.2010

Kandalam, V., Basu, R., Abraham, T., Wang, X., Soloway, P. D., Jaworski, D. M., . . . Kassiri, Z. (2010). TIMP2 deficiency accelerates adverse post-myocardial infarction remodeling because of enhanced MT1-MMP activity despite lack of MMP2 activation. *Circ Res, 106*(4), 796-808. doi: 10.1161/CIRCRESAHA.109.209189

Karwi, Q. G., Uddin, G. M., Ho, K. L., & Lopaschuk, G. D. (2018). Loss of Metabolic Flexibility in the Failing Heart. *Front Cardiovasc Med, 5*, 68. doi: 10.3389/fcvm.2018.00068

Katz, E. B., Stenbit, A. E., Hatton, K., DePinho, R., & Charron, M. J. (1995). Cardiac and adipose tissue abnormalities but not diabetes in mice deficient in GLUT4. *Nature, 377*(6545), 151-155. doi: 10.1038/377151a0

King, L. M., & Opie, L. H. (1998). Glucose delivery is a major determinant of glucose utilisation in the ischemic myocardium with a residual coronary flow. *Cardiovasc Res, 39*(2), 381-392. doi: 10.1016/s0008-6363(98)00100-x

Kolwicz, S. C., Jr., & Tian, R. (2009). Metabolic therapy at the crossroad: how to optimize myocardial substrate utilization? *Trends Cardiovasc Med, 19*(6), 201-207. doi: 10.1016/j.tcm.2009.12.005

Lansey, M. N., Walker, N. N., Hargett, S. R., Stevens, J. R., & Keller, S. R. (2012). Deletion of Rab GAP AS160 modifies glucose uptake and GLUT4 translocation in primary skeletal muscles and adipocytes and impairs glucose homeostasis. *Am J Physiol Endocrinol Metab, 303*(10), E1273-1286. doi: 10.1152/ajpendo.00316.2012

Larsen, T. S., & Aasum, E. (2008). Metabolic (in)flexibility of the diabetic heart. *Cardiovasc Drugs Ther, 22*(2), 91-95. doi: 10.1007/s10557-008-6083-1

Leney, S. E., & Tavare, J. M. (2009). The molecular basis of insulin-stimulated glucose uptake: signalling, trafficking and potential drug targets. *J Endocrinol, 203*(1), 1-18. doi: 10.1677/JOE-09-0037

Lenna, S., & Trojanowska, M. (2012). The role of endoplasmic reticulum stress and the unfolded protein response in fibrosis. *Curr Opin Rheumatol, 24*(6), 663-668. doi: 10.1097/BOR.0b013e3283588dbb

Leto, D., & Saltiel, A. R. (2012). Regulation of glucose transport by insulin: traffic control of GLUT4. *Nat Rev Mol Cell Biol, 13*(6), 383-396. doi: 10.1038/nrm3351

Liang, X., Butterworth, M. B., Peters, K. W., & Frizzell, R. A. (2010). AS160 modulates aldosterone-stimulated epithelial sodium channel forward trafficking. *Mol Biol Cell, 21*(12), 2024-2033. doi: 10.1091/mbc.E10-01-0042

Liu, J., Wang, H., & Li, J. (2016). Inflammation and Inflammatory Cells in Myocardial Infarction and Reperfusion Injury: A Double-Edged Sword. *Clin Med Insights Cardiol, 10*, 79-84. doi: 10.4137/CMC.S33164

Liu, M., & Dudley, S. C., Jr. (2015). Role for the Unfolded Protein Response in Heart Disease and Cardiac Arrhythmias. *Int J Mol Sci, 17*(1). doi: 10.3390/ijms17010052

Livak, K. J., & Schmittgen, T. D. (2001). Analysis of relative gene expression data using real-time quantitative PCR and the 2(-Delta Delta C(T)) Method. *Methods, 25*(4), 402-408. doi: 10.1006/meth.2001.1262

Martin-Timon, I., Sevillano-Collantes, C., Segura-Galindo, A., & Del Canizo-Gomez, F. J. (2014). Type 2 diabetes and cardiovascular disease: Have all risk factors the same strength? *World J Diabetes, 5*(4), 444-470. doi: 10.4239/wjd.v5.i4.444

Martínez, M. S., García, A., Luzardo, E., Chávez-Castillo, M., Olivar, L. C., Salazar, J., . . . Bermúdez, V. (2017). Energetic metabolism in cardiomyocytes: molecular basis of heart

ischemia and arrhythmogenesis. *Vessel Plus, 1*, 130-141. doi: 10.20517/2574-1209.2017.34

Mateus, D., Marini, E. S., Progida, C., & Bakke, O. (2018). Rab7a modulates ER stress and ER morphology. *Biochim Biophys Acta Mol Cell Res, 1865*(5), 781-793. doi: 10.1016/j.bbamcr.2018.02.011

Mazzaro Cdo, L., Costa Fde, A., Bombig, M. T., Luna Filho, B., Paola, A. A., Carvalho, A. C., . . . Povoa, R. M. (2008). Ventricular mass and electrocardiographic criteria of hypertrophy: evaluation of new score. *Arq Bras Cardiol, 90*(4), 227-231. doi: 10.1590/s0066-782x2008000400003

Mechanic, O. J., & Grossman, S. A. (2020). Acute Myocardial Infarction *StatPearls*. Treasure Island (FL).

Miinea, C. P., Sano, H., Kane, S., Sano, E., Fukuda, M., Peranen, J., . . . Lienhard, G. E. (2005). AS160, the Akt substrate regulating GLUT4 translocation, has a functional Rab GTPase-activating protein domain. *Biochem J, 391*(Pt 1), 87-93. doi: 10.1042/BJ20050887

Miklosz, A., Lukaszuk, B., Zendzian-Piotrowska, M., Branska-Januszewska, J., Ostrowska, H., & Chabowski, A. (2017). Challenging of AS160/TBC1D4 Alters Intracellular Lipid milieu in L6 Myotubes Incubated With Palmitate. *J Cell Physiol, 232*(9), 2373-2386. doi: 10.1002/jcp.25632

Moltke, I., Grarup, N., Jorgensen, M. E., Bjerregaard, P., Treebak, J. T., Fumagalli, M., . . . Hansen, T. (2014). A common Greenlandic TBC1D4 variant confers muscle insulin resistance and type 2 diabetes. *Nature, 512*(7513), 190-193. doi: 10.1038/nature13425

Moore, L., Fan, D., Basu, R., Kandalam, V., & Kassiri, Z. (2012). Tissue inhibitor of metalloproteinases (TIMPs) in heart failure. *Heart Fail Rev, 17*(4-5), 693-706. doi: 10.1007/s10741-011-9266-y

Mule, G., Calcaterra, I., Nardi, E., Cerasola, G., & Cottone, S. (2014). Metabolic syndrome in hypertensive patients: An unholy alliance. *World J Cardiol, 6*(9), 890-907. doi: 10.4330/wjc.v6.i9.890

Ng, J. M., Azuma, K., Kelley, C., Pencek, R., Radikova, Z., Laymon, C., . . . Kelley, D. E. (2012). PET imaging reveals distinctive roles for different regional adipose tissue depots in systemic glucose metabolism in nonobese humans. *Am J Physiol Endocrinol Metab, 303*(9), E1134-1141. doi: 10.1152/ajpendo.00282.2012

Oakes, N. D., Thalen, P., Aasum, E., Edgley, A., Larsen, T., Furler, S. M., . . . Severson, D. (2006). Cardiac metabolism in mice: tracer method developments and in vivo application revealing profound metabolic inflexibility in diabetes. *Am J Physiol Endocrinol Metab, 290*(5), E870-881. doi: 10.1152/ajpendo.00233.2005

Opie, L. H. (1992). Cardiac metabolism--emergence, decline, and resurgence. Part II. *Cardiovasc Res, 26*(9), 817-830. doi: 10.1093/cvr/26.9.817

Ornellas, F. M., Ornellas, D. S., Martini, S. V., Castiglione, R. C., Ventura, G. M., Rocco, P. R., . . . Morales, M. M. (2017). Bone Marrow-Derived Mononuclear Cell Therapy Accelerates Renal Ischemia-Reperfusion Injury Recovery by Modulating Inflammatory, Antioxidant and Apoptotic Related Molecules. *Cell Physiol Biochem, 41*(5), 1736-1752. doi: 10.1159/000471866

Ortiz-Martin, L., Picazo-Sanchez, P., Peris-Lopez, P., & Tapiador, J. (2018). Heartbeats Do Not Make Good Pseudo-Random Number Generators: An Analysis of the Randomness of Inter-Pulse Intervals. *Entropy, 20*(2). doi: 10.3390/e20020094

Piper, H. M., Garcia-Dorado, D., & Ovize, M. (1998). A fresh look at reperfusion injury. *Cardiovasc Res, 38*(2), 291-300. doi: 10.1016/s0008-6363(98)00033-9

Praagman, J., Vissers, L. E. T., Mulligan, A. A., Laursen, A. S. D., Beulens, J. W. J., van der Schouw, Y. T., . . . Sluijs, I. (2019). Consumption of individual saturated fatty acids and the risk of myocardial infarction in a UK and a Danish cohort. *Int J Cardiol, 279*, 18-26. doi: 10.1016/j.ijcard.2018.10.064

Prabhu, S. D., & Frangogiannis, N. G. (2016). The Biological Basis for Cardiac Repair After Myocardial Infarction: From Inflammation to Fibrosis. *Circ Res, 119*(1), 91-112. doi: 10.1161/CIRCRESAHA.116.303577

Quan, C., Xie, B., Wang, H. Y., & Chen, S. (2015). PKB-Mediated Thr649 Phosphorylation of AS160/TBC1D4 Regulates the R-Wave Amplitude in the Heart. *PLoS One, 10*(4), e0124491. doi: 10.1371/journal.pone.0124491

Ramachandra, C. J. A., Hernandez-Resendiz, S., Crespo-Avilan, G. E., Lin, Y. H., & Hausenloy, D. J. (2020). Mitochondria in acute myocardial infarction and cardioprotection. *EBioMedicine, 57*, 102884. doi: 10.1016/j.ebiom.2020.102884

Ribeiro, L. G., Louie, E. K., Hillis, L. D., Davis, M. A., & Maroko, P. R. (1979). Early augmentation of R wave voltage after coronary artery occlusion: a useful index of myocardial injury. *J Electrocardiol, 12*(1), 89-95. doi: 10.1016/s0022-0736(79)80050-3

Ronn, P. F., Lucas, M., Laouan Sidi, E. A., Tvermosegaard, M., Andersen, G. S., Lauritzen, T., . . . Jorgensen, M. E. (2017). The obesity-associated risk of cardiovascular disease and all-cause mortality is not lower in Inuit compared to Europeans: A cohort study of Greenlandic Inuit, Nunavik Inuit and Danes. *Atherosclerosis, 265*, 207-214. doi: 10.1016/j.atherosclerosis.2017.08.011

Shao, D., & Tian, R. (2015). Glucose Transporters in Cardiac Metabolism and Hypertrophy. *Compr Physiol, 6*(1), 331-351. doi: 10.1002/cphy.c150016

Siasos, G., Tsigkou, V., Kosmopoulos, M., Theodosiadis, D., Simantiris, S., Tagkou, N. M., . . . Papavassiliou, A. G. (2018). Mitochondria and cardiovascular diseases-from pathophysiology to treatment. *Ann Transl Med, 6*(12), 256. doi: 10.21037/atm.2018.06.21

Spurr, A. R. (1969). A low-viscosity epoxy resin embedding medium for electron microscopy. *J Ultrastruct Res, 26*(1), 31-43. doi: 10.1016/s0022-5320(69)90033-1

Stanley, W. C., Recchia, F. A., & Lopaschuk, G. D. (2005). Myocardial substrate metabolism in the normal and failing heart. *Physiol Rev, 85*(3), 1093-1129. doi: 10.1152/physrev.00006.2004

Stockli, J., Fazakerley, D. J., & James, D. E. (2011). GLUT4 exocytosis. *J Cell Sci, 124*(Pt 24), 4147-4159. doi: 10.1242/jcs.097063

Stone, S., Abkevich, V., Russell, D. L., Riley, R., Timms, K., Tran, T., . . . Shattuck, D. (2006). TBC1D1 is a candidate for a severe obesity gene and evidence for a gene/gene interaction in obesity predisposition. *Hum Mol Genet, 15*(18), 2709-2720. doi: 10.1093/hmg/ddl204

Sun, Y., Bilan, P. J., Liu, Z., & Klip, A. (2010). Rab8A and Rab13 are activated by insulin and regulate GLUT4 translocation in muscle cells. *Proc Natl Acad Sci U S A, 107*(46), 19909-19914. doi: 10.1073/pnas.1009523107

Szekeres, F., Chadt, A., Tom, R. Z., Deshmukh, A. S., Chibalin, A. V., Bjornholm, M., . . . Zierath, J. R. (2012). The Rab-GTPase-activating protein TBC1D1 regulates skeletal muscle glucose metabolism. *Am J Physiol Endocrinol Metab, 303*(4), E524-533. doi: 10.1152/ajpendo.00605.2011

Thygesen, K., Alpert, J. S., Jaffe, A. S., Chaitman, B. R., Bax, J. J., Morrow, D. A., . . . Executive Group on behalf of the Joint European Society of Cardiology /American College of Cardiology /American Heart Association /World Heart Federation Task Force for the Universal Definition of Myocardial, I. (2018). Fourth Universal Definition of Myocardial Infarction (2018). *J Am Coll Cardiol, 72*(18), 2231-2264. doi: 10.1016/j.jacc.2018.08.1038

Tian, R., & Abel, E. D. (2001). Responses of GLUT4-deficient hearts to ischemia underscore the importance of glycolysis. *Circulation, 103*(24), 2961-2966. doi: 10.1161/01.cir.103.24.2961

Tomczyk, M. M., & Dolinsky, V. W. (2020). The Cardiac Lipidome in Models of Cardiovascular Disease. *Metabolites, 10*(6). doi: 10.3390/metabo10060254

Uzunlulu, M., Telci Caklili, O., & Oguz, A. (2016). Association between Metabolic Syndrome and Cancer. *Ann Nutr Metab, 68*(3), 173-179. doi: 10.1159/000443743

Vanhoutte, D., Schellings, M., Pinto, Y., & Heymans, S. (2006). Relevance of matrix metalloproteinases and their inhibitors after myocardial infarction: a temporal and spatial window. *Cardiovasc Res, 69*(3), 604-613. doi: 10.1016/j.cardiores.2005.10.002

Virmani, R., Forman, M. B., & Kolodgie, F. D. (1990). Myocardial reperfusion injury. Histopathological effects of perfluorochemical. *Circulation, 81*(3 Suppl), IV57-68.

Waller, A. P., Kalyanasundaram, A., Hayes, S., Periasamy, M., & Lacombe, V. A. (2015). Sarcoplasmic reticulum Ca2+ ATPase pump is a major regulator of glucose transport in

the healthy and diabetic heart. *Biochim Biophys Acta, 1852*(5), 873-881. doi: 10.1016/j.bbadis.2015.01.009

Walters, A. M., Porter, G. A., Jr., & Brookes, P. S. (2012). Mitochondria as a drug target in ischemic heart disease and cardiomyopathy. *Circ Res, 111*(9), 1222-1236. doi: 10.1161/CIRCRESAHA.112.265660

Wang, H. Y., Ducommun, S., Quan, C., Xie, B., Li, M., Wasserman, D. H., . . . Chen, S. (2013). AS160 deficiency causes whole-body insulin resistance via composite effects in multiple tissues. *Biochem J, 449*(2), 479-489. doi: 10.1042/BJ20120702

Wang, L., Quan, N., Sun, W., Chen, X., Cates, C., Rousselle, T., . . . Li, J. (2018). Cardiomyocyte-specific deletion of Sirt1 gene sensitizes myocardium to ischaemia and reperfusion injury. *Cardiovasc Res, 114*(6), 805-821. doi: 10.1093/cvr/cvy033

Wang, S., Binder, P., Fang, Q., Wang, Z., Xiao, W., Liu, W., & Wang, X. (2018). Endoplasmic reticulum stress in the heart: insights into mechanisms and drug targets. *Br J Pharmacol, 175*(8), 1293-1304. doi: 10.1111/bph.13888

Weimershaus, M., Mauvais, F. X., Saveanu, L., Adiko, C., Babdor, J., Abramova, A., . . . van Endert, P. (2018). Innate Immune Signals Induce Anterograde Endosome Transport Promoting MHC Class I Cross-Presentation. *Cell Rep, 24*(13), 3568-3581. doi: 10.1016/j.celrep.2018.08.041

Wende, A. R., Kim, J., Holland, W. L., Wayment, B. E., O'Neill, B. T., Tuinei, J., . . . Abel, E. D. (2017). Glucose transporter 4-deficient hearts develop maladaptive hypertrophy in response to physiological or pathological stresses. *Am J Physiol Heart Circ Physiol, 313*(6), H1098-H1108. doi: 10.1152/ajpheart.00101.2017

Wieringa, G., Zerah, S., Jansen, R., Simundic, A. M., Queralto, J., Solnica, B., . . . European Communities Confederation of Clinical, C. (2012). The EC4 European syllabus for post-graduate training in clinical chemistry and laboratory medicine: version 4--2012. *Clin Chem Lab Med, 50*(8), 1317-1328. doi: 10.1515/cclm-2012-0019

Wiesner, C., El Azzouzi, K., & Linder, S. (2013). A specific subset of RabGTPases controls cell surface exposure of MT1-MMP, extracellular matrix degradation and three-dimensional invasion of macrophages. *J Cell Sci, 126*(Pt 13), 2820-2833. doi: 10.1242/jcs.122358

Wu, M. Y., Yiang, G. T., Liao, W. T., Tsai, A. P., Cheng, Y. L., Cheng, P. W., . . . Li, C. J. (2018). Current Mechanistic Concepts in Ischemia and Reperfusion Injury. *Cell Physiol Biochem, 46*(4), 1650-1667. doi: 10.1159/000489241

Xie, B., Chen, Q., Chen, L., Sheng, Y., Wang, H. Y., & Chen, S. (2016). The Inactivation of RabGAP Function of AS160 Promotes Lysosomal Degradation of GLUT4 and Causes Postprandial Hyperglycemia and Hyperinsulinemia. *Diabetes, 65*(11), 3327-3340. doi: 10.2337/db16-0416

Yang, S., Chen, C., Wang, H., Rao, X., Wang, F., Duan, Q., . . . Wang, D. W. (2012). Protective effects of Acyl-coA thioesterase 1 on diabetic heart via PPARalpha/PGC1alpha signaling. *PLoS One, 7*(11), e50376. doi: 10.1371/journal.pone.0050376

Yellon, D. M., & Hausenloy, D. J. (2007). Myocardial reperfusion injury. *N Engl J Med, 357*(11), 1121-1135. doi: 10.1056/NEJMra071667

Yu, S., Yehia, G., Wang, J., Stypulkowski, E., Sakamori, R., Jiang, P., . . . Gao, N. (2014). Global ablation of the mouse Rab11a gene impairs early embryogenesis and matrix metalloproteinase secretion. *J Biol Chem, 289*(46), 32030-32043. doi: 10.1074/jbc.M113.538223

Zhang, C., Tang, Y., Li, Y., Xie, L., Zhuang, W., Liu, J., & Gong, J. (2017). Unfolded protein response plays a critical role in heart damage after myocardial ischemia/reperfusion in rats. *PLoS One, 12*(6), e0179042. doi: 10.1371/journal.pone.0179042

Zimmet, P., Alberti, K., Stern, N., Bilu, C., El-Osta, A., Einat, H., & Kronfeld-Schor, N. (2019). The Circadian Syndrome: is the Metabolic Syndrome and much more! *J Intern Med, 286*(2), 181-191. doi: 10.1111/joim.12924

Zisman, A., Peroni, O. D., Abel, E. D., Michael, M. D., Mauvais-Jarvis, F., Lowell, B. B., . . . Kahn, B. B. (2000). Targeted disruption of the glucose transporter 4 selectively in muscle causes insulin resistance and glucose intolerance. *Nat Med, 6*(8), 924-928. doi: 10.1038/78693

6. Supplement/Appendix

6.1 Supplementary Figures

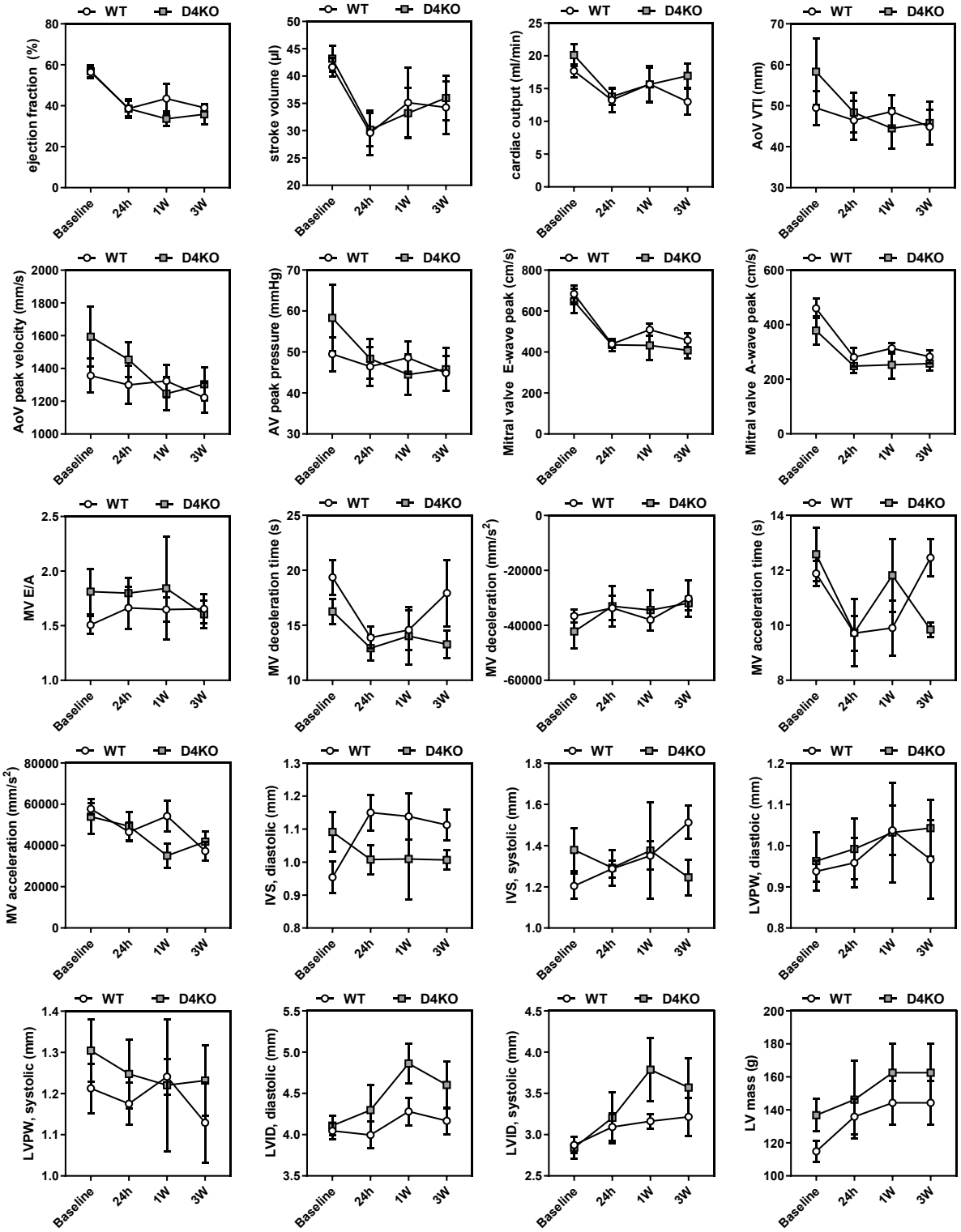

Supplementary figure 1: Time course of echocardiographic assessment of mouse heart function and morphology following I/R-intervention. Following the I/R-intervention phase in male mice at 36 weeks of age on a 60kcal% high-fat diet, animals were monitored for the 3 week reperfusion phase. During this, parameters of cardiac function and morphology were measured before the intervention (baseline) and

at time points of 24 hours, 1 week and 3 weeks after the intervention for type (WT; white) and *Tbc1d4*-deficient (D4KO; grey). Recordings were conducted at ZETT (HHU ion collaboration with Prof. J. Fischer, Heinrich-Heine University, Düsseldorf, Germany). AoV = aortic valve, VTI = velocity time integral, MV = mitral valve, IVS = intraventricular septum, LVPW = left ventricular posterior wall, LVID = left ventricular inner diameter, LV = left ventricle. Data are presented as mean values ± SEM (n = 6). Two-tailed unpaired Student´s t-test with Welch´s correction.

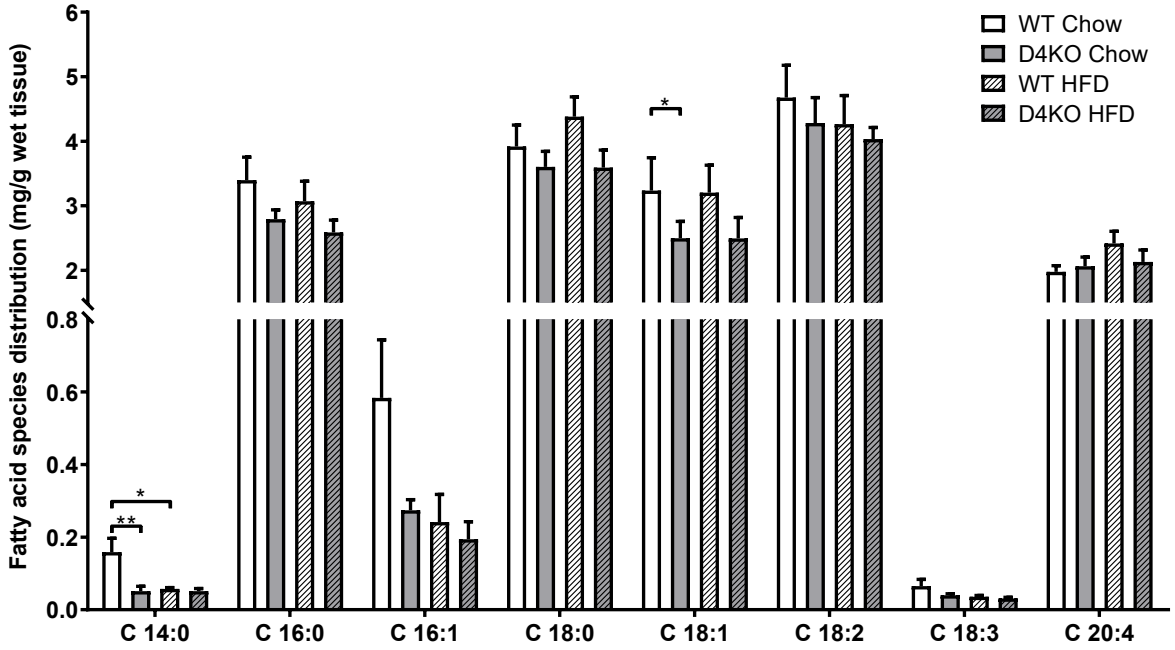

Supplementary figure 2: Fatty Acid profile of cardiac tissue of wild type and *Tbc1d4*-deficient mice. Total abundance of saturated and unsaturated fatty acid species was determined via gas chromatography (GC). Myristic acid (C14:0), palmitic acid (C16:0), palmitoleic acid (C16:1), stearic acid (C18:0), oleic acid (C18:1), linoleic acid (C18:2), α-linoleic acid (C18:3) and arachidonic acid (C20:4, blank bars) were detected in cardiac tissue samples of 36 weeks old male wild type (WT; white bars) and *Tbc1d4*-deficient (D4KO; grey bars) mice on a Chow or high-fat diet (HFD; hatched bars), respectively. Data are presented as mean values ± SEM (n = 5-10). Two-way ANOVA with Tukey multiple comparisons test. *p < 0.05; **p < 0.01

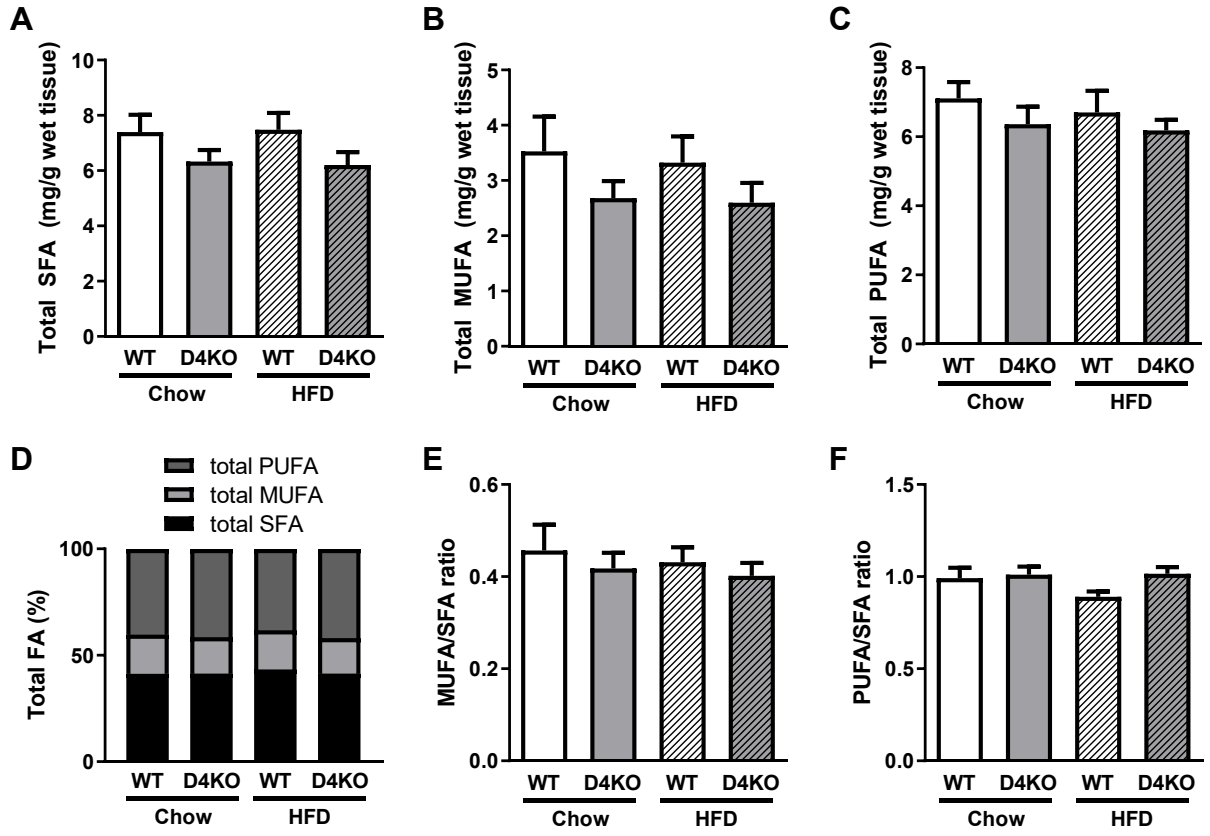

Supplementary figure 3: Composition of fatty acid classes in wild type and *Tbc1d4*-deficient mouse heart tissue. Total amount of (A) saturated fatty acids (SFA), (B) mono unsaturated fatty acids, and (C) poly unsaturated fatty acids (PUFA) was determined via GC analysis for 36 weeks old, male wild type (WT; white bars) and *Tbc1d4*-deficient (D4KO; grey bars) mice on a Chow or high-fat diet (HFD; hatched bars), respectively. Based on these results, the summary of each fatty acid class contribution to total fatty acid content (D) as well as the ratio of MUFAs to SFAs as indicator for total desaturation activity (E) and the ratio of PUFAs to SFAs (F) were generated. Data are presented as mean values ± SEM (n = 5-10). Two-way ANOVA with Tukey multiple comparisons test.

TOP 25 upregulated genes (Pre-I/R) (D4KO vs WT)			TOP 25 downregulated genes (Pre-I/R) (D4KO vs WT)		
gene	*log2 fold change*	*p-value*	*gene*	*log2 fold change*	*p-value*
Irs2	1,663	4,64E-03	*Sec14l3*	-25,683	1,43E-05
Hipk2	1,151	2,13E-03	*Wfdc2*	-5,951	3,85E-03
Ddit4	1,078	6,85E-04	*Aldh3b2*	-2,257	8,81E-03
Dnajb1	1,072	2,92E-03	*Bnc1*	-2,049	6,95E-05
Hcn4	1,060	1,56E-03	*Cpz*	-1,952	7,73E-03
Ammecr1	0,998	1,71E-05	*Cd163l1*	-1,930	1,40E-04
Frmd5	0,965	8,82E-06	*Slc14a1*	-1,833	3,85E-04
Igf2bp2	0,944	4,11E-04	*Cxcr6*	-1,790	2,23E-03
Ace2	0,908	1,12E-04	*Gm12522*	-1,711	3,45E-03
Fbxo40	0,903	7,40E-04	*Cd209g*	-1,385	6,38E-03
Adamts1	0,882	3,10E-04	*Lrrc17*	-1,344	3,87E-05
Ell2	0,877	8,82E-06	*Itih2*	-1,319	2,49E-03
Foxo3	0,868	2,62E-03	*Dbp*	-1,271	4,05E-03
Cpeb4	0,857	3,05E-04	*Clcn1*	-1,196	1,14E-04
Asb18	0,855	1,86E-04	*Mcpt4*	-1,192	3,43E-03
Kcna5	0,853	1,77E-03	*H2-Ob*	-1,189	8,39E-03
Ppp1r3a	0,844	2,76E-03	*Osr1*	-1,155	2,40E-03
Lrp11	0,839	3,88E-04	*Mdfi*	-1,151	2,12E-03
Slc25a25	0,821	9,97E-03	*Rspo1*	-1,128	5,85E-03
Ago2	0,816	1,06E-04	*Cth*	-1,116	8,44E-03
Rnf128	0,802	4,45E-04	*Rassf10*	-1,107	2,90E-04
Nfil3	0,802	1,14E-03	*Retnla*	-1,107	2,92E-03
Eif4ebp2	0,802	3,48E-03	*Per3*	-1,103	5,16E-03
Abca1	0,796	6,33E-03	*Stk32b*	-1,079	3,74E-03
Strn	0,793	2,81E-03	*Fxyd7*	-1,052	3,41E-03

Supplementary table 1: TOP 25 up- and downregulated genes of cardiac pre-I/R transcriptome due to *Tbc1d4*-deficiency and/or I/R-intervention. Cardiac transcriptome of wild type (WT) and *Tbc1d4*-deficient (D4KO) hearts from pre-I/R samples were sequenced using RNASequencing and subsequently tested for differential gene expression. Significance threshold was set at $p<0.01$ (n=4).

TOP 25 upregulated genes (3 weeks post-I/R) (D4KO vs WT)			TOP 25 downregulated genes (3 weeks post-I/R) (D4KO vs WT)		
gene	**log2 fold change**	**p-value**	**gene**	**log2 fold change**	**p-value**
Myh4	9,819	2,74E-03	*Cth*	-1,183	8,02E-03
Myh1	8,471	7,13E-05	*Hlf*	-0,964	5,84E-03
Myh2	7,305	7,13E-05	*Armc2*	-0,824	4,91E-03
Slpi	5,626	6,95E-04	*Nrg4*	-0,822	7,37E-03
Alb	5,618	1,31E-03	*Lonrf1*	-0,820	1,32E-03
Tnnc2	4,349	6,95E-04	*Rgs7bp*	-0,809	6,73E-03
Mybpc1	3,782	7,46E-05	*Ier3*	-0,761	6,95E-04
Pvalb	3,675	1,56E-04	*Mylk4*	-0,728	1,68E-03
Tnnt3	3,192	9,30E-04	*Wee1*	-0,724	1,57E-03
Actn3	3,137	9,72E-05	*Cry1*	-0,702	3,11E-03
Atp2a1	2,741	2,44E-03	*Gsta3*	-0,681	7,88E-03
Mylpf	2,732	2,90E-03	*Fam212b*	-0,661	2,74E-03
Arntl	2,050	1,38E-03	*Mid1ip1*	-0,658	7,33E-04
Gpr123	1,797	1,68E-03	*Nampt*	-0,620	2,90E-03
Gdf15	1,793	3,54E-03	*Fam213a*	-0,609	1,03E-03
Adamts4	1,705	2,90E-03	*Nr1d2*	-0,595	9,45E-03
Gdf6	1,422	7,65E-03	*Ankrd12*	-0,580	7,56E-03
Serinc2	1,205	6,36E-03	*Gcat*	-0,563	6,95E-04
Adamtsl2	1,204	6,95E-04	*Rps17*	-0,559	1,32E-03
Loxl3	0,892	1,89E-03	*Ppara*	-0,555	1,57E-03
Rcan1	0,876	4,46E-03	*Klf15*	-0,546	4,57E-03
Fbn1	0,866	7,73E-03	*Rps8*	-0,490	1,56E-04
Myl1	0,857	6,35E-03	*Bckdhb*	-0,489	5,22E-03
Orai2	0,834	2,44E-03	*Rps24*	-0,484	1,57E-03
Col5a2	0,821	9,48E-03	*Zcrb1*	-0,477	1,32E-03

Supplementary table 2: TOP 25 up- and downregulated genes of cardiac 3 weeks post-I/R transcriptome due to*Tbc1d4*-deficiency and/or I/R-intervention. Cardiac transcriptome of wild type (WT) and *Tbc1d4*-deficient (D4KO) hearts from 3 weeks post-I/R samples were sequenced using RNASequencing and subsequently tested for differential gene expression. Significance threshold was set at $p<0.01$ (n=4).

6.2 Index of figures

6.3 Index of tables

6.4 Abbreviations

Abbreviation	Full name
°C	Degree Celsius
µg	Microgram
µl	Microliter
AB	Antibody
ADP	Adenosine diphosphate
AKT	RAC-alpha serine/threonine-protein kinase, protein kinase B
AMP	Adenosine monophosphate
AMPK	5'-AMP-activated protein kinase
ANOVA	Analysis of variance
APS	Ammonium persulfate
AS160	Akt substrate of 160 kDa
ATF4	Activating transcription factor 4
ATF6	Activating transcription factor 6
ATP	Adenosine triphosphate
BAT	Brown adipose tissue
BCA	Bicinchoninic acid assay
bp	Base pair
BSA	Bovine serum albumin
BW	Body weight
$CaCl_2$	Calcium Chloride
CAD	Coronary artery disease
CBD	Ca+/calmodulin-binding domain
cDNA	Complementary DNA
CHOP	C/EBP homologous protein
CT	Computer tomography
Ct	Cycle threshold
CVD	Cardiovascular disease
CXR	Carboxy-X-rhodamine
D4KO	*Tbc1d4*-knockout
DB	Database
DDZ	Deutsches Diabetes Zentrum (German Diabetes Center)
DNA	Deoxyribonucleic acid
DNL	*de novo* lipogenesis
dNTP	Dideoxy-nucleoside triphosphate
DTT	Dithiothreitol
ECG	Electrocardiogram
ECL	Enhanced chemiluminescence
ECM	Extracellular matrix
EDL	*Extensor digitoris longum*
EDTA	Ethylene diamine tetraacetic acid
EGTA	Ethylene glycol tetraacetic acid

eIF2α	Eukaryotic translation initiation factor 2α
eIF4	Eukaryotic initiation factor 4
ER	Endoplasmic reticulum
ETOH	Ethanol
FATP4	Long-chain fatty acid transport protein 4
FCCP	Cyanide-4-(trifluoromethoxy)phenylhydrazone
FDG (^{18}F)	Fluorodeoxyglucose
GAP	GTPase-activating protein
GAPDH	Glyceraldehyde 3-phosphate dehydrogenase
GC	gas chromatography
gDNA	genomic DNA
GLUT1	Glucose transporter type 1
GLUT4	Glucose transporter type 4
GOD-PAP method	Glucose oxidase and peroxidase method
GSV	Glucose storage vesicle
GTP	Guanosine-5'-triphosphate
GTT	Glucose tolerance test
HCl	Hydrochloric acid
HDL	High-density lipoprotein
HE	Hematoxylin and eosin
HFD	High-fat diet
HHU	Heinrich-Heine University
HRP	Horse radish peroxidase
I/R	ischemia/reperfusion
IDF	International Diabetes Federation
IPA	Ingenuity Pathway Analysis
IR	Insulin receptor
IRE	Inositol-requiring enzyme 1
IRS1	Insulin receptor substrate 1
JNK	c-Jun N-terminal kinase
KCl	Potassium chloride
kDa	Kilodalton
KH_2PO_4	Monopotassium phosphate
KHB	Krebs-Henseleit buffer
KO	Knockout
KOH	Potassium hydroxide
LAD	Left anterior descending (coronary artery)
LCR	Leak control ratio
LV	Left ventricle
MeOH	Methanol
mg	Milligram
MHz	Megahertz
MI	Myocardial infarction
ml	Milliliter
MMP	Matrix metalloproteinase

mRNA	Messenger RNA
MUFA	Mono-unsaturated fatty acid
NaCl	Sodium chloride
NaH_2PO_4	Sodium dihydrogen phosphate
NaOH	Sodium hydroxide
NMR	Nuclear magnetic resonance
PA	Polyacrylamide
PAGE	Polyacrylamide gel electrophoresis
PBS	Phosphate-buffered saline
PCR	Polymerase chain reaction
PDK1	3-phosphoinositide-dependent protein kinase 1
PECAM-1	Platelet endothelial cell adhesion molecule 1
PERK	Protein kinase R (PKR)-like endoplasmic reticulum kinase
PET	Positron emission tomography
PGC1α	Peroxisome proliferator-activated receptor gamma coactivator 1-alpha
PI3K	Phosphatidylinositol-3-kinase
PKR	Protein kinase R
PPAR	Peroxisome proliferator-activated receptors
PTB-domain	Phosphotyrosine-binding domain
PUFA	Poly-unsaturated fatty acid
PVDF	Polyvinylidenfluoride
q(RT)PCR	Quantitative (real time) PCR
Rab	*Ras-related in brain*
RAC	*Ras-related C3 botulinum toxin substrate*
RCR	Respiratory control ratio
RNA	Ribonucleic acid
ROI	Region of interest
ROS	Reactive oxygen species
RT	Room temperature
RT-PCR	Reverse transcriptase PCR
SAPK	Stress-activated protein kinase
SCD1	Stearoyl-CoA desaturase-1
SDS	Sodium dodecyl sulfate
SEM	Standard error of the mean
SERCA1a	Sarco/endoplasmic reticulum Ca^{2+}-ATPase
SFA	Saturated fatty acid
siRNA	Small interfering RNA
STAR	Spliced Transcripts Alignment to a Reference
T1DM	Type 1 diabetes mellitus
T2DM	Type 2 diabetes mellitus
TAE buffer	Tris base, acetic acid and EDTA buffer
TBC1D1	TBC1 domain family member 1
TBC1D4	TBC1 domain family member 4
TBS	Tris-buffered saline
TBS-T	Tris-buffered saline with Tween20

TCA	Tricarboxylic acid cycle
TEM	Transmission electron microscopy
TEMED	Tetramethylethylenediamine
TIMP	Tissue inhibitor of metalloproteinase
UPR	Unfolded protein response
UV	ultraviolet
VCAM-1	Vascular cell adhesion molecule 1
WAT	White adipose tissue
WHO	World health organization
WT	wild type
XBP	X-box binding protein 1
ZETT	*Zentrale Einrichtung für Tierforschung und wissenschaftliche Tierschutzaufgaben*

6.5 Contributions

Overview of personal contributions to data shown in the results section:

Figure/Table	Personal Contributions	Collaborators
Figure 5	Conducted experiments and analysis	-
Figure 6	Conducted experiments and analysis	[^{3}H]-deoxyglucose uptake assay: Dr. David Barbosa (Institute for Clinical Biochemistry and Pathobiochemistry, German Diabetes Center (DDZ), Düsseldorf, Germany)
Figure 7	Data Analysis	PET imaging: Dr. Heiko Backes, Anna Lena Cremer, Prof. Dr. Jens Brüning (Max Planck Institute for Metabolism Research, Cologne, Germany)
Figure 8	Conducted experiments and analysis	-
Figure 9	Conducted experiments and analysis	-
Figure 10	Sample preparation, sectioning/ staining, data analysis	Histology and morphometry: Kay Jeruschke, Dr. Jürgen Weiß (Institute for Clinical Biochemistry and Pathobiochemistry, German Diabetes Center (DDZ), Düsseldorf, Germany) I/R-intervention: Dr. Simone Gorressen, Dominik Semmler, Prof. Dr. Jens W Fischer (Institute for Pharmacology and Clinical Pharmacology, Heine-University, Düsseldorf, Germany)
Figure 11	Conducted experiments and analysis	-

Figure 12	Data analysis	I/R-intervention and ECG monitoring: Dr. Simone Gorressen, Dominik Semmler, Prof. Dr. Jens W Fischer (Institute for Pharmacology and Clinical Pharmacology, Heine-University, Düsseldorf, Germany)
Figure 13	Conducted experiments and analysis	-
Table 20	Sample preparation, data analysis	Gas chromatography: Lothar Bohne (Institute for Clinical Biochemistry and Pathobiochemistry, German Diabetes Center (DDZ), Düsseldorf, Germany)
Figure 14-17	Conducted experiments and analysis	-
Figure 18	Sample preparation, data analysis	High-respirometry measurements: Dr. Tomas Jelenik (Institute for Clinical Diabetology, German Diabetes Center, Düsseldorf, Germany)
Figure 19	Sample preparation, data analysis	TEM imaging: Kay Jeruschke, Dr. Jürgen Weiß (Institute for Clinical Biochemistry and Pathobiochemistry, German Diabetes Center (DDZ), Düsseldorf, Germany)
Figure 20	Sample preparation, data preparation and analysis	Dr. Matthias Lienhard, Dr. Ralf Herwig (Max Planck Institute for Molecular Genetics, Berlin, Germany
Figure 21	Conducted experiments and analysis	-
Figure 22	Conducted experiments and analysis	-
Figure 23	Conducted experiments and analysis	-
Figure 24	Sample preparation, data analysis	TEM imaging: Kay Jeruschke, Dr. Jürgen Weiß (Institute for Clinical Biochemistry and Pathobiochemistry, German Diabetes Center (DDZ), Düsseldorf, Germany)
Figure 25	Conducted experiments and analysis	-
Figure 26	Conducted experiments and analysis	-
Figure 27	Conducted experiments and analysis	-
Figure 28	Conducted experiments and analysis	-

6.6 Acknowledgements

First of all, I would like to thank Prof. Dr. Hadi Al Hasani as the supervisor of my thesis for giving me the opportunity to work on my research project, for his valuable input, helpful discussions, his advice and recommendations, as well as the possibility to present my data of national and international congresses and symposia.

I would also like to thank Dr. Michael Feldbrügge for his willingness to be the second reviewer of my thesis.

Particularly, I would like to thank Alexandra Chadt for her great support and help along the development of this project, for always having great advice and fresh ideas as well as always having a sympathetic ear for this more “exotic” project in the working group.

I am extremely grateful to all the collaborators of this project who assisted and advised me with immense expertise. Dr. Simone Gorressen, Dominik Semmler and their team for their immense support with the I/R-interventions, Dr. rer. nat. Jürgen Weiß, Kay Jeruschke and Carmen Weidlich for their great aid and advice in all questions regarding the histological approaches of this study, Dr. Matthias Lienhard and Dr. Ralf Herwig for their great support on the field of bioinformatics, Prof. Dr. Jens Brüning and his team for the support in assessing the *in vivo* glucose uptake in mice and Dr. Thomas Jelenik for his great support regarding the respirometry measurements, My special thanks go to Dr. David Barbosa, for paving this projects way and allowing me to build on his great work.

Another big thank you goes to my students Anne Pfitzer, Marvin Hubert, Sarah Mae Hodge, Giovanna Hansen and Michelle Kolasa. It was my pleasure to supervise all of you during the preparation of your theses and I could teach you something for your bright future careers.

A big thank you goes to the technicians who assisted me throughout the whole project with their extraordinary technical expertise and supported me in all questions of the daily lab life. My special thanks to Anette Kurowski, Angelika Horrighs, Dagmar Grittner, Heidrun Podini, Carina Heitmann, Annette Schober, Antonia Osmers and Birgit Knobloch. In addition, I would like to thank Lothar Bohne for his splendid support with the gas chromatography measurements.

Of course, I will not forget my former and current colleagues and lab/office mates. Thank you for all the fruitful discussions, laughs and for creating such an extraordinarily great working atmosphere. Thank you to Dr. Samaneh Eickelschulte, Dr. Delsi Altenhofen, Dr. Tanja Schallschmidt, Lena Espelage, Sarah Görigk, Jenny Khuong and all the members of the research group Pathobiochemistry. Also, a big thank you goes to all the guys of the “Ilf güldene Zwülf”, Dr. Matthias Dille, David Barbosa, Dr. Tim Benninghoff, Dr. Christian Springer, Tim Brecklinghaus,

Christian de Wendt, Dr. Simon Göddeke, Dr. Sven Görgens and Dr. Torben Stermann for all the great times we had (and have) inside and outside the lab.

Last but definitely not least, I want to express my deep gratitude to my family, especially to my parents Renate and Hans for their endless and immense support during all these years and for always backing me up in all situations. All of this would not have been possible without you!

Eidesstattliche Erklärung

Hiermit erkläre ich, dass ich die vorliegende Dissertation selbstständig und ohne fremde Hilfe unter Beachtung der „Grundsätze zur Sicherung guter wissenschaftlicher Praxis an der Heinrich-Heine-Universität Düsseldorf“ verfasst habe. Es wurden nur die angegebenen Quellen und Hilfsmittel benutzt. Wörtlich und inhaltlich übernommene Gedanken wurden als solche kenntlich gemacht.

Düsseldorf, den _____

Christian Binsch